

REVIEW

View Article Online
View Journal | View IssueCite this: *Mater. Chem. Front.*,
2021, 5, 5897

Strategies, design and synthesis of advanced nanostructured electrodes for rechargeable batteries

Md Mokhlesur Rahman,^{ib}*^a Irin Sultana,^a Ye Fan,^a Baozhi Yu,^{ib}^a Tao Tao,^{ab}
Chunping Hou^{*cd} and Ying Chen^{ib}*^a

Nanotechnology and nanomaterials engineering have played a crucial role in the recent development of energy conversion and storage systems. Huge efforts have been made for advancing energy storage technologies particularly battery technologies including lithium-ion, sodium-ion, potassium-ion, and lithium-sulfur batteries. As electrodes (anodes and cathodes) are the key components of these rechargeable batteries, any improvement in electrode materials can effectively enhance the performance of these devices. The combination of nanotechnology and nanomaterials engineering has been proven to meet this challenge through the discovery or development of new materials chemistry, especially frontier materials at the nanoscale. In this review article, we briefly summarize our battery research based on the application of a wide range of nanomaterials over the last decade. The major goal of this review is to highlight various strategies to tackle problems associated with electrode materials and to discuss different approaches for the synthesis of nanomaterials with improved electrochemical performance. To achieve high performance rechargeable batteries, various design and synthesis strategies as well as new material properties are discussed. A number of future research directions are also suggested in this review article.

Received 18th February 2021,
Accepted 2nd June 2021

DOI: 10.1039/d1qm00274k

rsc.li/frontiers-materials

^a Institute for Frontier Materials, Deakin University, Waurn Ponds, Victoria 3216, Australia. E-mail: m.rahman@deakin.edu.au, ian.chen@deakin.edu.au^b School of Materials and Energy, Guangdong University of Technology, Guangzhou 510006, China. E-mail: houcp@nmu.edu.cn^c College of Materials Science and Engineering, North Minzu University, Yinchuan 750021, China^d Bolt Technologies Co. Ltd, Yinchuan Technology Building, South Tongda Street, ETDZ, Yinchuan 750011, China**Md Mokhlesur Rahman**

Dr Md Mokhlesur Rahman received his PhD degree in Materials Science and Engineering in 2011 from the University of Wollongong, Australia. Currently, Dr Rahman is a Senior Research Fellow and a Chief Investigator of ARC (Australian Research Council) Research Hub in New Safe and Reliable Energy Storage and Conversion Technologies, at the Institute for Frontier Materials, Deakin University, Australia. He is an expert in smart nano and circular energy materials synthesis, characterization at the nanoscale, new battery material and battery cell design and electrochemical performance evaluation by adopting most advanced ex situ and in situ techniques.

**Irin Sultana**

Dr Irin Sultana received her PhD degree in Materials Engineering in 2018 from Institute for Frontier Materials, Deakin University, Australia, and her MEng (by research) in 2012 from the University of Wollongong, Australia. She is currently a Research Fellow at the School of Materials and Energy, Guangdong University of Technology, China, and is working at the Institute for Frontier Materials, Deakin University, Australia. Her research interests include the synthesis and characterization of electrode materials for metal-ion (Li-ion, Na-ion, and K-ion) batteries.

1. Introduction

Recently, great effort has been focused on various kinds of batteries to store energy from renewable sources.¹ Electrochemical energy storage (EES) systems, particularly alkali-ion batteries including lithium-ion batteries (LIBs), sodium-ion batteries (SIBs) and potassium-ion batteries (PIBs), are considered as typical rechargeable battery systems due to ions travelling between anode and cathode during the charging/discharging process.² Among alkali-ion batteries, LIB technology is playing a major role in powering a wide range of mobile devices for quite a long-time. Currently, the application of LIBs is shifted to another level and LIBs are being considered for energy/power storage on a large-scale, such as electric vehicles (EVs) and electric power grids.^{3–5} It is, however, expected that the increase in the demand for lithium on a large-scale will dramatically drive up the cost of raw lithium-containing precursors and could make the technology very expensive. Therefore attention has been paid to sodium (Na), which is the next sister element to lithium (Li) in the periodic table. Na resources are virtually unlimited as Na is one of the

most abundant elements in the Earth's crust and ocean.⁶ Nontoxic and inexpensive raw materials are available for preparing Na-based electrodes, which make SIBs the most promising technology for stationary large-scale energy storage applications.^{6,7} Furthermore, PIBs are a new type of electrochemical energy storage cells with many advantages. Both theoretical calculations and experimental observations have revealed that the K^+/K couple exhibits the lowest redox potential compared to Li and Na in some non-aqueous electrolytes, suggesting that K-ion high voltage batteries with high energy density are possible.^{8–10} It is expected that this next-generation technology could have potential for a wide range of energy storage applications, such as electric power grids and storage of electricity from renewable sources.¹¹ In addition to alkali-ion batteries, the lithium–sulfur (Li–S) system is another type of rechargeable battery, which consists of a Li metal anode and an environmentally friendly low cost sulfur (S) cathode with a high theoretical specific energy (2600 W h kg^{-1}) and specific capacity (1675 mA h g^{-1}).^{12,13} Due to their high energy density and low cost sulfur cathode, Li–S batteries are considered as promising future energy storage devices to power



Ye Fan

Dr Ye Fan obtained his BEng degree from the University of Science and Technology Beijing (China), MEng degree from Hokkaido University (Japan) and PhD degree from Deakin University (Australia). Dr Fan is currently working as a Research Fellow at the Institute for Frontier Materials, Deakin University, Australia. His research focuses on lithium–sulfur and lithium-ion batteries, the applications of boron nitride materials in battery technologies and the development of novel sodium and potassium battery systems.



Baozhi Yu

Dr Baozhi Yu is currently a Research Fellow at the Institute for Frontier Materials, Deakin University, Australia. He received his BSc degree from the Northwestern Polytechnical University in 2011 and PhD degree from Northwest University in 2016. His current research focuses on the development of advanced materials for high-performance energy storage systems including Li-ion batteries, Li–metal batteries, Li–S batteries, and supercapacitors.



Tao Tao

Dr Tao Tao is currently an associate professor at the School of Materials and Energy, Guangdong University of Technology, China. He obtained his BSc, Master's degree, and PhD degree from Central South University, China, and worked for over 3 years at the Institute for Frontier Materials at the Deakin University, Australia. His current research mainly focuses on the development of lithium batteries.



Chunping Hou

Dr Chunping Hou obtained his Master of Engineering degree (2006) from Yanshan University and PhD degree (2018) in Materials Science from Northwestern Polytechnical University, respectively. He became a senior engineer in 2015 and was appointed as CTO in Bolt Technologies Co. Ltd. Since 2018, he has been working in North Minzu University as an associate professor. His main research focuses on electrochemical energy storage engineering, nanocomposite electrode materials for LIBs and carbon-based functional materials.

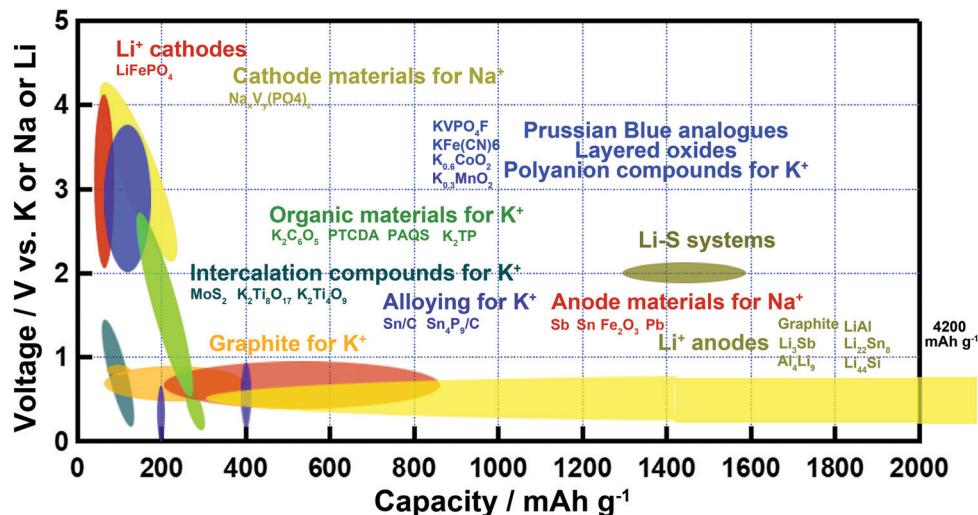


Fig. 1 Comparison of various electrode materials (cathode and anode) in terms of capacity and voltage within the field of rechargeable batteries (alkali-ions: Li⁺, Na⁺, K⁺ and Li-S).

electric vehicles (EVs). As rechargeable batteries are powering and/or expected to power a wide variety of applications,¹⁴ the development of components as well as understanding of the microstructural evolution and atomic scale storage mechanism of these devices is critical.¹⁵ All rechargeable batteries consist of three functional components: (i) electrode (anode and cathode), (ii) separator, and (iii) electrolyte. Among them, electrode materials are regarded as the key elements dominating the capacity of these devices,^{2-5,16-18} as shown in Fig. 1. It is observed from Fig. 1 that most cathode systems exhibit a similar specific capacity (except the Li-S system) between 50 and 250 mA h g⁻¹ within the voltage range of 2–4.3 V for all metal-ion systems. In the case of anode electrodes, the specific capacity of anode materials is significantly different among metal-ion systems. LIB anodes exhibit a wide range of capacity (200–4200 mA h g⁻¹) in which aluminium and

silicon based alloys provide the highest specific capacity. On the other hand, the specific capacity of the anodes is limited to 900 mA h g⁻¹ for SIBs and 500 mA h g⁻¹ for PIBs. Since anode materials are capable of storing ions *via* conversion, alloying, or combined reactions, they typically have much higher theoretical capacity compared with insertion-based cathode materials. It is realised that a number of materials are indeed capable of alloying with sodium or potassium and display a promising level of capacity in excess of that of a typical graphite anode.

Until now, a substantial amount of battery research with respect to both fundamental studies and practical applications has been conducted. Huge efforts have been made for improving rechargeable battery performance by adopting a wide range of strategies. However, many challenges (such as low energy/power density, high cost, low safety, and short lifespan) are still present in alkali-ion batteries whereas Li-S batteries could face the issue of the shuttle effect. Many of these challenges are related to the electrode host structure because fundamental structures of electrode materials play a more crucial role in lifting battery performance as well as in understanding battery chemistry. Undoubtedly, the electrochemical properties of both cathode and anode materials (*e.g.*, specific capacity, cycling stability, Coulombic efficiency, potential, rate performance, *etc.*) are fully dependent on the correlation between host chemistry and structure, the ion diffusion mechanisms, and phase transformations as well.^{17,18} Even though the chemical properties of lithium, sodium, and potassium are very similar to each other, phase stability, transport properties and interphase formation among the three systems are quite different because of the size difference of ions (Li⁺ < Na⁺ < K⁺; 0.76 Å < 1.02 Å < 1.38 Å).¹⁹⁻²¹ It is, therefore, more challenging to develop electrode hosts to accommodate and reversibly transfer large Na⁺ and K⁺ ions (compared to Li⁺ ions) which cause a greater change in the host structures and damage upon extraction/insertion, leading to a poorer electrochemical performance. In comparison with metal-ion batteries, the Li-S system exhibits the highest energy density



Ying Chen

Professor Ying (Ian) Chen received his PhD in Chemistry from the University of Paris-Sud, Orsay, France. He had worked at the Australian National University, Canberra, for 15 years before moving to Deakin University, Melbourne, in 2009. Professor Chen is the Alfred Deakin Professor, Chair of Nanotechnology, and the Director of a national research centre funded by the Australian Research Council – ARC Research Hub in New Safe

and Reliable Energy Storage and Conversion Technologies, at the Institute of Frontier Materials of Deakin University. He has been working on nanotechnology and energy storage for 25 years and his current research focuses on fundamental research in nanomaterials for energy storage in batteries and fuel cells.

which results in a different reaction mechanism. Although the system has matured, many problems with electrodes still exist such as the insulating nature of sulfur, formation of polysulfides, large volumetric expansion of sulfur during lithiation, polysulfide shuttle effect, unstable solid electrolyte interphase layer and growth of Li dendrites.

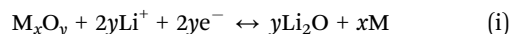
To solve many of the above mentioned problems related to the electrode host structure, nanostructuring of electrodes is being explored as a suitable method for developing large varieties of electrode materials where materials engineering is adopted as a key technique to build electrode architecture at the nanoscale.^{11,13,22–24} Tuning the electrode architecture at the nanoscale offers unique properties which result in high performance electrodes, suitable for application in various energy storage devices. It is important to note that the electrochemical performance of nanostructured electrodes not only depends on the nanoscale but also mostly on the design as well as the synthesis method of materials including phase fraction, phase purity, morphology, and particle/crystal size distribution. In the past several years, our group have demonstrated a significant advancement in the field of nanostructured electrode materials for rechargeable batteries. In this review article, we provide a comprehensive summary and discussion of various strategies, diverse designs and different synthesis approaches for the fabrication of varied electrode architectures and the impacts of proper nanostructuring and advanced compositing on enhanced physicochemical/electrochemical properties of electrode materials for rechargeable battery technologies. Even though nanomaterials have shown significant advantages in the field of electrode materials, the latest nanotechnology is required to further advance battery technology.

2. Nanostructured anodes for LIBs and SIBs

Nanomaterials are expected to provide solutions suitable for designing advanced electrode architectures.^{23–25} The use of nanoparticles, in particular, helps to overcome the issues of ionic conductivity (by reducing the length scale for ionic transport) and, to some extent, excessive stress developing in the electrode upon charge and discharge. The smaller particles are generally able to tolerate the repeated expansion and contraction better and, in addition, the electrode composed of such particles is highly porous, thus providing enough internal space for the expansion of its components. Moreover, the use of nanostructured material as an electrode leads to improved electrochemical performance as it provides a large surface area, numerous active sites, and a short mass and charge diffusion distance.²⁶

Among various anode electrodes, nanostructured metal oxides are promising electrode materials for LIBs, SIBs, and supercapacitors because of their high specific capacity/capacitance, typically 2–3 times higher than that of carbon/graphite based materials. Metal oxides, particularly transition metal oxides (TMOs), are, by far, the family of compounds that react through conversion reactions deserving the most attention.^{27–29} The

mechanism of reaction with lithium or sodium is different from that of the carbon-based materials. Lithium or sodium ions react reversibly with metal oxides *via* a conversion reaction that involves the formation and decomposition of Li_2O or Na_2O and is accompanied by the reduction and oxidation of metal nanoparticles. Generally, the electrochemical reactions can be summarized by the following equations:^{30–32}



The forward reaction is thermodynamically favourable and involves multiple electron transfer per unit of metal atom leading to a high theoretical lithium or sodium storage capacity (400–1100 mA h g^{-1}).^{27,32} However, most metal oxides in SIBs usually deliver a relatively small reversible capacity of less than 400 mA h g^{-1} , in spite of their high theoretical capacity.³² The realization of a practical battery with TMO anodes that undergo reversible conversion reactions during cycling is not straightforward. The oxides reacting electrochemically with lithium/sodium through conversion reactions often experience significant volume changes upon lithiation/sodiation and delithiation/desodiation. More specifically, metal oxides suffer from several problems when used as anode materials, which limit their use. Swelling and shrinking of active material particles upon insertion and extraction of Li^+ or Na^+ ions induce poor contact due to pulverization between the active materials and the electron conducting agents, leading to low electric and ionic conductivity, which directly affects the electrochemical performance of the electrodes.^{33–37} As a result, stable cyclic behaviour and good rate capability are difficult to achieve in conversion reaction anodes. Therefore, it is quite challenging to satisfy these issues with metal oxide anodes and these issues need to be addressed. To tackle these problems, some elegant strategies have been proposed. To verify the strategies, a couple of metal oxide electrode systems including $\text{Fe}_2\text{O}_3\text{-SnO}_2/\text{C}$, $\text{Co}_3\text{O}_4\text{-Fe}_2\text{O}_3/\text{C}$, $\text{ZnFe}_2\text{O}_4/\text{C}$, $\text{Nb}_2\text{O}_5\text{-TiO}_2$, $\text{Co}_3\text{O}_4/\text{CNTs}$ and $\text{SnO}_2/\text{graphene}$ have been synthesised and investigated.

2.1 Hybridization of binary metal oxides and their composites

Despite the huge advantages of nanoparticles, the transition metal oxide electrodes based on nanoparticles of only one phase still suffer from poor cyclic stability and rate capability. To circumvent the issue with single-phase transition metal oxide electrodes, a hybridization concept is proposed.³⁸ The idea is to include dissimilar nanostructured components within a single electrode of a battery anode that operates *via* conversion reaction mechanisms. Although, in general, any conversion reaction in anode materials occurs within the same potential range of 0.01–3.0 V vs. Li/Li^+ or 0.01–3.0 V vs. Na/Na^+ or possibly 0.01–3.0 V vs. K/K^+ , the exact potentials responsible for particular stages of the conversion reactions are varied between different materials. This results in the fact that the maxima of the volume expansion/contraction *via* conversion reactions and the associated stresses in electrodes are different for various transition metal compounds. If two suitable materials are combined together in the same anode within an appropriate working potential with a

nanostructured architecture, the volume change is expected to occur sequentially, potentially reducing the level of stress in the electrode and resulting in better structural stability of the combined metal oxide system (compared to a single system). Therefore, the combination of two different metal oxides is critical for stress management in a single electrode system whereas formation of a conducting network with a conductive agent is also essential for more efficient electronic transport in the electrode.

Fe₂O₃-SnO₂/C for LIBs. A common issue with SnO₂ and Fe₂O₃ electrode materials delaying their commercial implementation is the significant volume change (~300% for SnO₂³⁹⁻⁴¹ and ~96% for Fe₂O₃^{34,35}) upon reaction with lithium, resulting in unstable cycling behaviour and poor rate capability. It is challenging to

accommodate this level of volume alterations without damaging the structure of the electrode. An interesting strategy that our group have applied to combat the effects of a drastic volume change more effectively is to combine the two phases that react with lithium at different potentials *vs.* Li/Li⁺ in one electrode and simultaneously disperse them on chains of the conductive carbon matrix of super P LiTM carbon black.⁴² A large-scale synthesis approach of combination of a molten salt method and a low energy ball milling was demonstrated to create such a fascinating hybrid structure of Fe₂O₃-SnO₂/C (Fig. 2a). The electrochemical performance of the hybrid Fe₂O₃-SnO₂/C electrode was superior to that of the Fe₂O₃-SnO₂ electrode assembled *via* a conventional procedure. The Fe₂O₃-SnO₂/C

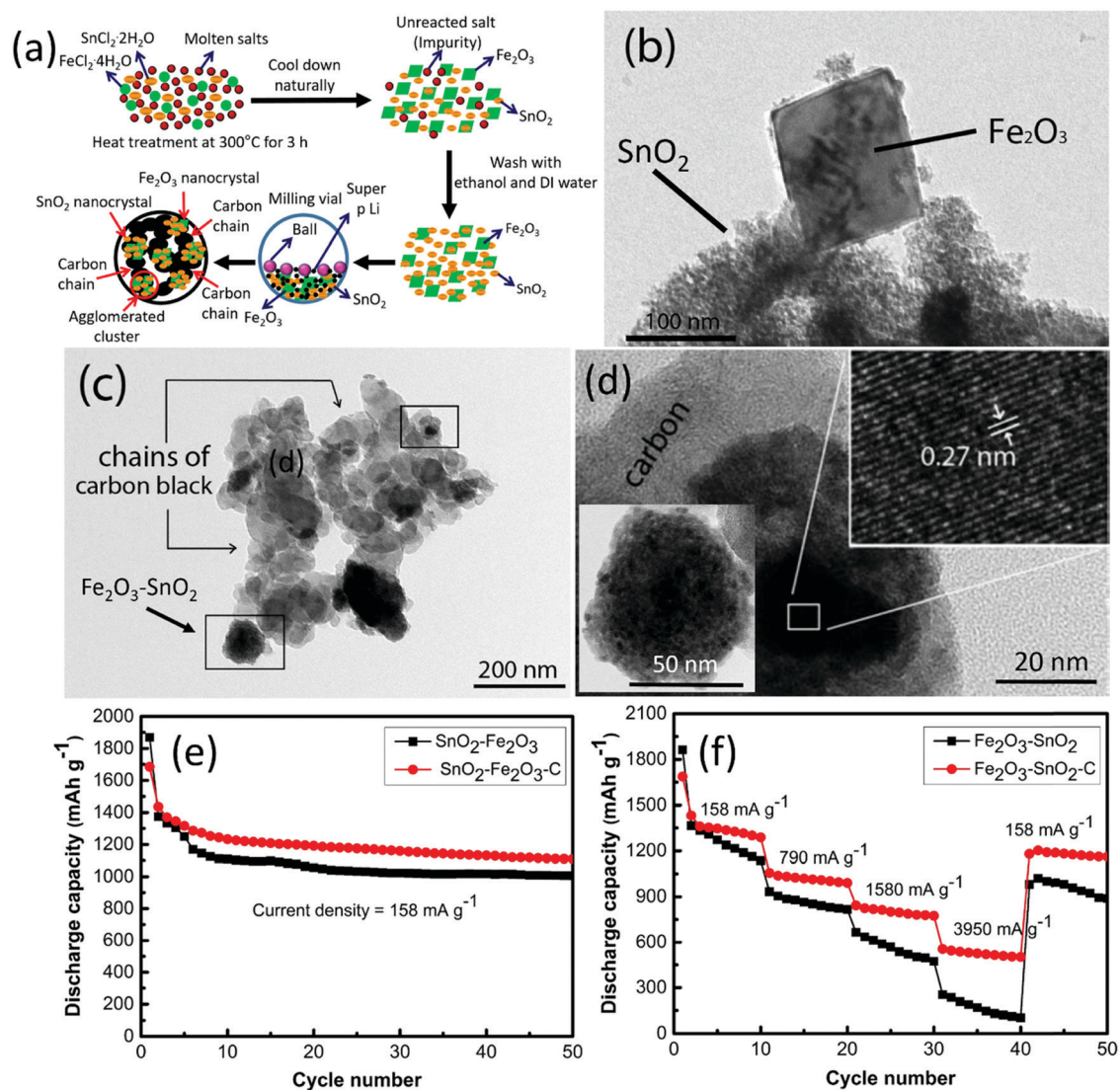


Fig. 2 (a) Schematic representation of the hybridization and material preparation procedure; (b–d) TEM images of (b) a bright-field of Fe₂O₃-SnO₂ where the Fe₂O₃ particle is adjacent to the aggregated nanoparticles of SnO₂, (c) a bright-field of Fe₂O₃-SnO₂/C where Fe₂O₃-SnO₂ particles are dispersed along the chains of super P LiTM carbon black, (d) a selected region (top mark) of (c) containing a Fe₂O₃ particle surrounded by SnO₂ nanocrystals with an HRTEM image (inset in the top right corner) revealing lattice fringes of the Fe₂O₃ crystal. The inset in the lower left corner shows a selected region (bottom mark) of (c) containing SnO₂ nanoparticles; (e and f) electrochemical performance of (e) cycling stability up to 50 cycles at 158 mA g⁻¹ and (f) consecutive cycling behaviour at different rates of the Fe₂O₃-SnO₂/C and Fe₂O₃-SnO₂ electrodes.⁴² (Adapted with copyright permission, The Royal Society of Chemistry.)

electrode exhibited a stable reversible capacity of 1110 mA h g⁻¹ at a current rate of 158 mA g⁻¹ with only 31% of initial irreversible capacity in the first cycle. A high reversible capacity of 502 mA h g⁻¹ was obtained at a high current rate of 3950 mA g⁻¹ (Fig. 2f). A few attempts of combining SnO₂ and Fe₂O₃ into one electrode have been reported. Zeng *et al.*⁴³ have produced microelectrodes based on Fe₂O₃-SnO₂ nanotube arrays, capable of delivering higher gravimetric capacity (965 mA h g⁻¹) than that of previously reported Fe₂O₃ nanotube arrays⁴⁴ and better cyclic stability than that of SnO₂ nanotube arrays.⁴⁵ Fe₂O₃-SnO₂ nanocombs and nano-heterostructures have been studied by Singaporean groups,^{46,47} with a modest electrochemical performance; however, their initial capacity gradually faded away over extended cycles. Another type of Fe₂O₃-SnO₂ heterostructure, representing sub-10 nm iron oxide rods on a micron-sized primary SnO₂ sheet, was evaluated by Wang *et al.*⁴⁸ and a capacity of 325 mA h g⁻¹ was measured after 50 cycles. Chen *et al.*⁴⁹ have indicated that the performance of Fe₂O₃-SnO₂ nanorattles is superior to that of SnO₂ hollow nanospheres. Zhu *et al.*⁵⁰ have assessed the electrochemical properties of SnO₂-Fe₂O₃ nanoparticles dispersed over reduced graphene oxide sheets, capable of delivering 958 mA h g⁻¹ at a current density of 395 mA g⁻¹. The content of Fe₂O₃ nanoparticles in their work was, however, rather low (weight ratio of 1:11 with respect to SnO₂), and the iron oxide nanoparticles were believed to contribute merely as spacers preventing the agglomeration of the SnO₂ nanoparticles. Various groups have also developed robust nanocomposites of Fe₂O₃/SnO₂/graphene. Xia *et al.*⁵¹ fabricated a Fe₂O₃/SnO₂/graphene composite with improved reversible capacity (700 mA h g⁻¹ at 400 mA g⁻¹) and rate capability (154 mA h g⁻¹ at 4205 mA g⁻¹) by adopting a time consuming complicated synthesis process of combination of *in situ* precipitation and chemical reduction. The same composite of Fe₂O₃/SnO₂/graphene was prepared by employing a hydrothermal method.⁵² A combination of 0D (zero-dimensional) SnO₂ nanoparticles and 1D (one-dimensional) Fe₂O₃ nanorods was homogeneously attached onto the nanosheets of 2D (two-dimensional) reduced graphene oxide. The electrode exhibited a high reversible capacity of 1530 mA h g⁻¹ at 100 mA g⁻¹ and a rate capability of 615 mA h g⁻¹ at 2000 mA g⁻¹. Even though reversible capacity was quite good in both cases, rate capability was not promising.

The excellent electrochemical performance of the hybrid Fe₂O₃-SnO₂/C electrode prepared by our group can be attributed to the elegant combination of SnO₂ and Fe₂O₃, two promising anode materials, into an integrated structure of small clusters dispersed on top of conductive chains of carbon black.⁴² The high surface area (147 m² g⁻¹) and clusters of SnO₂-Fe₂O₃ nanoparticles enable better contact between active materials and the electrolyte, reducing the traverse time for both electrons and lithium ions. The combination of two materials, SnO₂ and Fe₂O₃, provides breathable aggregates and makes sequential expansion and contraction of the electrode possible, mitigating the problems associated with volume change. The conductive chains of carbon black among the small clusters serve as a conductive scaffold that maintains a reliable electrical contact between SnO₂-Fe₂O₃ and

the current collectors. The presence of extra space between the carbon black particles and the clusters is also beneficial for diffusion of the electrolyte into the bulk of the electrode, providing fast transport channels for the Li ions, and more effectively accommodating the volume variation. All of these factors could increase the structural stability of the electrode, leading to the superior electrochemical performance. This strategy was further extended to produce other hybrids/nanocomposites of functional oxides.

Co₃O₄-Fe₂O₃/C for LIBs and SIBs. Despite high theoretical capacity, it is very difficult to minimise dramatic volume variations of as high as ~100% with Co₃O₄ in LIBs.⁵³ To minimise this volume change, a hybrid anode of Co₃O₄-Fe₂O₃/C was prepared using low-energy ball milling by mixing together Co₃O₄-Fe₂O₃ nanoparticles synthesized by the molten salt method and super P Li carbon black powder.⁵⁴ The hybrid Co₃O₄-Fe₂O₃/C electrode exhibited outstanding cycling stability in LIBs with a retained reversible capacity of 703 mA h g⁻¹ (96% retention of the calculated theoretical capacity of 731 mA h g⁻¹) at 0.5C rate after 300 cycles (Fig. 3c). A high reversible capacity of 400 mA h g⁻¹ was achieved at a very high current rate of *ca.* 3 A g⁻¹ (4C). Even after 50 cycles of discharge/charge at different current rates, the Co₃O₄-Fe₂O₃/C electrode still delivered a reversible capacity of 780 mA h g⁻¹, which represents >99% capacity recovery (Fig. 3d). Hybridization of Co₃O₄ and Fe₂O₃ into hybrid Co₃O₄-Fe₂O₃ electrodes has also been explored by several groups. Wu *et al.*⁵⁵ have reported the direct growth of Co₃O₄/α-Fe₂O₃ branched nanowire heterostructures prepared by a two-step hydrothermal method. The Co₃O₄/α-Fe₂O₃ branched nanowires exhibited significantly enhanced Li⁺ storage capacity and stability, with a high reversible capacity of 980 mA h g⁻¹ after 60 cycles at a current density of 100 mA g⁻¹. Although the reversible capacity was attractive in this study, the capacity retention was unsatisfactory (~63%) with respect to the initial capacity (1534 mA h g⁻¹). A hierarchical Fe₂O₃@Co₃O₄ nanowire array based on the sacrificial template accelerated hydrolysis (using ZnO as the template) has also been reported.⁵⁶ The Fe₂O₃@Co₃O₄ nanowire array exhibited good cycling performance (1005 mA h g⁻¹ after 50 cycles at 200 mA g⁻¹) with improved rate performance (788 mA h g⁻¹ at 5000 mA g⁻¹) but significant capacity fading was observed. Luo *et al.*⁵⁷ demonstrated another novel hierarchical Co₃O₄@α-Fe₂O₃ core-shell nanoneedle array (Co₃O₄@α-Fe₂O₃ NAs) produced by a step-wise, seed-assisted, hydrothermal approach with a high reversible capacity of 1045 mA h g⁻¹ after 100 cycles at 120 mA g⁻¹. However, the capacity retention (~53%) and rate capability were not satisfactory. Recently, a high performance composite of Fe₂O₃-Co₃O₄/polypyrrole (PPy) has been constructed for LIBs through hybridization of Fe₂O₃ and Co₃O₄ nanosheets and their subsequent encapsulation into conductive polypyrrole.⁵⁸ The Fe₂O₃-Co₃O₄/polypyrrole (PPy) composite exhibits high capacity (922 mA h g⁻¹ after 100 cycles), very good rate capability (712 mA h g⁻¹ at 5 A g⁻¹) and excellent long-term cycling stability (414 mA h g⁻¹ at 10 A g⁻¹ after 1000 cycles).

We have prepared a Co₃O₄-Fe₂O₃/C electrode with attractive electrochemical performance which originates from the presence of the percolating carbon host in the hybrid electrode and

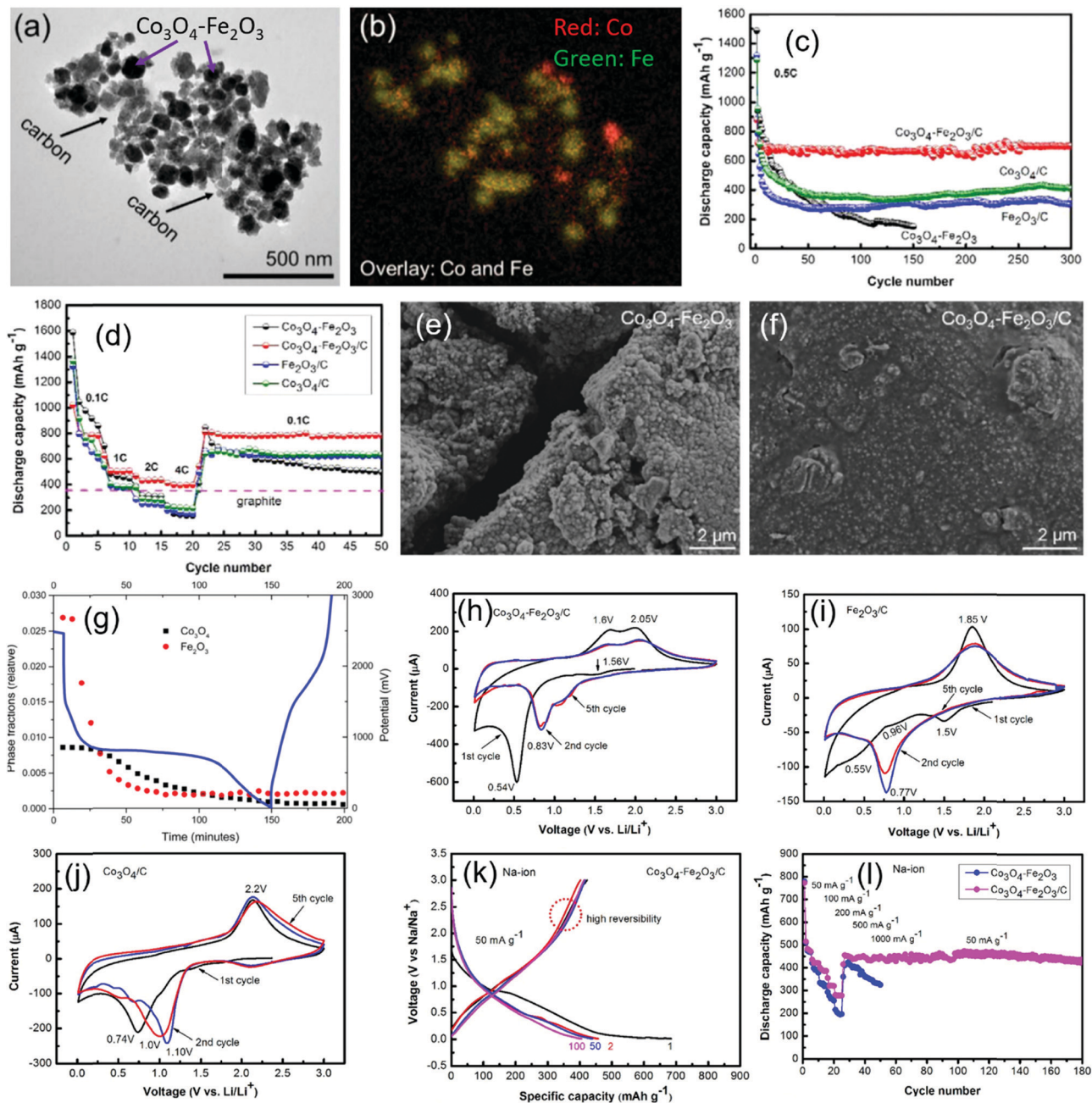


Fig. 3 (a–j) Characterization of $\text{Co}_3\text{O}_4\text{-Fe}_2\text{O}_3/\text{C}$ in LIBs⁵⁴ (reproduced with permission, Copyright 2015, American Chemical Society): (a and b) TEM analysis of (a) a bright-field image and (b) the corresponding energy filtered map of Co and Fe; (c and d) electrochemical performance of the $\text{Co}_3\text{O}_4\text{-Fe}_2\text{O}_3/\text{C}$ electrodes; (e and f) post cycling SEM images of the electrodes extracted from lithium half-cells after 50 cycles of the rate capability test; (g) evolution of the phase fractions of the Co_3O_4 and Fe_2O_3 components as a function of time correlated to the electrochemical charge/discharge curve in blue; and (h–j) cyclic voltammetry. (k and l) Electrochemical performance of the $\text{Co}_3\text{O}_4\text{-Fe}_2\text{O}_3/\text{C}$ electrode in SIBs⁶¹ (adapted with copyright permission, The Royal Society of Chemistry).

sequential volume expansion in the oxide components.⁵⁴ Post cycling SEM images (Fig. 3e and f) clearly demonstrate that structural stability of the hybrid $\text{Co}_3\text{O}_4\text{-Fe}_2\text{O}_3/\text{C}$ electrode is significantly better than that of $\text{Co}_3\text{O}_4\text{-Fe}_2\text{O}_3$ due to the presence of the carbon host. A large crack is developed in the $\text{Co}_3\text{O}_4\text{-Fe}_2\text{O}_3$ electrode, leading to an unstable structure, resulting in deterioration in electrochemical performance. It is evidenced that Fe_2O_3 reacts first, followed by the Co_3O_4 component in the hybrid system. Each

component starts being active at different parts of the first discharge and the activity appears to be sequential rather than simultaneous in their reactions in the first discharge of the half-cell. It is realized from Fig. 3g that the sloping potential region is predominantly due to the Fe_2O_3 phase reacting during discharge and the plateau region signals the onset of the Co_3O_4 phase reacting. It is also worthwhile to note that the Co_3O_4 phase fraction remains stable while the majority of Fe_2O_3 reacts with

lithium first. Although both materials react with lithium within the same potential range of 3–0.01 V vs. Li/Li⁺, the exact potential for the maximal electrochemical activity differs for Co₃O₄ and Fe₂O₃, as was supported by CV curves (Fig. 3h–j). Sequential volume expansion was also found in the nanocomposite of multilayer CuO@NiO hollow spheres,⁵⁹ in which the sequence of lithium insertion was first in CuO at ~1.2–1.1 V and then in NiO at ~0.7–0.6 V. Due to the discrepancy in electrochemical active potentials, SnO₂ has been used as an inert matrix for Fe₂O₃ particles and it keeps them from agglomerating. Both the lithium insertion and extraction potentials of SnO₂ are below 0.7 V and just beyond the active potential range of Fe₂O₃ (0.7 to 2.0 V), leading to a sequential volume expansion in the systems of graphene/Fe₂O₃/SnO₂⁶⁰ and Fe₂O₃–SnO₂/C,⁴² respectively.

Furthermore, the obtained hybrid of Co₃O₄–Fe₂O₃/C was used in SIBs for the first time,⁶¹ with a capacity retention of 410 mA h g^{−1} after 100 cycles at 50 mA g^{−1} within the potential range of 0.1–3.0 V vs. Na/Na⁺ (Fig. 3k). The hybrid also exhibited superior rate capability in SIBs with a capacity recovery of 440 mA h g^{−1} (93% retention) after 180 long-term cycles at 50–1000 mA g^{−1} and back to 50 mA g^{−1} (Fig. 3l). This work led to several follow-up studies in the metal oxide based anodes for SIBs.^{62,63}

2.2 Construction of ternary metal oxide composites

Ternary metal oxides involve both the conversion and alloying reaction mechanisms, leading to high theoretical capacity. Complex chemical composition, interfacial effects, and synergic effects of multiple metal species make ternary metal oxides much more competitive than single metal oxides and possess a better electrical conductivity than their simple oxide counterparts.^{64–66} However, the sluggish diffusion of lithium ions and relatively low electronic conductivity are two major barriers for their practical application in energy storage in higher rate environments.⁶⁴ To make these materials viable, rational design with favourable structural features is needed. Over the past several years, various strategies have been introduced to improve the electrochemical performance of ternary metal oxides with a spinel structure (AB₂O₄, A = Mn, Zn, Fe, Co, Ni, or Cu; B = Mn, Fe, Zn, Co, Ni, or Cu; A ≠ B) in LIBs such as (i) synthesis of very special morphologies (hollow microspheres,⁶⁷ hollow nanospheres,⁶⁸ macroporous particles,⁶⁹ and flakes),⁷⁰ (ii) surface coating with carbon,⁷¹ and (iii) decreasing of particle size to the nanometre range.⁷² Carbon coating and special morphologies are capable of improving their cyclability; however, the complicated synthesis procedure along with high temperature carbon coating is time-consuming, which significantly hinders the process scale-up. It is anticipated that ball milling could be an exceptionally suitable method for this purpose because ball milling can efficiently reduce oxide particle size down to the nanometre level and simultaneously mix them homogeneously with the carbon matrix to form a composite microstructure. A simple, cost effective and high yield ball milling method is thus required to overcome problems with ternary metal oxide anodes, particularly ZnFe₂O₄ based anodes.

ZnFe₂O₄/C for LIBs. The anode of ZnFe₂O₄ (a member of AB₂O₄) with a spinel lattice structure has attracted much attention because lithium insertion into the ZnFe₂O₄ electrode involves both the conversion and alloying reaction mechanisms, leading to a high theoretical capacity of 1000 mA h g^{−1}.^{73,74} This material, however, experiences first cycle irreversibility and fast capacity decay, which are challenging to mitigate. An effective method for the preparation of a ternary metal oxide composite of ZnFe₂O₄–C by combining sol–gel and ball milling techniques is proposed,⁷⁵ as shown in Fig. 4a. The crucial feature of this structure is that sol–gel synthesised ZnFe₂O₄ nanoparticles are dispersed and attached uniformly along the chains of the Super P LiTM carbon black host by adopting low energy ball milling which gives a number of advantages such as (i) high electronic conductivity; (ii) reduction in the traverse time for both electrons and lithium ions; (iii) increase in the structural stability; and (iv) high Coulombic efficiency in the first cycle because of sufficient infiltration of the electrolyte and fast diffusion of Li⁺ ions. As a result, the electrochemical performance (in terms of cycling stability, rate capability, and capacity retention) of the ZnFe₂O₄–C electrode is outstanding (Fig. 4c and d). The cycling stability and rate capability of the ZnFe₂O₄–C electrode were improved dramatically with a reversible capacity of 681 mA h g^{−1} (96% retention of the calculated theoretical capacity of ~710 mA h g^{−1}) at 0.1C after 100 cycles with a remarkable coulombic efficiency (82%) improvement in the first cycle. The rate capability was as high as 702 at 0.1, 648 at 0.5, 582 at 1, 547 at 2 and 469 mA h g^{−1} at 4C (2.85 A g^{−1}). The capacity recovery was ~98% when the cell was returned to 0.1C. It is demonstrated that a smart electrode design enables ZnFe₂O₄–C materials to be a high quality anode for LIBs.

2.3 Fabrication of metal oxide–carbon nanotube (CNT) composites

In Sections 2.1 and 2.2, super P LiTM carbon black and graphene were used as the conductive matrix for the formation of transition metal oxide based composites and mixed metal oxide based composites. To achieve high performance electrodes, another effective strategy is to fabricate composites of metal oxides with carbon nanotubes (CNTs). Compared to graphite, carbon nanotubes (CNTs) (an allotrope of graphite) might be another interesting conductive matrix for the formation of composites with metal oxides because of the unique properties of CNTs including strong mechanical properties, excellent electronic conductivity, and large surface areas.⁷⁶ Moreover, composites with CNTs could retain the sizes of nanoparticles due to their tight anchoring by the CNTs. Most importantly, CNTs exhibit higher Na ion storage properties than other carbon materials such as activated carbon, mesoporous carbon, and graphene nanosheets,⁷⁷ which encourages one to fabricate metal oxide–CNT composites for more efficient sodium storage.

Co₃O₄/CNTs for SIBs. Little attention has been paid to study the electrochemical behaviours of Co₃O₄ with sodium. In 2014, we first attempted to extend the electrochemical investigation of cobalt oxides (Co₃O₄) with sodium and demonstrated a possible conversion reaction with a reversible capacity of 447 mA h g^{−1}.⁷⁸

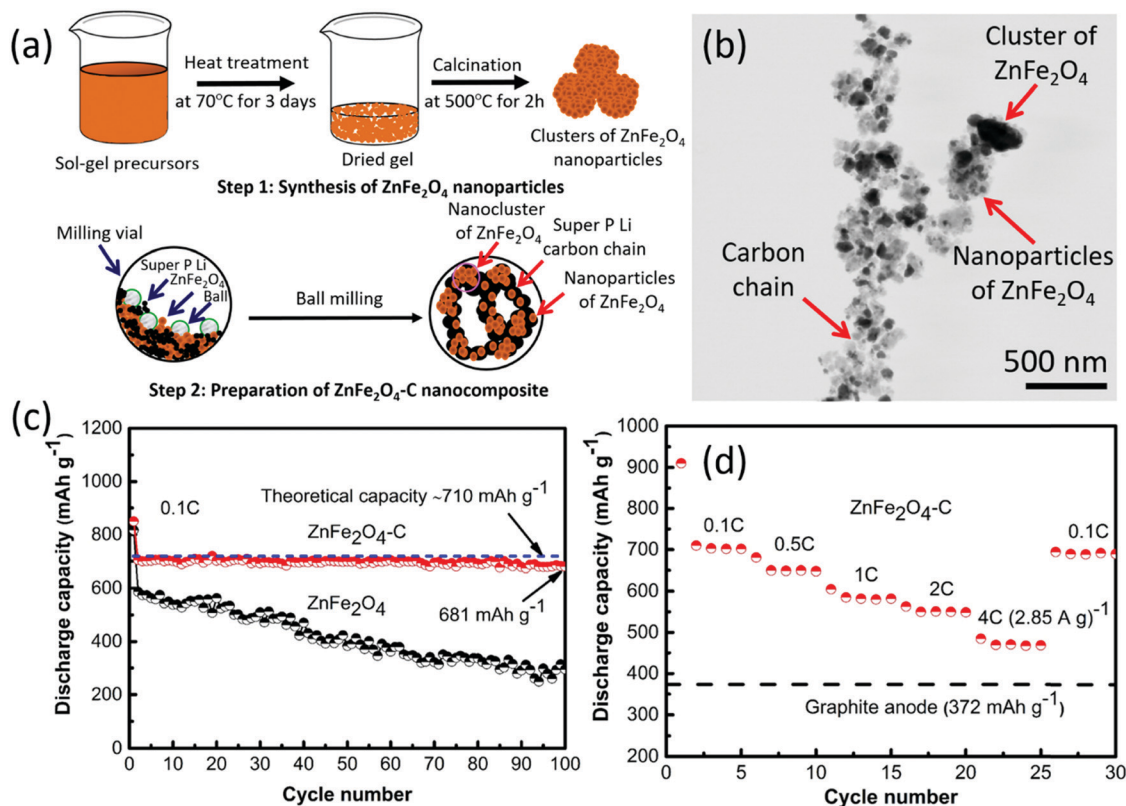


Fig. 4 Schematic illustration of the composite preparation procedure (combination of a sol-gel process and a ball milling method); (b) a bright-field TEM image of the $\text{ZnFe}_2\text{O}_4\text{-C}$ sample; (c and d) electrochemical performance: (c) cycling performance up to 100 cycles at a low current rate of 0.1C (0.1C = $\sim 100 \text{ mA g}^{-1}$ for ZnFe_2O_4 and $\sim 71 \text{ mA g}^{-1}$ for $\text{ZnFe}_2\text{O}_4\text{-C}$) and (d) consecutive cycling performance of the $\text{ZnFe}_2\text{O}_4\text{-C}$ electrode at different current rates, ranging from low to moderate to very high.⁷⁵ (Reproduced with permission, Copyright 2015, Elsevier.)

This work was undoubtedly helpful to further advance towards sodium electrochemistry of Co_3O_4 based electrodes. Later on, Wen *et al.*⁷⁹ also synthesized bowl-like hollow spherical Co_3O_4 structures and studied their sodium-storage behaviour; however, electrochemical performance was unsatisfactory. To achieve high performance electrodes, Jian *et al.*⁸⁰ developed $\text{Co}_3\text{O}_4@\text{CNT}$ composites wherein monodispersed hierarchical Co_3O_4 spheres were intertwined with carbon nanotubes, providing both facile electron and Na^+ ion diffusion in the system simultaneously. As a consequence, the composite $\text{Co}_3\text{O}_4@\text{CNT}$ electrodes exhibited improved cycling and rate performance. Mesoporous Co_3O_4 nanosheet/3D graphene network ($\text{Co}_3\text{O}_4\text{MNS}/3\text{DGN}$) nanohybrids have also been reported.⁸¹ It is noticed that the $\text{Co}_3\text{O}_4\text{MNS}/3\text{DGN}$ nanohybrids exhibit better SIB performance with enhanced reversible capacity, good cycle performance and rate capability as compared to Co_3O_4 MNSSs and Co_3O_4 nanoparticles, but the rate capability was not as good as that of $\text{Co}_3\text{O}_4@\text{CNT}$ composites, which may be due to different conductive agents used in both cases. It was found that the Na-ion storage properties of carbon nanotubes (CNTs) are better than those of other carbon materials such as activated carbon, mesoporous carbon, and graphene nanosheets.⁸² By considering this information, we have produced a robust composite electrode of $\text{Co}_3\text{O}_4/\text{CNT}$.⁸³ A single step process of the “liquid plasma” method with a nanosecond pulse atmospheric pressure plasma (NPAPP) system

was used (Fig. 5a), where Co_3O_4 nanoparticle clusters were uniformly dispersed into the CNT networks.⁸³ When used as a SIB anode, the $\text{Co}_3\text{O}_4/\text{CNT}$ electrode exhibits a high reversible capacity of 403 mA h g^{-1} at 50 mA g^{-1} after 100 cycles and shows a remarkable rate capability of 212 mA h g^{-1} at 1.6 A g^{-1} and 190 mA h g^{-1} at 3.2 A g^{-1} . Such a high rate capability is understood to be a consequence of incorporation of CNTs into Co_3O_4 clusters to form a $\text{Co}_3\text{O}_4/\text{CNT}$ composite. In this composite, Co_3O_4 guarantees high electrochemical reactivity towards sodium, while the CNT improves the conductivity and stabilizes the anode structure during repeated cycling (Fig. 5f). Due to the simple synthesis technique with high electrochemical performance, the $\text{Co}_3\text{O}_4/\text{CNT}$ composite could have great potential as an anode material for SIBs.

2.4 Fabrication of metal oxide-graphene composites

Fabrication of metal oxide-graphene composites is another effective strategy to combat against volume expansion of the electrodes used in LIBs and SIBs. As an electrode host material, mono-layer graphene, known as graphene, has attracted worldwide attention since 2004.⁸⁴ The impact of incorporation of graphene into battery electrodes is huge because monolayer or few-layer graphene can provide high conductivity and more active sites for lithium and sodium ions, not only on both sides of the carbon sheets but also on the edges and covalent sites of

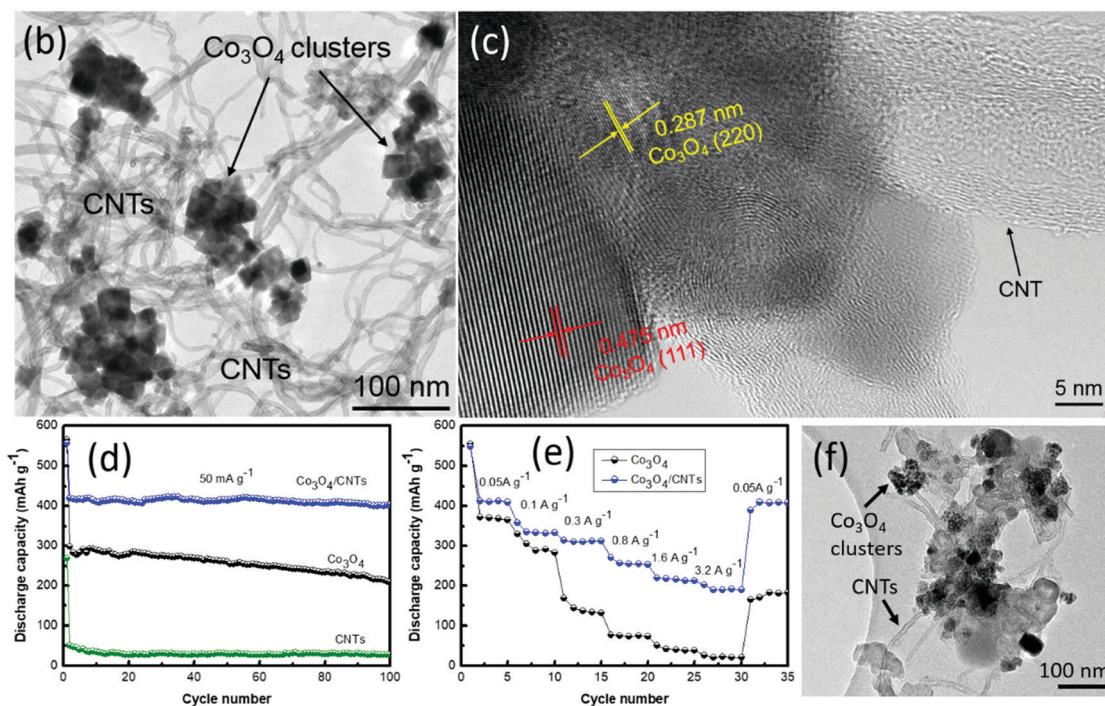
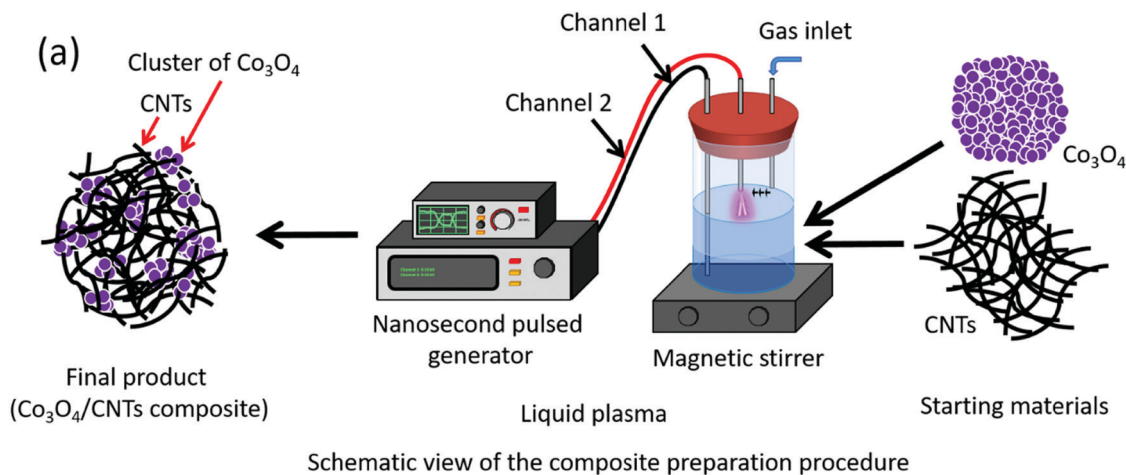


Fig. 5 (a) Schematic illustration of the preparation of the $\text{Co}_3\text{O}_4/\text{CNTs}$ composite; (b and c) bright-field and HRTEM images; (d and e) electrochemical performance; and (f) post cycling TEM analysis.⁸³ (Adapted with copyright permission, The Royal Society of Chemistry.)

graphene fragments. Furthermore, elastic graphene layers are excellent buffers for anisotropic volumetric expansion.^{85,86} As a result, to achieve high performance metal oxide anodes with excellent electrical conductivity and superior structural stability, graphene is widely utilised for the fabrication of metal oxide based graphene composites. For instance, Su *et al.*⁸⁷ have synthesised SnO_2 -graphene nanocomposites by adopting an *in situ* hydrothermal process. Although SnO_2 can deliver a high theoretical sodium storage capacity of 1378 mA h g^{-1} , huge volume variation during the cycling process leads to rapid capacity loss. To tackle the volume variation of the SnO_2 anode in SIBs, SnO_2 nanocrystals were uniformly anchored on graphene nanosheets in their synthesis process, in which individual SnO_2 nanocrystals were wrapped with graphene nanosheets, creating a

superior electrode architecture (Fig. 6a and b). The obtained SnO_2 -graphene nanocomposites demonstrated a high reversible capacity of over 700 mA h g^{-1} in SIBs with an excellent cyclability as compared to bare SnO_2 electrodes (Fig. 6c). Commendable rate capabilities were also achieved (Fig. 6d). Inspired by this work, various research groups also prepared a wide range of Sn or SnO_2 -graphene nanocomposites for SIBs.⁸⁸⁻⁹¹

Recently, Kong *et al.*⁹² have reported a facile synthesis approach of three-dimensional (3D) hollow spheres of the SnO_2/rGO composite with a porous wall by adopting a sol-gel assisted spray drying method combined with solid-state calcination (Fig. 6e). In these composite spheres, the reduced graphene oxide (rGO) acts as a substrate as well as a super conductive matrix, in which SnO_2 nanoparticles play the dual role of a reinforcement agent and

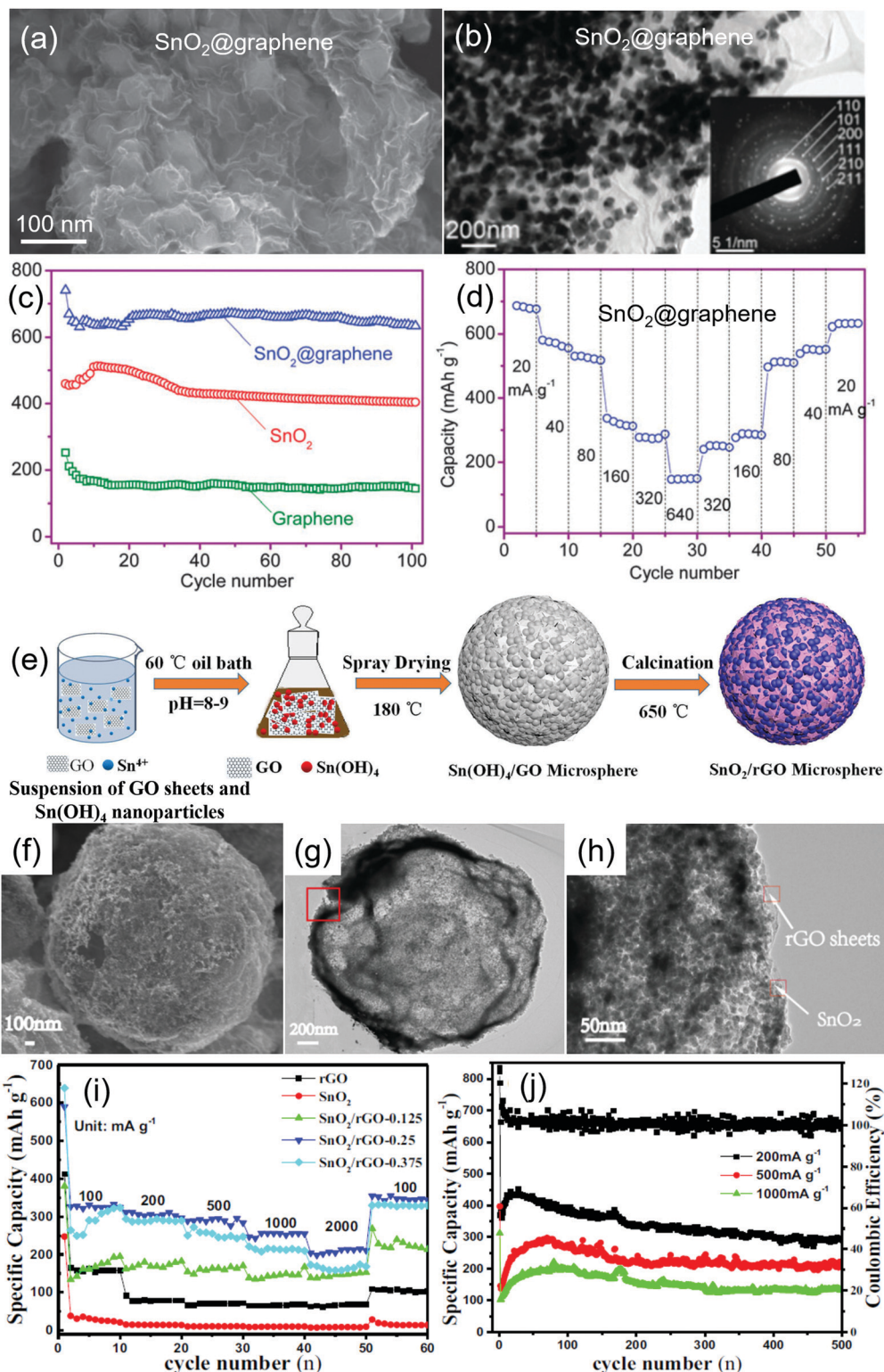


Fig. 6 (a–d) Characterization of the SnO₂–graphene nanocomposite in SIBs⁸⁷ (reproduced with permission, Copyright 2021, The Royal Society of Chemistry): (a and b) electron microscopy analysis of (a) FESEM image and (b) low magnification TEM bright-field image (inset: SAED pattern); and (c and d) electrochemical performance of (c) cycling stability and (d) rate capability. (e–j) Characterization of 3D porous SnO₂/rGO hollow spheres in SIBs⁹² (reproduced with permission, Copyright 2019, Elsevier): (e) schematic illustration of the preparation of SnO₂/rGO hollow spheres; (f–h) electron microscopy analysis of (f) SEM image of a microsphere and (g and h) TEM bright-field images; and (i and j) electrochemical performance of (i) rate capability and (j) cycling stability.

essentially as an active material for Na⁺ storage, providing the most advanced electrode architecture (Fig. 6f–h). As a result, the as-prepared 3D porous/hollow SnO₂/rGO anode maintained an enhanced rate capability of 231 mA h g⁻¹ at 2000 mA g⁻¹ (Fig. 6i and j). In addition to SnO₂ based graphene oxide composites, many other different systems including MO/graphene, M₂O₃/graphene, M₃O₄/graphene, MO₂/graphene, M₂O₅/graphene, MO₃/graphene, and ternary M_xM'_yO_z/graphene (M, M' = low-cost metals of Cu, Ni, Co, Zn, Fe, Mo, V, Mn, Ti, etc.) have been synthesised and characterized in LIBs and SIBs with promising electrochemical performances.^{93–96}

2.5 Additive-free hybridization

Most traditional syntheses of battery materials and subsequent electrode preparation methods are time consuming involving unhealthy multiple steps, including material synthesis with toxic reagents, slurry formation, coating onto current collectors, and drying in vacuum. Furthermore, carbon black, polymeric binders and organic solvents (*N*-methyl-2-pyrrolidone) are commonly included during slurry preparation for electrical conduction and better physical contacts between particles and current collector, respectively.^{97–101} Basically, addition of various additives to the electrodes generates 3 major problems:^{102,103} (i) an extra weight (10–40%, depending on the electrode materials used) of the electrode is increased; (ii) inhomogeneous blend of carbon black, binders, and nanoparticles (active materials) makes the diffusion paths of the ions and electrons unclear, leading to modeling and characterization difficulties; and (iii) complicated procedure and various additives lead to environmental hazard as well as high cost of the electrodes. Therefore, it would be beneficial but also challenging to develop a simplistic method of fabrication of hybrid electrode systems without incorporation of any additives/chemicals but with excellent electrochemical performance.

Nb₂O₅-TiO₂ for LIBs. Earlier, nanomaterials, particularly nanowires and nanotubes, have been developed and investigated as additive-free electrodes for energy storage.^{104–108} However, additive-free electrode films based on fully nanoparticles, specifically hybridization of both nanoparticles of TiO₂ and Nb₂O₅ in one electrode, are hardly reported. In 2016, Yu *et al.*¹⁰⁹ hybridized Nb-doped TiO₂ and Nb₂O₅ as a core-shell heterostructure where the Nb-doped TiO₂ rod was used as a core and the Nb₂O₅ nanosheet was used as a shell. Combination of nanoparticles of TiO₂ and nanosheets of Nb₂O₅ is also reported as a heterogeneous composite of TiO₂-Nb₂O₅.¹¹⁰ Even though they successfully hybridized TiO₂ and Nb₂O₅, both systems cannot be claimed as additive-free systems as they used binder and carbon black for the preparation of the electrode as well as various reagents in the synthesis process. Recently, a hybrid Nb₂O₅-TiO₂ electrode without incorporation of any chemicals/additives in the synthesis/electrode fabrication process is developed. A radio frequency sputtering technique was employed to deposit directly hybrid Nb₂O₅-TiO₂ on the copper foil (Cu) current collector by combining the titanium (Ti) and niobium (Nb) target together.¹¹¹ The obtained Nb₂O₅-TiO₂ electrode delivers high gravimetric capacity (214 mA h g⁻¹ at 50 mA g⁻¹), high areal capacity (0.0214 mA h cm⁻² at 5 μA cm⁻²), and high volumetric capacity

(1813 mA h cm⁻³ at 5 μA cm⁻²) (Fig. 7d). A long-term cycling stability with a gravimetric capacity of 174 mA h g⁻¹ at 0.4 A g⁻¹, an areal capacity of 0.0174 mA h cm⁻² at 40 μA cm⁻², and a volumetric capacity of 1474 mA h cm⁻³ at 40 μA cm⁻² after 1000 cycles was recorded (Fig. 7f). Such a superior electrochemical performance of the electrode is credited to its distinctive electrode architecture and the synergistic effects between components. The duration of deposition time plays a crucial role in this regard. The 1 h deposition film features pearl-chain like morphology consisting of numerous nanoparticles, which are attached one after one, capable of creating a void due to interconnection gaps among chains (Fig. 7a and b). As a result, the voids function as an electrolyte reservoir, facilitating electrolyte diffusion into the bulk of the electrode, thus improving the Li⁺ ion transport path. Moreover, 1 h deposition provides small particle size in the Nb₂O₅-TiO₂ film, enabling charge transfer (both ionic and electronic) over shorter distances (Fig. 7c). Most importantly, grain boundaries and interface charge transfer resistance are likely to be reduced significantly due to the binder free electrode, leading to high electron transport along the lattices of electroactive Nb₂O₅-TiO₂. The obtained electrochemical performance of the additive-free hybrid Nb₂O₅-TiO₂ electrode is better than that of other reported additive-based Nb₂O₅ and TiO₂ systems.^{112–118}

A safe LIB anode of Nb₂O₅ with a new morphology of a vein-like nanoporous network was produced using a simple electrochemical anodization method (Fig. 7g).¹¹⁹ The porous Nb₂O₅ electrode, even without surface coating or cation doping, could deliver a high reversible capacity of 201 mA h g⁻¹ within 1.0–3.0 V and 175 mA h g⁻¹ within 1.2–3.0 V after 300 cycles at a current density of 0.4 A g⁻¹ (Fig. 7k and l). However, this system cannot be claimed as an additive-free electrode because carbon black and binder were used during slurry mixing for electrode fabrication. The electrode could also tolerate very high current and exhibited commendable rate capabilities of 208 mA h g⁻¹ at 0.2 A g⁻¹, 186 mA h g⁻¹ at 0.4 A g⁻¹ and 161 mA h g⁻¹ at 0.8 A g⁻¹ with a cut-off voltage window of 1.0–3.0 V (Fig. 7m). The demonstrated synthesis method can potentially be used to produce a wide range of functional nanomaterials.

3. Nanostructured cathodes for LIBs and SIBs

The impact of cathode materials in LIBs and SIBs is remarkable as they play a crucial role in determining the power density and fast charging/discharging. The key to improving the electrochemical performance of LIBs and SIBs is the smart design and controlled synthesis of cathode materials. The cathode materials for LIBs and SIBs are expected to work well if they function as a host material for Li and Na; the volume variation should be negligible during cycling for Li⁺ and Na⁺ in and out, and this capability is critical for achieving high performance devices.^{120,121} Although a significant number of cathode hosts for LIBs have already been commercialized, potential cathodes for successful commercial implementation in SIBs are still far away.^{121–123}

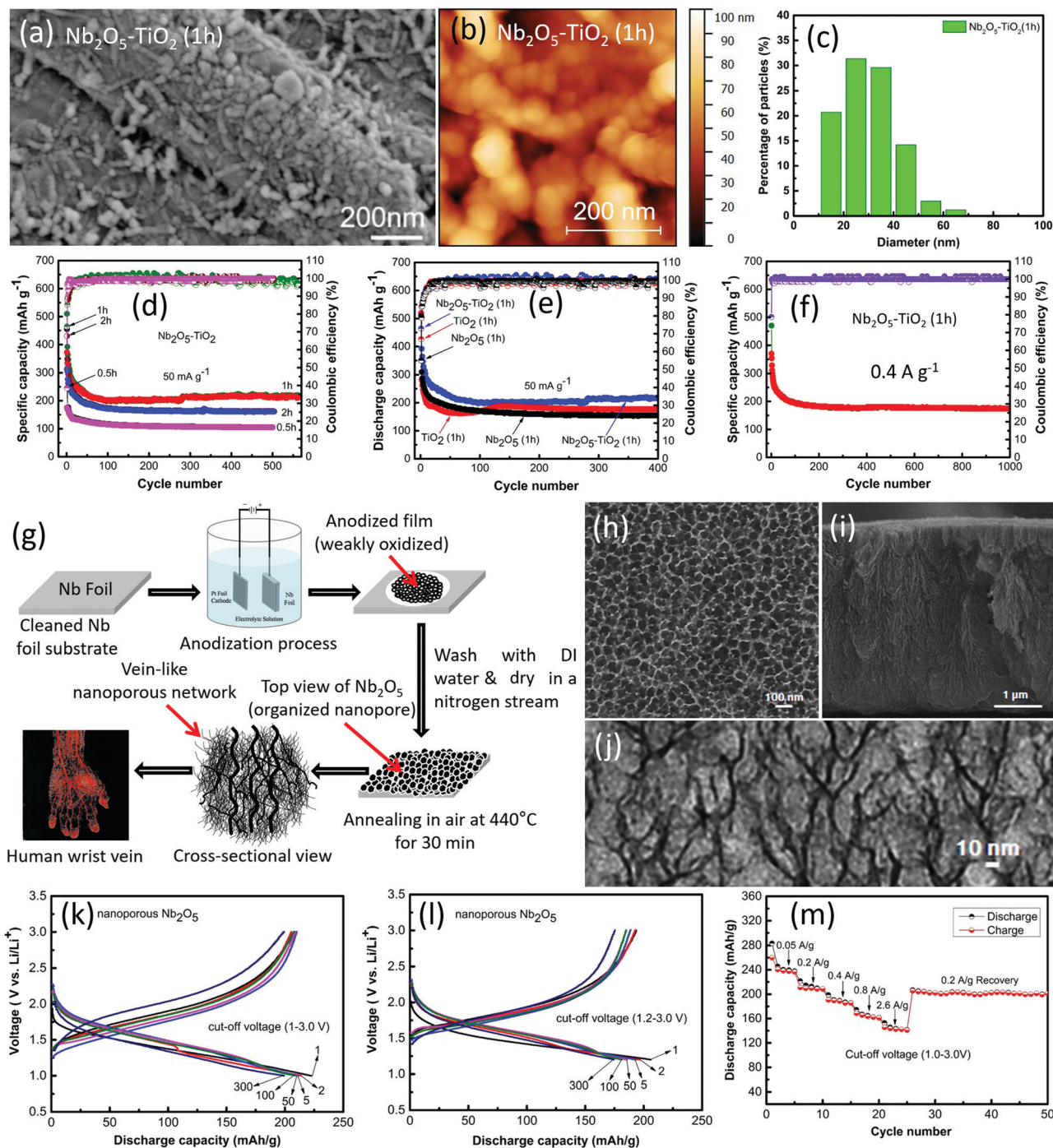


Fig. 7 (a–f) Characterization of additive-free electrode films of $\text{Nb}_2\text{O}_5\text{-TiO}_2$, Nb_2O_5 , and TiO_2 fabricated with different deposition time durations of 0.5, 1.0, and 1.0 h, respectively¹¹¹ (reproduced with permission, Copyright 1969, John Wiley and Sons); (a–c) SEM image, AFM topography image, and particle size distribution of the $\text{Nb}_2\text{O}_5\text{-TiO}_2$ electrode film fabricated with 1.0 h deposition time; and (d–f) electrochemical performance of the electrodes. (g–m) Characterization of nanoporous Nb_2O_5 ¹¹⁹ (adapted with copyright permission, The Royal Society of Chemistry): (g) schematic of the nanoporous Nb_2O_5 preparation procedure; (h and i) SEM images of (h) top view, and (i) cross-sectional view of the entire nanoporous structure; (j) a TEM image of a cross-section of the nanoporous network; and (k–m) electrochemical performance.

Basically, unstable structure and limited electrochemical performance make cathode materials difficult to meet the requirement of practical application in SIBs. However, the requirements of stable cathodes with high sodium storage capacity and excellent cycling stability have facilitated the exploration of various

cathode materials (metal oxides, polyanionic compounds, Prussian blue analogs, and organic electrodes) for SIBs.^{124,125} Among various cathode systems, layered transition metal oxides and poly-anionic compounds are identified as suitable cathode hosts for LIBs and SIBs. Even though many important cathode

materials based on metal oxides or layered transition metal oxides and poly-anionic compounds have attracted attention for potential use, some challenges still exist with these cathodes; particularly their poor cycling stability and rate capability need to be overcome for their successful implementation. A number of strategies have been adopted to achieve high performance cathodes as summarised below.

3.1 Double carbon coating

The carbon coating strategy is widely considered for the construction of battery materials due to several advantages:^{126,127} (i) carbonaceous materials are available and cheap with excellent electronic conductivity; (ii) they are physically and chemically stable with high mechanical strength and structural flexibility, and are capable of acting as a buffer layer to protect active materials from fracture during reaction; and (iii) most importantly, carbonaceous materials with various allotropes and geometric structures are available to meet architectural requirements. Even though carbon coating improves electrochemical performance by increasing conductivity, buffering volume expansion and/or stabilizing the reaction interface, single carbon coating is unable to meet all the requirements in terms of conformal coverage of active materials and a continuous conductive network for the electrodes. As a result, single carbon-coated active materials themselves still suffer from inefficient electrical connections between particles, where a random and discontinuous electron-transport path leads to inadequate conductivity in the bulk electrodes, resulting in poor rate capability of the materials. To circumvent this problem, a dual carbonaceous coating strategy is proposed. In this section, we mainly focus on the development of polyanion compound cathodes through their rational design by adopting the double carbon coating strategy.

Polyanion compound cathodes. In 1997, Goodenough *et al.*¹²⁸ reported olivine LiMPO_4 ($M = \text{Mn, Fe, Co and Ni}$) with high thermal stability as a promising cathode family. Among them, olivine LiFePO_4 is the most competitive material for electric vehicle application and it has now been commercialized. Later on, a wide range of follow-up studies have been conducted to discover or improve LiMPO_4 based cathodes for different applications.¹²⁹ For instance, $\text{LiFe}_{1-x}\text{Mn}_x\text{PO}_4$ is being considered as a potential cathode for LIBs owing to its high theoretical capacity ($\sim 170 \text{ mA h g}^{-1}$) and high operating voltage of 3.5–4.1 V. However, low electronic and ionic conductivity with $\text{LiFe}_{1-x}\text{Mn}_x\text{PO}_4$ based cathodes leads to unsatisfactory electrochemical performance. To advance $\text{LiFe}_{1-x}\text{Mn}_x\text{PO}_4$ based cathodes, a more robust preparation strategy as well as structural design is required. In 2013, Liu *et al.*¹³⁰ fabricated spherical $\text{LiFe}_{0.6}\text{Mn}_{0.4}\text{PO}_4/\text{C}$ particles with much improved electrochemical performance by employing a double carbon coating process. However, the overall material preparation process was difficult to be scaled up for mass production. In this regard, we proposed a $\text{LiFe}_{0.4}\text{Mn}_{0.6}\text{PO}_4/\text{C}$ composite microstructure which was produced using a double carbon coating process by employing traditional industrial techniques (a combination of ball milling, spray drying and annealing) (Fig. 8a–g).¹³¹ The composite microspheres exhibited a reversible capacity of 152 mA h g^{-1} at 1C

after 500 cycles with excellent rate capabilities of 132, 103, and 72 mA h g^{-1} at 5, 10, and 20C, respectively (Fig. 8e–g). Such an excellent electrochemical performance is attributed to the micrometer-sized spheres of double carbon-coated $\text{LiFe}_{0.4}\text{Mn}_{0.6}\text{PO}_4$ nanoparticles with improved electric conductivity and higher Li ion diffusion coefficients, ensuring full redox reactions of all nanoparticles. The strategy of double carbon coating ensures that all particles get electrons from all directions and contribute to the charge–discharge process.

3.2 Entwining/anchoring nanoparticles with conductive networks

The strategy of entwining/anchoring of nanoparticles with conductive networks is widely considered to enhance the electrochemical performance of battery electrodes. To achieve high performance batteries, a smart electrode architecture with high electrical and thermal conductivity, an appropriate high specific surface area, as well as high thermal and chemical stability is required. To meet these requirements, both carbon nanotubes (CNTs) and graphene are widely considered for the fabrication of battery electrodes due to their multiple roles (such as conductive, active, flexible and supportive roles) at the same time.¹³² However, it is challenging to construct a superior electrode architecture by combining nanoparticles and conductive agents, particularly CNTs and graphene. In most cases, many particles/materials of the electrode are unable to participate in the charge–discharge process because they are segregated or isolated from the conductive networks, leading to poor cycling performance. It is thus required to develop effective fabrication techniques which are capable of entwining/anchoring of nanoparticles in graphene or CNT networks where both electron transfer and ion diffusion could occur simultaneously and most particles can contribute to the charge/discharge process. Development of various cathode materials, electrochemical performance, and entwining/anchoring fabrication techniques are discussed in this section.

Maricite NaFePO_4 cathodes. Olivine NaFePO_4 does not work in SIBs due to its non-reversible charge/discharge process. Additionally, the conventional synthesis process is unable to produce olivine NaFePO_4 .¹³³ Even though carbon coated maricite NaFePO_4 in the form of nanometre-sized particles exhibits reversible charge/discharge processes in SIBs,^{134,135} success is limited. An innovative approach of combination of a solid-state reaction and a ball milling technique was adopted to produce more reactive maricite NaFePO_4 nanoparticle entwined graphene sheets by dispersing the nanoparticles of NaFePO_4 in the *in situ* generated graphene sheets (Fig. 9a and b).¹³⁶ Entwining particles in a graphene network ensured both electron transfer and ion diffusion simultaneously and most particles contributed to the charge/discharge process. The obtained hybrid $\text{NaFePO}_4/\text{C}/\text{graphene}$ exhibited an outstanding cycling performance with a capacity of 142 mA h g^{-1} after 300 cycles (98% capacity retention) (Fig. 9c). The rate capabilities were also appealing with reversible capacities of 79 at 1, 67 at 3, and 51 mA h g^{-1} at 5C (Fig. 9d). This study demonstrates a significant advance in the field of NaFePO_4 based cathodes, which includes an industry acceptable synthesis method, a new robust electrode architecture, and a high performance cathode for SIBs.

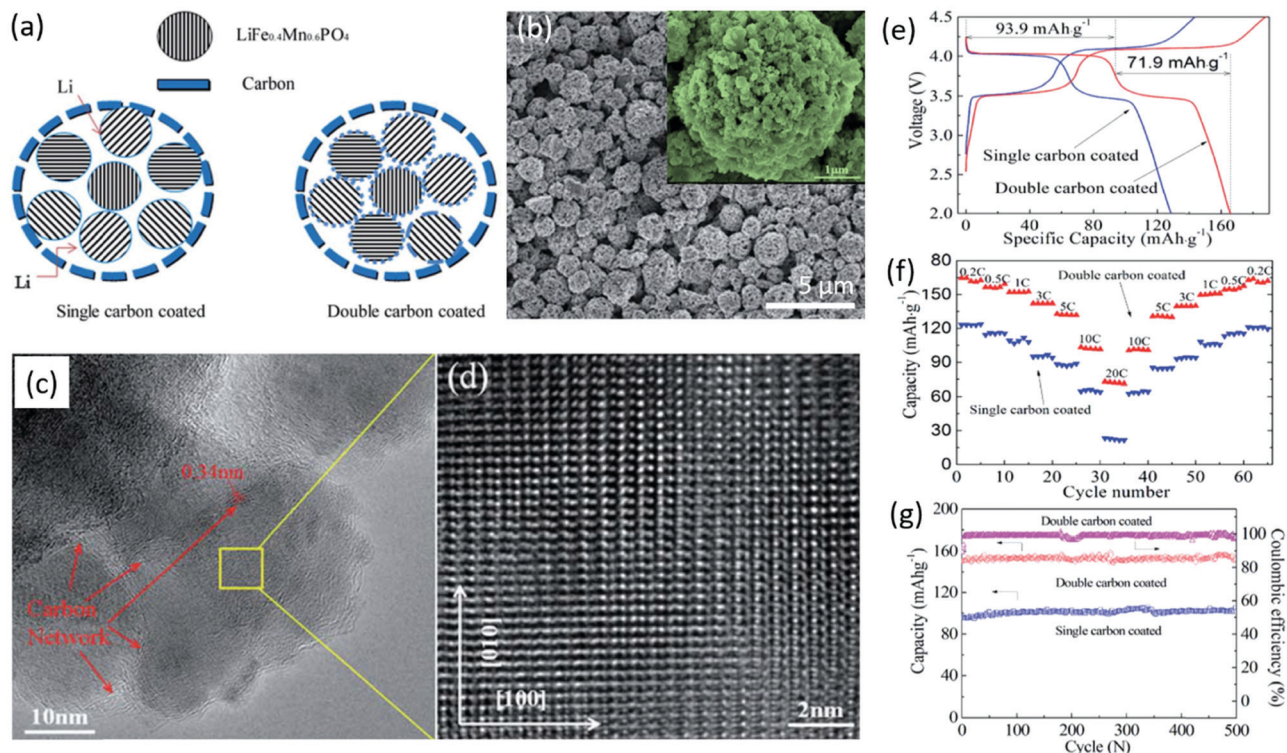


Fig. 8 (a–g) Characterization of the LiFe_{0.4}Mn_{0.6}PO₄ cathode for LIBs: (a) schematic structures of the single and double carbon coated LiFe_{0.4}Mn_{0.6}PO₄; (b–d) SEM and TEM images of the double carbon-coated LiFe_{0.4}Mn_{0.6}PO₄: (b) low and (inset) high-magnification SEM images, (c and d) typical TEM images of LiFe_{0.4}Mn_{0.6}PO₄/C particles containing several primary crystallites; and (e–g) comparison of electrochemical performance between the double and single carbon coated LiFe_{0.4}Mn_{0.6}PO₄.¹³¹ (Adapted with copyright permission, The Royal Society of Chemistry.)

Metal oxide cathodes. A metal oxide based alternative cathode of the α -LiFeO₂-multiwalled carbon nanotubes (MWCNTs) nanocomposite,¹³⁷ with a similar rock-salt structure to LiCoO₂, has been developed for LIBs due to its low cost, more environmentally benign nature and safety during operation. A significant improvement in the reversible capacity and rate capability of the α -LiFeO₂-MWCNTs cathode is realised due to the unique composite structure of MWCNTs with α -LiFeO₂ nanoparticle clusters achieved by combining a molten salt precipitation process and a radio frequency oxygen plasma (Fig. 9e–h). The α -LiFeO₂-MWCNTs nanocomposite can deliver a reversible capacity of 147 mA h g⁻¹ after 100 cycles at 1C, and exhibits an excellent rate capability with about 96% retention of its original initial capacity at a high current rate of 10C (2820 mA g⁻¹) (Fig. 9g and h). Both rate capability and cycling stability can be a result of introduction of the unique composite structure of clusters of α -LiFeO₂ nanoparticles integrated into the conductive network of MWCNTs. A nanocomposite of LiFeTiO₄-MWCNTs prepared by combination of low energy ball milling and annealing was also demonstrated as a novel cathode for LIBs (Fig. 9i–k). The composite shows a high capacity (105–120 mA h g⁻¹) at a slow current rate, and can operate at a relatively high current.¹³⁸ A simple wet ball-milling method was used to construct another hybrid cathode of V₂O₅/graphene for LIBs.¹³⁹ In this hybrid structure, nanometre-sized V₂O₅ particles/aggregates were well embedded and uniformly dispersed in the conductive networks of crumpled and flexible graphene sheets generated by *in situ*

conversion of bulk graphite during ball milling (Fig. 9l–n). The V₂O₅/graphene hybrid shows good cycling stability with a high discharge capacity of 185 mA h g⁻¹ at 1C (1C = 294 mA g⁻¹) after 100 cycles (Fig. 9m). Moreover, a huge improvement in rate performance, particularly at high rates (10C) (Fig. 9n), suggests that the *in situ* incorporation of graphene into V₂O₅ crystals not only tremendously increases the electronic conductivity (both interparticle and intra-particle conductivity) but also improves the ionic conductivity of the hybrid electrodes.

3.3 Surface nanocoating

The term nanocoating refers to nanoscale (thickness of a few tens to a few hundreds of nanometers) thin-films that are applied to surfaces to improve material's functionalities. Due to the significant benefits of nanocoating, this strategy is widely used in various industries. Among different strategies, the carbon-based coating technique is well-known in the battery industry; however, safety issues with carbon materials encourage to develop carbon-free coatings.¹⁴⁰ To achieve superior rate performance, high tap density, and surface stability of the electrode materials, the strategy of nanocoating is very popular and it is routinely used for the electrochemical improvement of nickel–manganese–cobalt (NMC) based Li-rich layered oxide cathodes in LIBs.^{141,142} However, the electrochemical performance of surface coated cathode materials is determined by qualities of the coated oxides in terms of thickness, conformity, uniformity, and integrity. In most cases, the resultant coating layers are often very thick and

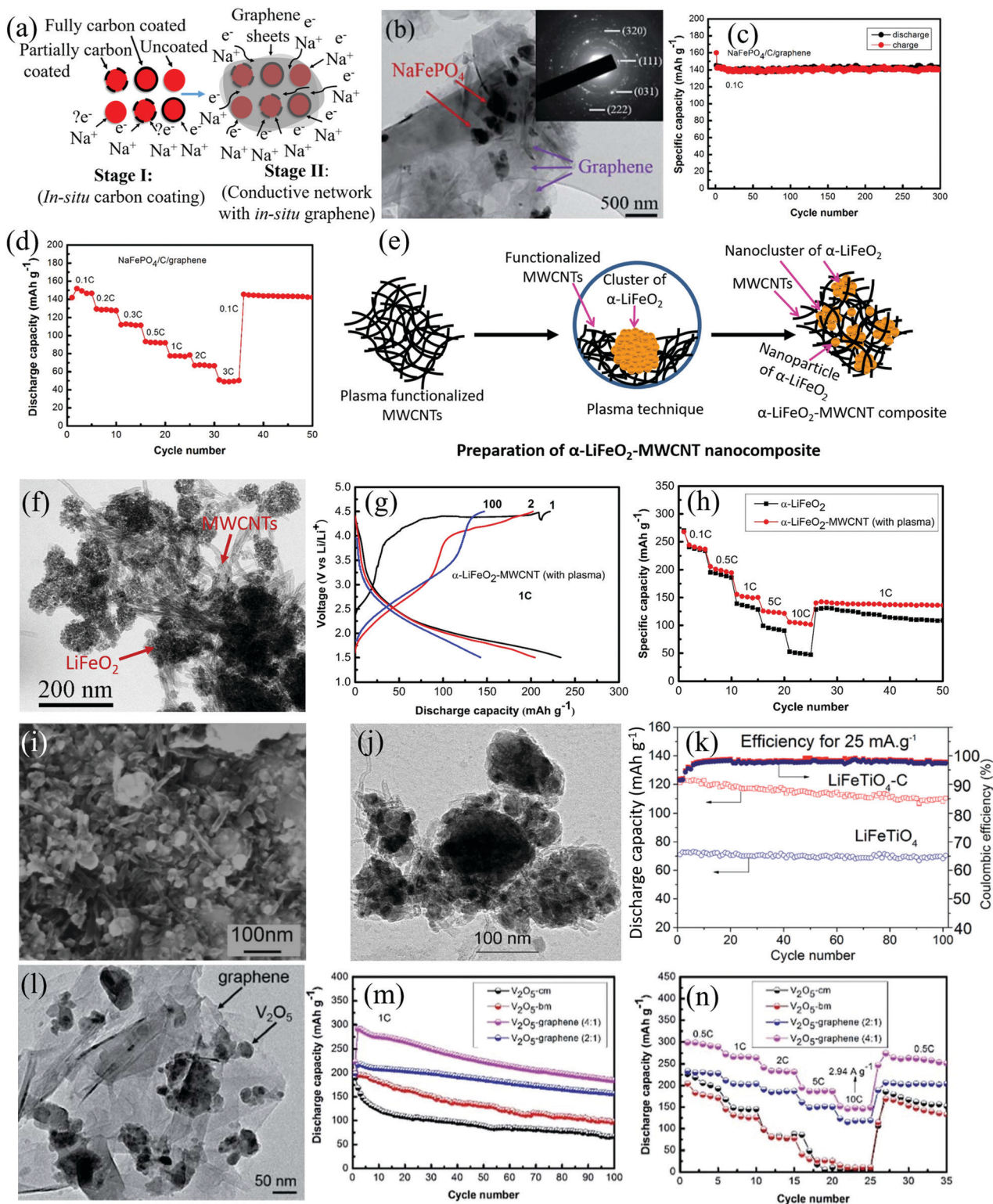


Fig. 9 (a–d) Characterization of the NaFePO₄/C/graphene cathode for SIBs¹³⁶ (adapted with copyright permission, The Royal Society of Chemistry): (a) schematic illustration of the electrode architecture; (b) TEM image; (c and d) electrochemical performance of (c) cycling at 0.1C (1C = 155 mA g⁻¹) up to 300 cycles and (d) rate capability; (e–h) characterization of α-LiFeO₂ and α-LiFeO₂-MWCNTs cathodes for LIBs¹³⁷ (adapted with copyright permission, The Royal Society of Chemistry): (e) schematic illustration of the preparation procedure of α-LiFeO₂-MWCNTs; (f) a bright-field TEM image; and (g and h) cycling performance; (i–k) characterization of the LiFeTiO₄-MWCNTs cathode for LIBs¹³⁸ (adapted with copyright permission, The Royal Society of Chemistry): (i and j) SEM and TEM images; and (k) cycling stability; (l–n) characterization of the V₂O₅/graphene cathode for LIBs¹³⁹ (adapted with copyright permission, The Royal Society of Chemistry): (l) a bright-field TEM image and (m and n) electrochemical performance of V₂O₅/graphene hybrids.

thereby impede the transport of lithium ions and electrons. In this section, we discuss the development of nickel–manganese–cobalt (NMC) based layered oxide cathodes by employing surface nanocoating with various materials.

Nickel–manganese–cobalt (NMC) based layered cathodes. Layered transition metal oxide electrodes, particularly nickel–manganese–cobalt (NMC) based electrodes, are considered the most promising candidates for metal-ion batteries.^{143,144} However, the NMC based cathodes suffer from sluggish diffusion of ions and electron transfer, which results in a rapid capacity decay and inferior rate capability. Among them, nickel-rich cathodes, $\text{LiNi}_{1-x-y}\text{Mn}_x\text{Co}_y\text{O}_2$ ($0 \leq x + y \leq 0.5$), have been one of the most important cathodes for next generation LIBs due to their high reversible capacity of about 200 mA h g^{-1} , excellent capacity retention, low cost and high working voltage, as compared with LiCoO_2 . Basically $\text{LiNi}_{1-x-y}\text{Mn}_x\text{Co}_y\text{O}_2$ systems face two major obstacles: (i) poor capacity retention and (ii) poor thermal stability. The undesirable side reactions between the transition metal ions, in particular Ni^{4+} , and the electrolyte and the phase

transition from the layered to the rock-salt structure on the particles' surfaces cause a decline in the lithiation kinetics at the electrode–electrolyte interfaces, leading to poor capacity retention.^{145,146} On the other hand, a highly de-lithiated state releases oxygen from the lattice structure which is responsible for poor thermal stability.^{147,148} De-lithiated nickel-rich cathodes are highly reactive with organic electrolytes because of a substantial overlap between the 3d band of Ni and the 2p band of oxygen.

Surface nanocoatings have been considered to lower the electrochemically reactive surface with improved cycle life. To enhance the capacity retention and thermal stability of Ni-rich layer structured cathodes, a surface nanocoating with metal oxides, such as SiO_2 ,¹⁴⁹ ZrO_2 ,¹⁵⁰ and antimony,¹⁵¹ is developed (Fig. 10a–i). These surface coatings suppress the side reaction in the interface between electrolyte and electrode, reduce the transition-metal dissolution, and hinder the decomposition of the electrolyte, leading to improved electrochemical performance. It is obvious that the rate performances of the ZrO_2 -modified (Fig. 10f) and antimony doped tin oxide (ATO) (Fig. 10i) coated samples are

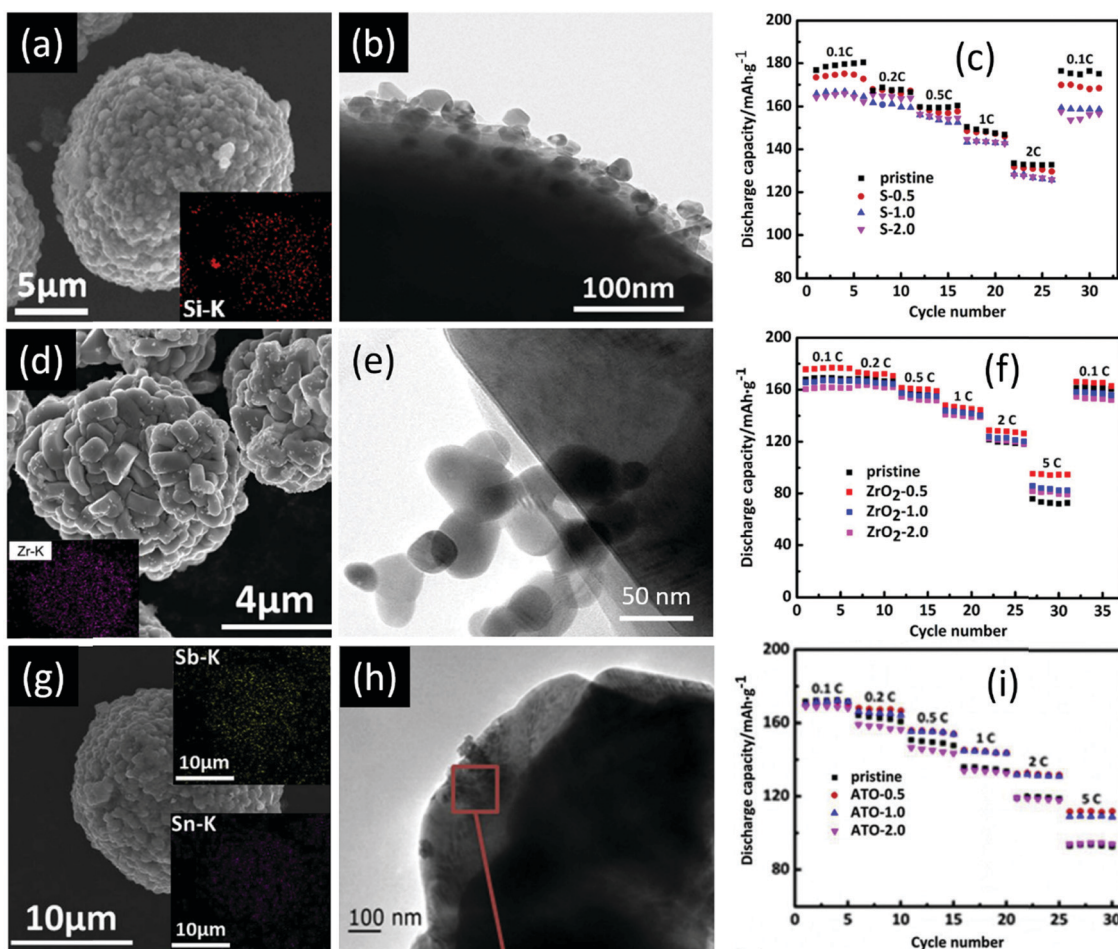


Fig. 10 (a–c) Characterization of the 0.5 wt% SiO_2 -coated $\text{LiNi}_{0.5}\text{Co}_{0.2}\text{Mn}_{0.3}\text{O}_2$ microsphere cathode¹⁴⁹ (reproduced with permission, Copyright 2017, Elsevier): (a) SEM image and corresponding Si map (inset); (b) a bright-field TEM image; and (c) rate capability at different current rates; (d–f) characterization of the 0.5 wt% ZrO_2 modified $\text{LiNi}_{0.6}\text{Co}_{0.2}\text{Mn}_{0.2}\text{O}_2$ cathode¹⁵⁰ (reproduced with permission, Copyright 2017, Elsevier): (d) SEM image and corresponding EDS mapping of Zr (inset); (e) TEM image; and (f) rate capability at different current rates; (g–i) characterization of the 0.5 wt% antimony doped tin oxide (ATO)-coated $\text{LiNi}_{0.5}\text{Co}_{0.2}\text{Mn}_{0.3}\text{O}_2$ cathode¹⁵¹ (reproduced with permission, Copyright 2018, Elsevier): (g) SEM image and corresponding EDS mappings of Sn and Sb elements; (h) HRTEM image; and (i) rate capability at different current rates.

better than that of the pristine materials. However, the electrochemical performance of the cathodes could be very sensitive to the amount of coating materials. An excess amount (2.0 wt%) of ZrO₂ and ATO has a negative effect on the improvement of rate capability. On the other hand, the rate performance of the pristine material is better than that of the SiO₂-coated sample (Fig. 10c). The poor rate capability of the SiO₂-coated sample could be ascribed to the bad electrical conductivity of excess SiO₂, because the low ion and electron conductivity of SiO₂ results in a high interfacial resistance between the cathode and the electrolyte.¹⁵² This observation reveals that an appropriate amount of coating plays a critical role in the electrical conductivity of the LiNi_{1-x-y}Mn_xCo_yO₂ cathodes during cycling which affects electrochemical performance.

4. Nanostructured alloy anodes for PIBs

Despite the exceptionally valuable features of the PIBs, the device faces two major barriers: (i) achieving a stable cycle life with high reversible capacity of electrode hosts (anode and cathode), and (ii) achieving sufficiently high energy density of a full-cell. All of these barriers are related to the heavier and larger size of K⁺ ions (1.38 Å),¹⁹⁻²¹ which causes a greater change in the electrode host structure and damage upon extraction/insertion of the ions, leading to a poorer cycle life and lower capacity. Although conversion/alloying reaction based anodes show high potential in these new-generation large-scale energy storage applications, the main challenge with conversion/alloying-based anodes in PIBs is to buffer the unavoidable volume expansion and maintain the structural integrity during the repeated insertion and extraction of K⁺ ions.^{153,154} Among various PIB anodes, antimony (Sb)-based anodes including pure Sb and its composites, Sb-based alloys, Sb-oxides and Sb-selenides have attracted much attention.^{153,154}

Recently, Wang *et al.*¹⁵⁴ have developed a superior stable antimony selenide (Sb₂Se₃) based anode by adopting a combined strategy of conductive encapsulation and 2D confinement. The obtained N-doped carbon encapsulated and graphene oxide (rGO) confined Sb₂Se₃ nanorod composites (Sb₂Se₃@NC@rGO) exhibited significantly improved reversible capacity (~590 mA h g⁻¹) and outstanding cycling stability over 350 cycles, demonstrating a significant advance in the field of research. Besides, we have also developed a series of alloy-based anode materials such as tin (Sn), phosphorus (P), antimony (Sb) and silicon for PIBs, which are summarized and discussed in this section.

4.1 Construction of alloy electrodes

Tin (Sn) based composites. As an anode, pure tin (Sn) shows unsatisfactory electrochemical performance in LIBs and SIBs because of mechanical degradation of the electrodes caused by large volume variation during the cycling process (~420% in sodium cells and ~260% in lithium cells).¹⁵⁵ To make this material viable, an approach of composite formation with the carbon matrix is widely demonstrated where fine nanoparticles of Sn are dispersed/embedded in a carbon matrix. This strategy

is quite successful to prevent mechanical degradation of the electrodes because of the advantages of nanometre dimensions of tin for controlling mechanical strain.¹⁵⁶⁻¹⁵⁸ The same strategy was adopted and the composite of Sn-C was produced and reported for the first time as the PIB anode.¹⁵⁹ The Sn-C composite was prepared by mixing tin and graphite powders in the weight ratio of 7 : 3 and nanoparticles of Sn were distributed in the carbon component (Fig. 11a and b). Even though the tin-graphite (Sn-C) composite electrode exhibited a reversible capacity of 150–170 mA h g⁻¹ in the first few cycles, capacity contribution from graphite was significant but slightly lower than that of the composite (Fig. 11d). This study also demonstrated a storage mechanism of the reversible alloy-de-alloying process in the Sn-C electrode (Fig. 11e and f). In the study of *ex situ* XRD, K₄Sn₂₃ and K₂Sn₅ phases were detected in the first discharge but the final phase of the alloying process was not detected. However, during charging, the diffraction peak of Sn re-appeared confirming that Sn is capable of alloying and de-alloying with potassium in a reversible manner. Later on, follow-up studies have been conducted on Sn electrodes in potassium-cells and a final potassiation phase of KSn has been suggested.¹⁶⁰⁻¹⁶² This study certainly underpins the importance of developing tin-based electrodes further. Another anode of the tin sulfide-reduced graphene oxide (SnS₂-rGO) composite in potassium cells is also reported for the first time (Fig. 11g-j).¹⁶³ In this composite, nanocrystalline SnS₂ was dispersed on sheets of reduced graphene oxide (rGO) produced *via* a chemical route. An impressive capacity of 350 mA h g⁻¹ was achieved, exceeding the capacity of graphite. A high capacity of above 250 mA h g⁻¹ was retained for the first 30 cycles but capacity decay was observed afterwards. This study discloses a new type of tin-sulfide anode for PIBs and stimulates the development of non-graphitic anode materials.

Antimony (Sb) based composites. Antimony (Sb) has been considered as a well-known alloy anode for both LIBs and SIBs because of its high theoretical capacity of 660 mA h g⁻¹ due to the formation of Li₃Sb and Na₃Sb alloys, respectively.¹⁶⁴⁻¹⁶⁶ In 2015, McCulloch *et al.*¹⁶⁷ first reported an antimony-carbon anode for PIBs with a capacity of 600 mA h g⁻¹ after 10 cycles, corresponding to a final alloy phase of K₃Sb. A steady capacity of 250 mA h g⁻¹ with 98% coulombic efficiency has been observed for 50 cycles when restricted cyclic conditions were applied. The capacity fall and the impairment of cyclic stability seem to be distinctive phenomena in Sb-C electrodes in potassium half-cells, which differ drastically from lithium and sodium half-cells of the same electrode material. To gain insight into the failure mechanism in electrodes and possible avenues to improve cyclic stability, a comprehensive examination of the Sb-C electrodes prepared from different amounts of graphite with varied Sb particle size has been carried out (Fig. 12a-f).¹⁶⁸ It is observed that abrupt capacity decay in the cycling experiments is sensitive to the Sb particle size and graphite content. The *ex situ* investigation of the electrodes and separators extracted from the cycled cells suggests that mechanical degradation of the electrodes is likely to be the dominant cause of the capacity fall. For achieving improved cycling stability,

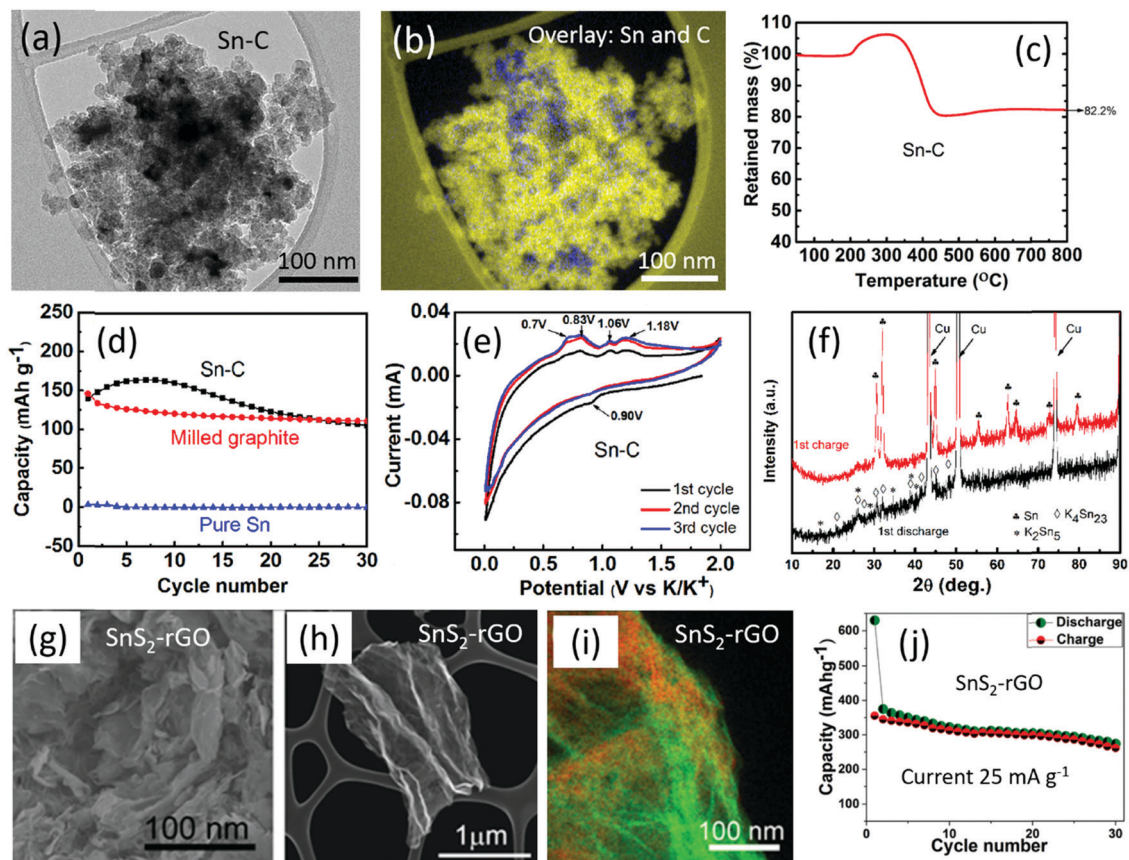


Fig. 11 (a–f) Characterization of the Sn–C anode for PIBs¹⁵⁹ (adapted with copyright permission, The Royal Society of Chemistry): (a and b) bright-field TEM image and an energy-filtered image with an elemental contrast (color scheme: C – yellow; Sn – blue); (c) thermogravimetric curve; and (d–f) electrochemical analysis of (d) cycling performance at a current rate of 25 mA g⁻¹ within the potential window of 2.00–0.01 V vs. K/K⁺; (e) cyclic voltammogram; and (f) *ex situ* XRD patterns after the first discharge and the first charge in potassium half-cells of the Sn–C anode. (g–j) Characterization of the SnS₂–rGO composite anode for PIBs¹⁶³ (adapted with copyright permission, The Royal Society of Chemistry): (g) SEM image of an area in the sample; (h) SEM image of an individual SnS₂-coated sheet of rGO; (i) energy-filtered TEM image (color scheme: red – sulfur, green – carbon); and (j) cycling stability at 25 mA g⁻¹ of the SnS₂–rGO composite.

three possible strategies (such as the use of an electrolyte additive, changing the binder type used and the addition of an extra alloying element to composites) are proposed. The strategy of replacement of the standard electrode binder (CMC) with gum arabic, substituting a certain fraction of Sb with another high capacity alloying component, black phosphorus (P), and incorporation of an electrolyte additive (FEC) is capable of enhancing the cyclability of the Sb based anodes in potassium cells. The new composite of Sb–P–C coupled with an alternative binder (gum arabic) appears to be more effective in improving the cyclic stability with a retained capacity of above 400 mA h g⁻¹ in the first 50 cycles (Fig. 12g–i).¹⁶⁸ These results demonstrate a significant advance in the field of Sb based anodes for PIBs.

Phosphorus (P) based composites. Zhang *et al.*¹⁶⁹ have recently reported red phosphorus-based anodes for PIBs with a demonstrated capacity higher than that of graphitic materials. In their study, the authors suggested a three-electron charge storage mechanism with the formation of a K_{3-x} P-type alloy, which is similar to the reaction mechanisms known in lithium and sodium cells. It was concluded that pure phosphorus-based electrodes are not suitable because of unstable cyclic behaviour.

They suggested Sn₄P₃ alloy materials as a substitute. Later on, an alternative type of anode based on black phosphorus encapsulated in a carbon matrix was developed by our group.¹⁷⁰ Two phosphorus–carbon composite samples (weight ratios of 7 : 3 and 1 : 1) were prepared by mechanical milling of mixtures of black phosphorus and graphite powders. The typical morphology of a phosphorus–carbon nanocomposite and an excellent degree of mixing were observed (Fig. 13a). The stable electrochemical performance of black phosphorus–carbon (BP–C 1 : 1) was evaluated and a high reversible capacity of 617 mA h g⁻¹ was measured in the first cycle for the BP–C 7 : 3 sample, indicating the maximal level of reversible capacity that can be achieved for the material in a potassium cell (Fig. 13d). The *ex situ* XRD analysis of the potassiation products in the electrodes suggests that the mechanism in the electrodes is electrochemical alloying of phosphorus with potassium to form a KP alloy, leading to a theoretical capacity of 843 mA h g⁻¹ for phosphorus (Fig. 13f). This investigation certainly reinforces the importance of developing phosphorus-based electrodes for PIBs further. As follow-up studies, several groups have demonstrated phosphorus based electrodes in potassium cells.^{171,172}

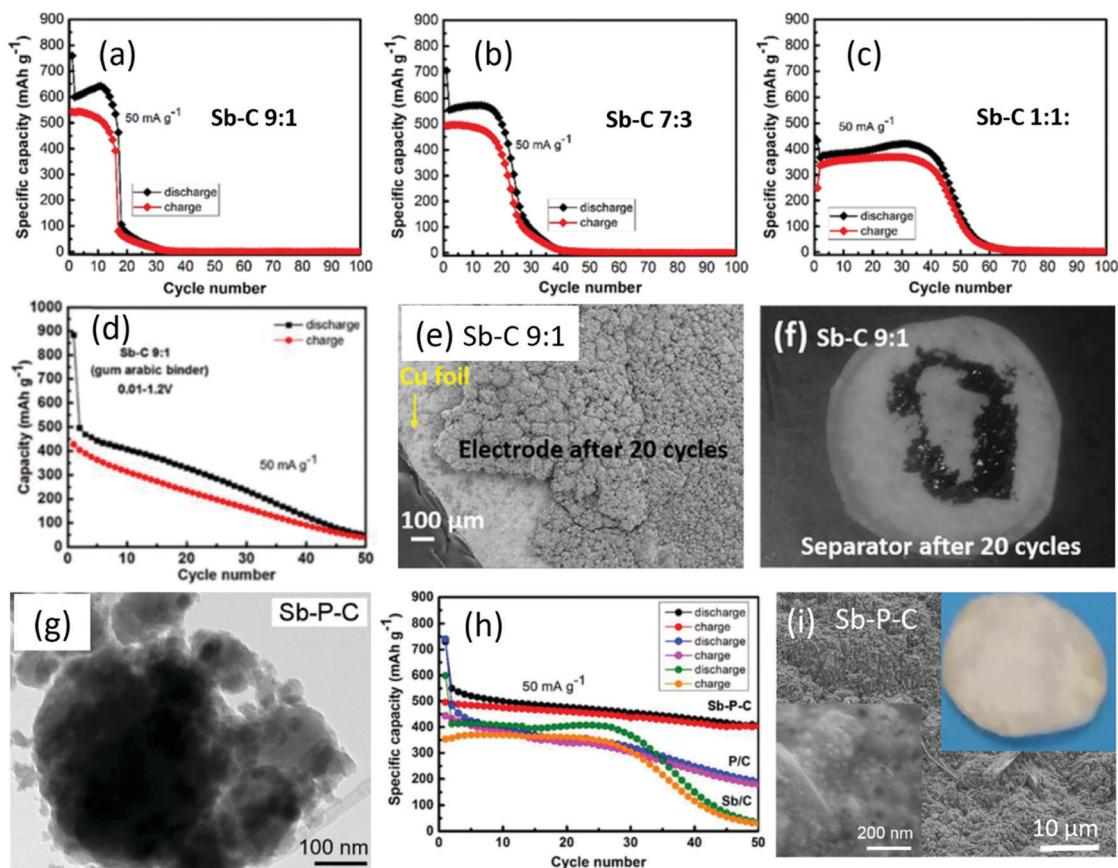


Fig. 12 (a–f) Characterization of Sb–C anode electrodes for PIBs¹⁶⁸ (reproduced with permission, Copyright 2019, Elsevier): (a–c) cycling stability of the electrodes with the CMC binder; (d) cycling stability of the Sb–C 9 : 1 electrode with the gum arabic binder; and (e and f) SEM image of the Sb–C 9 : 1 electrode after twenty galvanostatic discharge–charge cycles and corresponding digital photograph of the separator extracted from the same cell. (g–i) Characterization of Sb–P–C anode electrodes for PIBs: (g) a bright-field TEM image; (h) cycling stability at 50 mA g^{−1} with the gum arabic binder up to 50 cycles; and (i) SEM image of the Sb–P–C electrode extracted from the potassium cell after 50 cycles (the inset in top right corner shows the digital photograph of the separator extracted from the same cell after 50 cycles).

Silicon based composites. Among various alloy materials, silicon is the most attractive anode for LIBs because of its high theoretical capacity (silicon produces Li_{4.4}Si alloy with lithium, which is corresponding to the capacity of 4200 mA h g^{−1}), low cost, abundance, and environmental friendliness.^{173,174} Inspired by the attractive alloying properties of silicon with lithium, we have investigated the alloying properties of silicon with potassium for the first time.¹⁷⁵ As silicon experiences significant volume variations during alloying with lithium, a composite structure of Si/graphene was constructed where micrometre-sized aggregates consisting of Si nanoparticles and graphene were observed (Fig. 14a). The Si/graphene electrode was tested in potassium-ion cells; however, no alloying–de-alloying electrochemistry was observed in this study as evidenced by the triangular shape of the charge–discharge profile of the Si–graphene electrode (Fig. 14c). The Si/graphene electrode displayed a capacity around 100 mA h g^{−1} in the course of 50 cycles in which the most capacity contribution came from graphene whereas silicon seemed to be inactive (Fig. 14d and e). The *ex situ* XRD of the electrode after the first discharge and charge further confirmed that Si remains inert towards the alloying process with potassium (Fig. 14f).

In this experiment, it is concluded that the formation of the reactive structure of silicon with potassium is challenging, although Si can theoretically alloy with potassium to form a KSi phase with a capacity of 955 mA h g^{−1}.¹⁷⁶

5. Electrodes for Li–S batteries

The lithium–sulfur (Li–S) battery comprises of a lithium metal anode and a sulfur cathode. In a typical Li–S battery (Fig. 15a),^{177–179} the elemental sulfur (S₈) is gradually reduced during the discharge process and forms a wide range of long-chain lithium polysulfides (Li₂S₈ and Li₂S₆), short-chain lithium polysulfides (Li₂S₄ and Li₂S₂), and finally lithium sulfide (Li₂S). On the other hand, the charge process takes reversibly from Li₂S to S₈. The intermediate polysulfide products formed during the discharge process are soluble in common electrolyte solvents, and they migrate through the separator from the cathode to the anode and irreversibly deposit on the surface of the Li anode, causing the shuttle effect (Fig. 15a and c). Basically, redox reactions between solid-state S and Li₂S occur stepwise, causing several

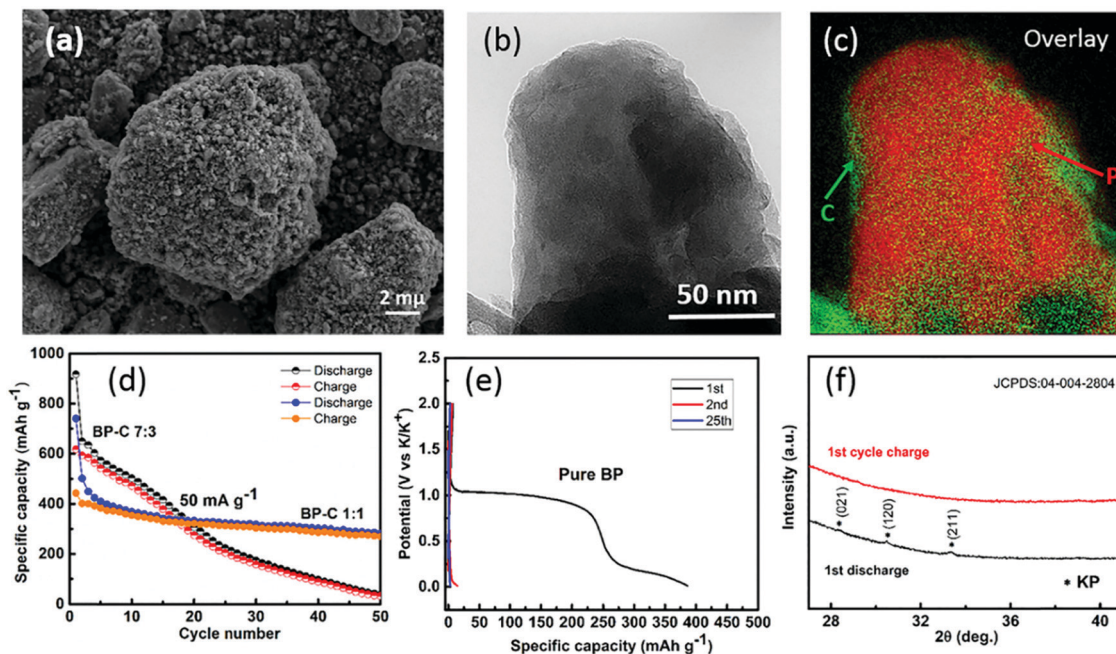


Fig. 13 (a) SEM image of the typical appearance of a phosphorus-carbon nanocomposite material; (b) an elastic TEM image of a black phosphorus-carbon nanocomposite (BP-C 1:1); (c) an overlay of energy-filtered three window maps (color scheme: red – phosphorus, green – carbon); (d) cyclic stability of the two samples (BP-C 7:3 and BP-C 1:1); (e) charge-discharge profiles of pure black phosphorus; and (f) *ex situ* XRD pattern of the BP-C 1:1 electrode after the first discharge and the first charge.¹⁷⁰ (Adapted with copyright permission, The Royal Society of Chemistry.)

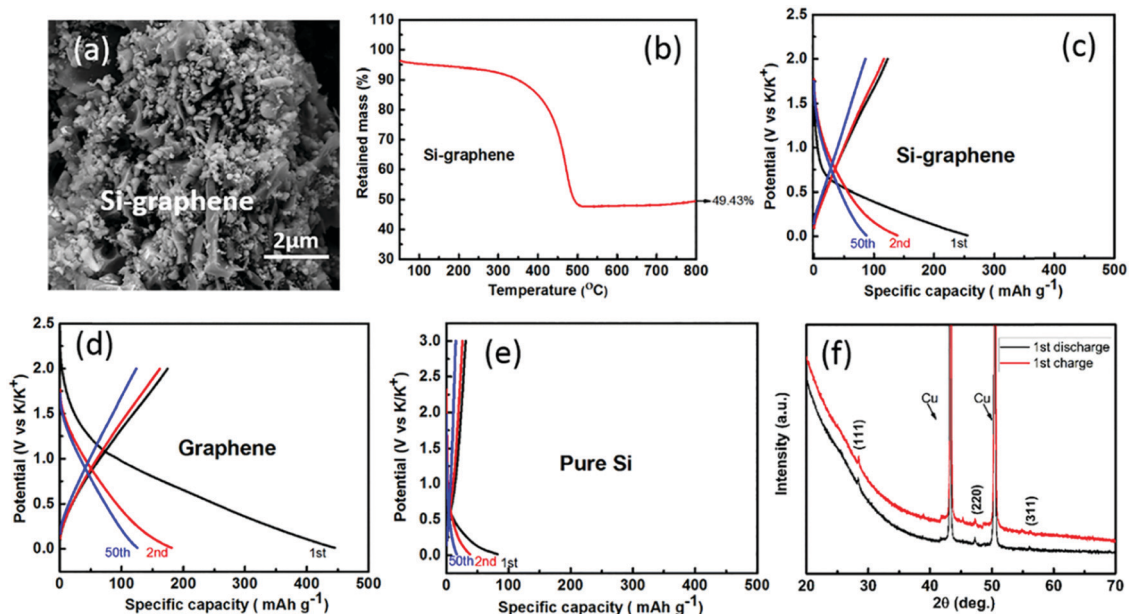


Fig. 14 Characterization of Si/graphene, pure silicon, and graphene electrodes: (a and b) SEM image and TGA analysis of the Si-graphene material; (c–e) electrochemical behavior of Si/graphene, graphene and pure silicon electrodes in potassium cells; and (f) *ex situ* XRD patterns of Si/graphene electrodes after the first discharge and the first charge in a potassium half-cell.¹⁷⁵ (Reproduced with permission, Copyright 1969, John Wiley and Sons.)

compositional and structural transformations as demonstrated in Fig. 15b.¹⁸⁰ Step I. During the initial discharge, a plateau at ~ 2.4 V is observed which represents the two-phase reaction from solid S_8 to liquid long-chain lithium polysulfides (LiPSs) (Li_2S_x , $6 < x \leq 8$). Step II. A pronounced slope is observed just below ~ 2.4 V, suggesting single-phase reaction and the

formation of liquid short chain LiPSs (Li_2S_x , $2 < x \leq 6$). As a result, both steps (step I and step II) deliver 0.5 electrons transfer per S, which corresponds to 25% theoretical capacity.¹⁸¹ Step III. A typical low discharge very long plateau at around 2.1 V is observed, confirming two-phase transition from short-chain LiPSs to solid Li_2S_2 . Step IV. A single-phase

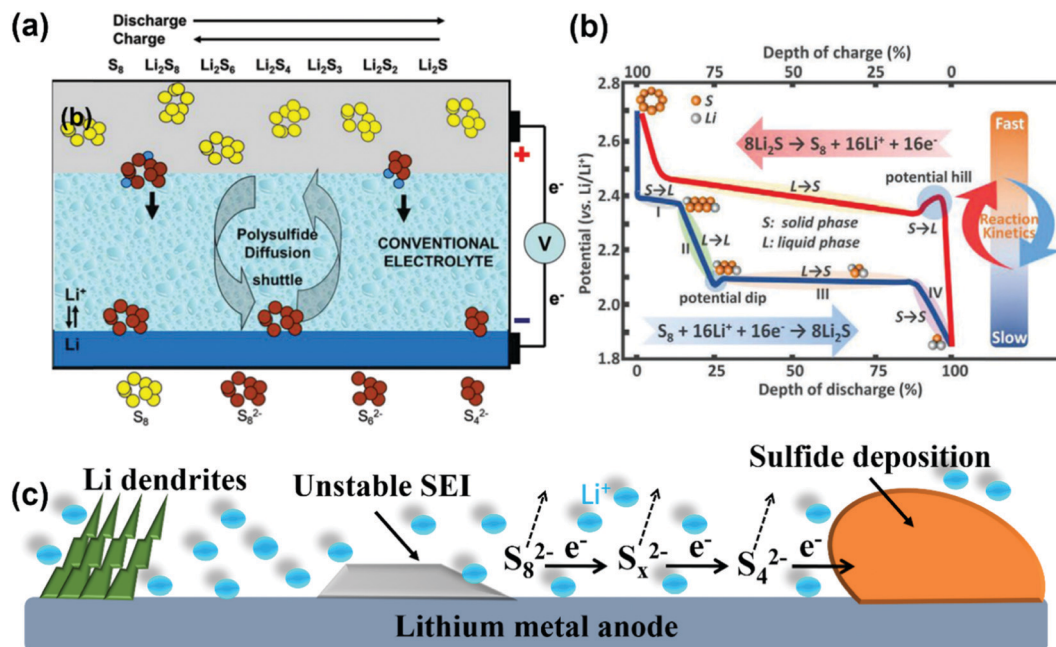


Fig. 15 Schematic illustrations of the Li-S system: (a) shuttle effect¹⁷⁸ (reproduced with permission, Copyright 2013, John Wiley and Sons), (b) discharge/charge profiles and corresponding products of the sulfur cathode¹⁸⁰ (reproduced with permission, Copyright 2020, John Wiley and Sons), and (c) challenges with the lithium metal anode.

transition from Li_2S_2 to solid Li_2S is observed at the end of the final slope. However, a potential dip is seen at the beginning of the second plateau which is ascribed to the concentration polarization. As a result, Li^+ transport is delayed due to the increased electrolyte viscosity where overpotential is required for the crystallization of insulating Li_2S_2 .^{182,183} Overall, both steps III and IV contribute 75% of theoretical capacity through 1.5 electrons transfer per S in the liquid–solid transition.¹⁸⁴ On the other hand, a potential hill is also observed during the initial charging which is related to the phase nucleation of $\text{Li}_2\text{S}_2/\text{Li}_2\text{S}$ (Fig. 15b). Such a potential hill displays a sluggish oxidation process of $\text{Li}_2\text{S}_2/\text{Li}_2\text{S}$ as well as low S utilization.¹⁸⁵ Additionally, $\text{Li}_2\text{S}/\text{Li}_2\text{S}_2$ is deposited on the cathode surface which hinders access of both electrons and Li^+ , leading to difficulties for the final products to completely convert back to S. Therefore, the obtained practical charge capacity of the Li-S battery is lower than the theoretical value.¹⁸⁶ At the same time, the lithium metal anode also faces many problems as shown in Fig. 15c. As a result, the device faces several problems, particularly low sulfur utilization in the cathode and unstable SEI layer/dendrite formation on the surface of the electrode leading to severe capacity fading and a low Coulombic efficiency, which hinder the real application of Li-S batteries.^{187,188} To overcome these inherent limitations of Li-S systems, many strategies including novel cell configurations, rational design of sulfur cathodes, and incorporation of the protective layers on the surface of the lithium metal have been proposed.

5.1 Rational design of sulfur cathodes

Significant materials have been identified as potential sulfur hosts, which led to the development of a wide range of

nanostructured sulfur cathodes. Nanostructured sulfur cathodes can be divided into several categories depending on the composition and structure of the electrodes,^{189,190} including (i) nanoporous carbon–sulfur composites, (ii) graphene–sulfur composites, (iii) one dimensional (1D) carbon–sulfur composites, (iv) conductive polymer–sulfur composites, (v) porous oxide additives, and (vi) nanostructured Li_2S cathodes. Even though the first three categories use carbon as a conductive pathway and as a matrix to trap polysulfides, different carbon structures have their own advantages and limitations. Among all the host materials, carbon-based materials are widely investigated as their structures and properties can readily be tailored for specifically addressing the issues of sulfur cathodes in Li-S batteries.

Carbon–sulfur based cathodes. Most of the traditional approaches for the preparation of sulfur electrodes involve physical mixing of sulfur with conductors such as super P or carbon black and binders. No matter which method is used for the preparation of sulfur cathodes, selection of carbon materials (both conductor and sulfur loading carbon) and proper design of the cathode architecture need to be considered to achieve an appropriate interface between electrode and electrolyte to ensure maximum utilization of sulfur. In this respect, the electrode architecture should be intertwined with stable three phase networks of $e^-/\text{S}_8/\text{Li}^+$ where lithium ions and electrons can smoothly contact with sulfur and react easily, ensuring maximum utilization of sulfur. Therefore, high sulfur loading or sulfur host materials with a high content of sulfur, good conductivity and structural stability are very important to fabricate carbon based robust sulfur composite cathodes for the development of high-performance Li-S batteries.

To physically trap the soluble lithium polysulfides, carbons with various pore structures and morphologies including microporous

carbon spheres/sheets, mesoporous carbon nanoparticles, hierarchical porous carbon nanotubes, and 3D (three-dimensional) carbon nanostructures have been developed.^{191–194} Macropores and mesopores with large pore volumes are expected to host a high content of sulfur; however, they are less effective to trap polysulfides due to their much larger pore size. Moreover, microporous carbon negatively influences the battery performance because of the very small pore volume (typically lower than $1 \text{ cm}^3 \text{ g}^{-1}$), which could only host a small fraction of sulfur in its pores. As a result, conventional microporous carbons are practically useless for real applications in Li–S batteries. To solve some of these key issues, a yolk–shell carbon nanosphere (denoted as YSCN) with a microporous shell, a mesoporous core, and a large void between them is proposed as an effective sulfur host structure prepared by a modified Stöber coating method (Fig. 16a).¹⁹⁵ Such a robust electrode architecture gives a number of advantages over the conventional structure such as (i) connection between yolk and shell fundamentally eliminates the poor electron transfer problem, which occurs in all hollow structure hosts because of the gap formation between hollow host and polysulfide in the long-term cycles; (ii) the yolk-supported shell can provide a more robust physical architecture to deal with the sulfur volume expansion problem; (iii) both yolk and shell effectively block soluble lithium polysulfides; and (iv) both sulfur storage and utilization are improved significantly. These advantages result in a stable and increased reversible capacity as well as an improved rate capability. This yolk–shell carbon

nanosphere can provide effective barriers to prevent the shuttle effect by confining small sulfur molecule allotropes in both porous yolk and shell. A high sulfur loading of 76 wt% with a high initial capacity of 1106 mA h g^{-1} is achieved. The electrode exhibits commendable rate capability with a capacity of about 400 mA h g^{-1} at 2C (Fig. 16e). Besides, when cycled at a high rate of 0.5C, the material still maintains a capacity of 337 mA h g^{-1} with a very small capacity decay as low as 0.05% per cycle up to 1000 cycles (Fig. 16f).

5.2 Fabrication of interlayers

Boron nitride–graphene based interlayer. An effective strategy of incorporation of an interlayer between sulfur cathode and separator has been proposed for the absorption of soluble polysulfides as well as reuse of the absorbed active material. Until now, a number of interlayers such as carbon paper,¹⁹⁶ carbon nanocube multilayered reservoirs,¹⁹⁷ carbon nanotube paper,¹⁹⁸ and an acetylene black mesh¹⁹⁹ have been developed. The major problems with all of these interlayers are their complex preparation procedure, weak interaction between interlayer and polar polysulfide anions, and unacceptable thickness with heavy mass of the interlayer, which affect battery performance significantly. Therefore, development of a lightweight interlayer that can not only increase the electric conductivity but can also alleviate polysulfide transport from the cathode to anode is a challenge. To decrease charge transfer resistance and alleviate polysulfide diffusion, a thin and selective

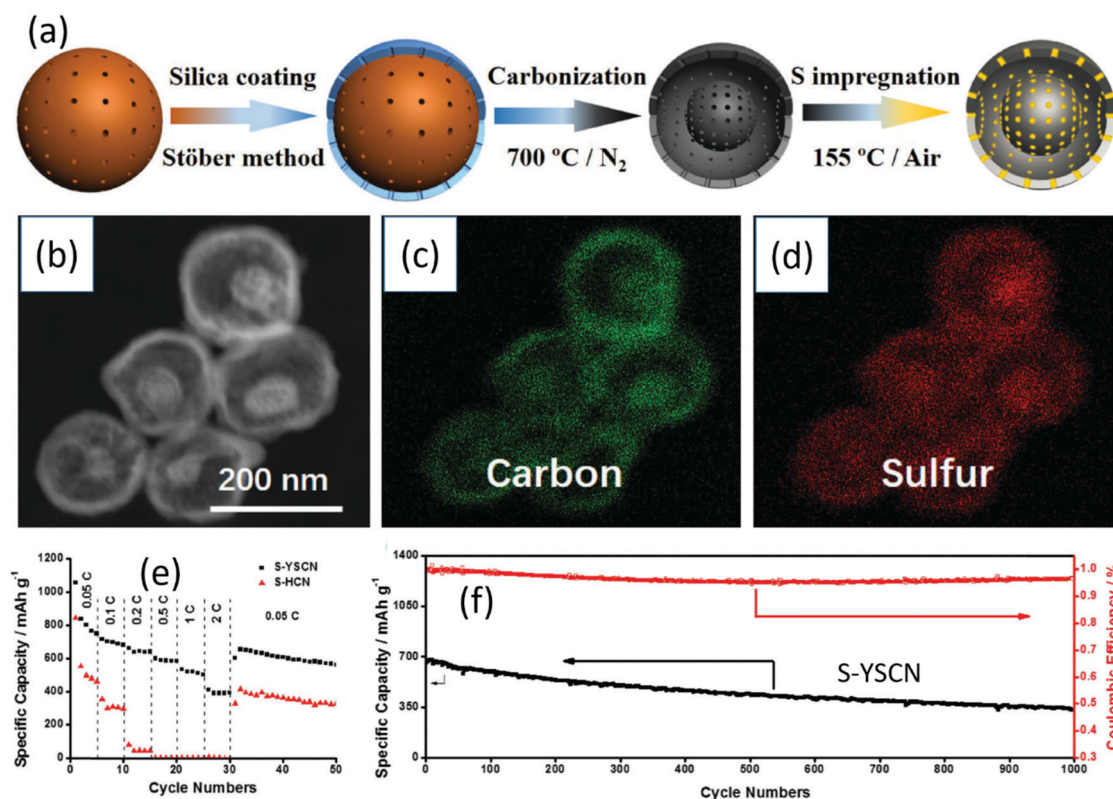


Fig. 16 (a) Schematic synthesis protocol of the yolk–shell carbon nanospheres (YSCNs) and the subsequent sulfur impregnation (S-YSCNs); (b) STEM image and (c and d) corresponding elemental distributions (areal); (e and f) electrochemical performance of (e) rate capability and (f) cyclic stability of the S-YSCN electrodes.¹⁹⁵ (Reproduced with permission, Copyright 1969, John Wiley and Sons.)

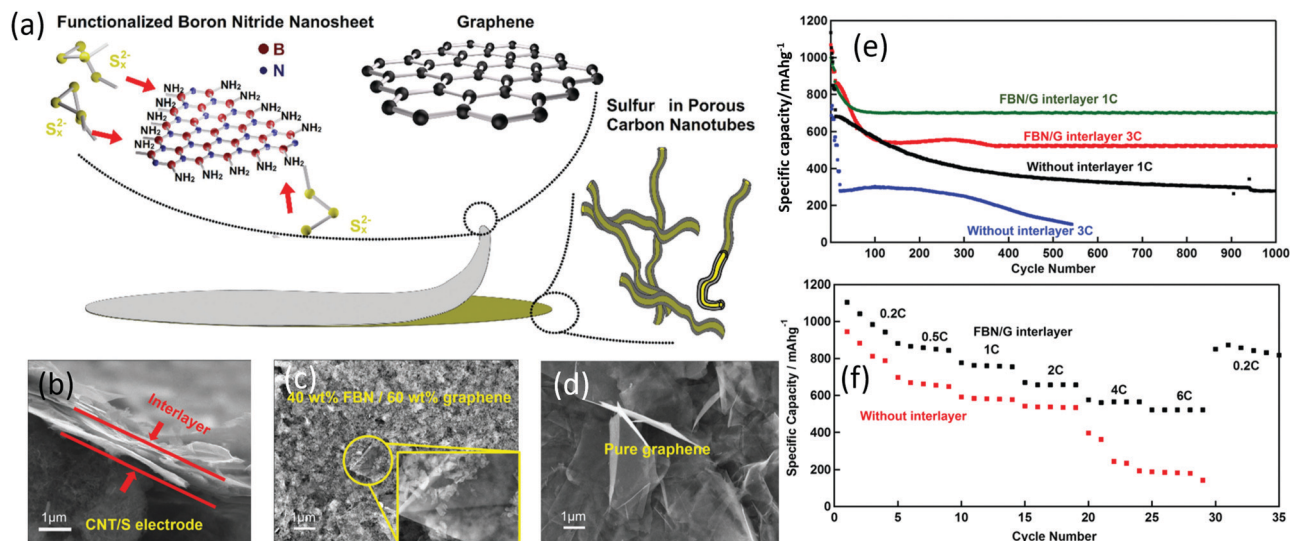


Fig. 17 (a) Schematic configuration of a Li-S cell with a FBN/G interlayer; (b) SEM image of cross section of the FBN/G interlayer and CNT/S cathode; (c) SEM image of the surface of a FBN/G interlayer; (d) SEM image of the surface of a pure graphene; and (e and f) electrochemical performance of (e) cyclic stability and (f) rate capability.²⁰⁰ (Reproduced with permission, Copyright 1969, John Wiley and Sons.)

interlayer was prepared by coating the surface of a carbon nanotube/sulfur (CNT/S) cathode with a thin layer of a functionalized boron nitride (FBN)/graphene (G) composite.²⁰⁰ The interlayer of FBN/G not only leads to the reduction of charge transfer resistance but also mitigates the shuttling problem. The incorporation of positively charged amino groups into FBN makes it to act as an ion-attracting site of negatively charged polysulfide products due to the electrostatic interaction, where graphene as a conductor and skeleton provides enough conductivity to the system. Consequently, a low capacity degradation rate of 0.0067% per cycle at 1C and 0.0037% per cycle at 3C is measured for the cell with interlayers over 1000 cycles (Fig. 17e). The Li-S cell with a FBN/G interlayer also exhibits a superior high-rate capability (Fig. 17f). This new interlayer provides a promising approach to significantly enhance Li-S battery performance. Such a novel configuration strategy can potentially be applied to other energy storage systems.

5.3 Advanced infusion of molten lithium

Li metal anodes. The lithium (Li) metal is considered as an ultimate choice for the anode for Li-S batteries due to its highest theoretical capacity (3860 mA h g^{-1} or $2061 \text{ mA h cm}^{-3}$) and lowest electrochemical potential (-3.04 V versus the standard hydrogen electrode) among all possible candidates.^{201,202} The Li anode, however, poses two critical issues: (i) the virtually infinite relative volume change, resulting in cracks of the solid-electrolyte-interface (SEI),²⁰³ and (ii) uncontrollable formation of Li dendrites during charge/discharge cycles, leading to low Coulombic efficiency, poor cyclic stability, and serious safety problems.²⁰⁴⁻²⁰⁷ To address the problem of relative volume change, the molten lithium infusion strategy has been developed to pre-store Li in the stable hosts,^{208,209} which delivers several advantages: first, a stable host minimizes volume variation by dividing dense Li into smaller domains; second, the increased

active Li surface greatly reduces the effective current density, homogenizing the ion flux and further suppressing dendrites; third, stable volume can be maintained at the electrode level to avoid stress fluctuation within a cell, thus minimizing safety concerns. However, the most challenges are to find out suitable host materials with excellent lithiophilicity for molten Li infusion because most available materials cannot be well wetted by molten Li.

Exploring new lithiophilic materials and finding a new surface functionalization strategy are of significant importance to the broader application of the molten Li infusion and the carbon-based hosts for stable Li-metal anodes. Recently, our group has identified a series of metal oxides including MnO_2 , Co_3O_4 and SnO_2 as superior lithiophilic materials. In this study, MnO_2 was used to functionalize graphene foams (G) by simply touching the edge of the functionalized graphene foams to molten Li (Fig. 18a-d).²¹⁰ Such a novel design of metal oxide nanoflake-decorated graphene foams (GFs) as 3D hosts exhibits several attractive features such as high porosity, high conductivity, and good mechanical flexibility, which ensure structural integrity during cycling. The 3D network acts as a cage to effectively confine lithium, realize minimum volume change, stabilize the electrolyte/electrode interface, and effectively suppress large dendrite formation during cycling. The obtained Li-Mn/graphene anode demonstrates a super-long and stable lifetime for repeated Li plating/stripping of 800 cycles at 1 mA cm^{-2} without voltage fluctuation, which is eight times longer than the normal lifespan of a bare Li foil under an identical testing condition (Fig. 18e). In addition, excellent rate capability and cyclability are also realized in full-cell batteries with Li-Mn/graphene anodes and LiCoO_2 cathodes (Fig. 18f and g). This study demonstrates a major advancement in developing a stable Li anode for Li-S batteries.

In addition to the above mentioned strategies, fabrication of hollow multishell structured (HoMS)/hollow micro/nanostructured

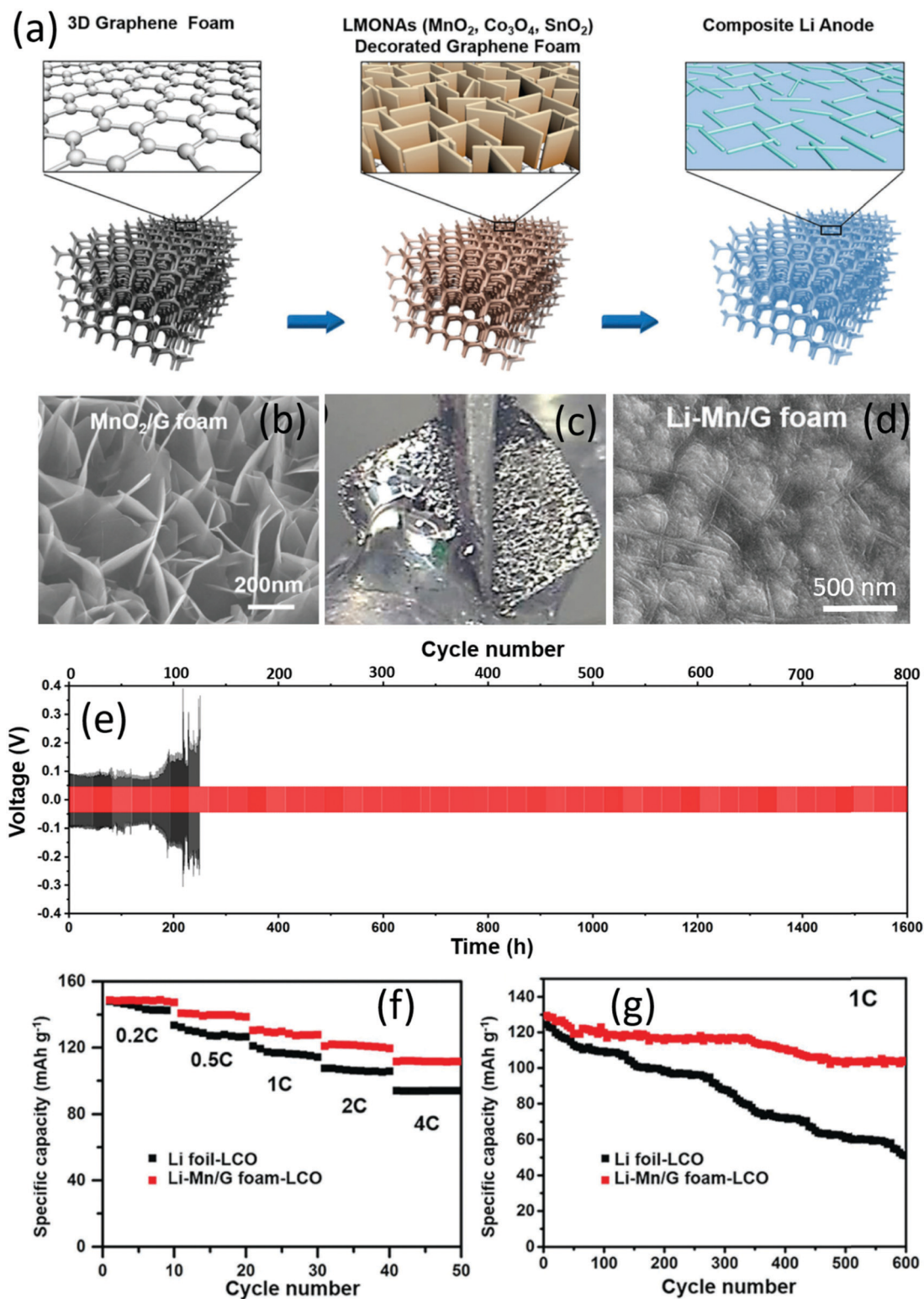


Fig. 18 (a) Schematic of the material design and the consequent synthetic procedures; (b) top-view SEM image of the MnO₂/graphene foam; (c) digital camera image of MnO₂/graphene foam after contacting with molten Li; (d) SEM image of the Li-Mn/G composite anode; (e) long-term cycling performance of a symmetric Li-Mn/G composite anode (red) and bare Li foil (black) with a stripping/plating capacity of 1 mA h cm⁻² at 1 mA cm⁻²; and (f and g) cycling performance of full-cell batteries with Li-Mn/graphene anodes and LiCoO₂ cathodes (1C = 120 mA g⁻¹).²¹⁰ (Reproduced with permission, Copyright 2018, John Wiley and Sons.)

materials and their application in rechargeable batteries as electrodes and/or sulfur carrier have received serious attention.^{211–214} Hollow structures have been shown to be fruitful in addressing the cycling-stability problem of high capacity electrode materials. HoMS materials have unique properties including large specific surface area, high loading capacity and/or buffering effect, benefiting the mass/energy transmission and effective surface area. As a result, hollow structured electrodes can maintain good structural integrity and achieve much better cycling stability than their solid counterparts. Besides, to resolve dendrite growth of alkali metals (typically Li, Na and K), an effective approach of anode engineering on structured current collectors can potentially be adopted.²¹⁵

6. Conclusions and future perspectives

In this review article, we have discussed our battery research carried out over the last decade. Table 1 summarizes all electrode materials and their critical properties which have been reflected here. This review article clearly demonstrates the development from bulk to nanoscale materials by adopting nanotechnology and how nanoscale materials profoundly change the performance of various energy storage systems including LIBs, SIBs, PIBs, and Li-S batteries. Various strategies, different nanostructural

electrode design, synthesis methods as well as some future works are discussed to overcome existing limitations with different storage systems.

LIBs and SIBs

Metal oxides exhibit several serious problems, specifically swelling and shrinking of active metal particles during Li^+ or Na^+ ion insertion/de-insertion, causing pulverization between active materials and electron conducting agents, leading to low electric and ionic conductivity, which directly affect battery performance, in particular cycling stability and rate capability. Minimization of the high level of volume alterations with metal oxide anodes is a challenge. To combat the effects of a drastic volume change in metal oxides, a hybridization strategy is employed where two phases that react with lithium at different potentials *vs.* Li/Li^+ are combined together in one electrode and are simultaneously dispersed in a conductive carbon matrix by adopting the industry acceptable ball milling technique. As a result, the obtained hybridized $\text{Fe}_2\text{O}_3\text{-SnO}_2/\text{C}$ and $\text{Co}_3\text{O}_4\text{-Fe}_2\text{O}_3/\text{C}$ composite anodes deliver improved cycle life and high rate capability due to the mitigation of volume change through sequential expansion and contraction in one electrode where the carbon matrix serves as a conductive scaffold that maintains a reliable electrical contact between active particles and current collectors. Such an electrode architecture is beneficial for diffusion of the electrolyte into the

Table 1 A summary of the various electrode materials (synthesis methods and properties) for rechargeable batteries

Materials	Systems	Synthesis methods	Cycling stability	Rate capability (mA h g^{-1})	Ref.
$\text{Fe}_2\text{O}_3\text{-SnO}_2/\text{C}$	LIB anode	Molten salt and ball milling	1110 mA h g^{-1} (50 cycles)	502 at 3950 mA g^{-1}	42
$\text{Co}_3\text{O}_4\text{-Fe}_2\text{O}_3/\text{C}$	LIB anode	Molten salt and ball milling	703 mA h g^{-1} (300 cycles)	400 at 3 A g^{-1}	54
$\text{Co}_3\text{O}_4\text{-Fe}_2\text{O}_3/\text{C}$	SIB anode	Molten salt and ball milling	410 mA h g^{-1} (100 cycles)	278 at 1 A g^{-1}	61
$\text{ZnFe}_2\text{O}_4/\text{C}$	LIB anode	Sol-gel and ball milling	681 mA h g^{-1} (100 cycles)	469 at 2.85 A g^{-1}	75
$\text{Co}_3\text{O}_4/\text{CNTs}$	SIB anode	Molten salt and liquid plasma	403 mA h g^{-1} (100 cycles)	190 at 3.2 A g^{-1}	83
Additive-free $\text{Nb}_2\text{O}_5\text{-TiO}_2$	LIB anode	Radio frequency sputtering	218 mA h g^{-1} (400 cycles)	174 at 0.4 A g^{-1} (1474 mA h cm^{-3} at 40 $\mu\text{A cm}^{-2}$)	111
Nanoporous Nb_2O_5	LIB anode	Electrochemical anodization	201 mA h g^{-1} (1.0–3.0 V) and 175 mA h g^{-1} (1.2–3.0 V) (300 cycles)	161 at 0.8 A g^{-1}	119
$\text{LiFe}_{0.4}\text{Mn}_{0.6}\text{PO}_4/\text{C}$ composite	LIB cathode	Combination of ball milling, spray drying and annealing	152 mA h g^{-1} (500 cycles)	72 at 20C	131
Maricite NaFePO_4	SIB cathode	Solid-state reaction and ball milling	142 mA h g^{-1} (300 cycles)	51 at 5C	136
$\alpha\text{-LiFeO}_2\text{-MWCNTs}$ nanocomposite	LIB cathode	Molten salt and a radio frequency oxygen plasma	147 mA h g^{-1} (100 cycles)	101 at 10C	137
$\text{LiFeTiO}_4\text{-MWCNTs}$	LIB cathode	Ball milling and annealing	110 mA h g^{-1} (100 cycles)	65 at 500 mA g^{-1}	138
Hybrid $\text{V}_2\text{O}_5/\text{graphene}$	LIB cathode	Wet ball-milling	185 mA h g^{-1} (100 cycles)	149 at 10C	139
$\text{SiO}_2\text{-coated LiNi}_{0.5}\text{Co}_{0.2}\text{Mn}_{0.3}\text{O}_2$ microspheres	LIB cathode	Wet chemistry and solid state reaction	153.4 mA h g^{-1} (50 cycles)	131 at 2C	149
ZrO_2 modified $\text{LiNi}_{0.6}\text{Co}_{0.2}\text{Mn}_{0.2}\text{O}_2$	LIB cathode	Wet chemistry and solid state reaction	146 mA h g^{-1} (100 cycles)	94.5 at 5C	150
Antimony doped tin oxide coated- $\text{LiNi}_{0.5}\text{Co}_{0.2}\text{Mn}_{0.3}\text{O}_2$	LIB cathode	Wet chemistry and solid state reaction	123 mA h g^{-1} (50 cycles)	110 at 5C	151
Sn/C nanocomposite	PIB anode	Ball-milling	120 mA h g^{-1} (30 cycles)	—	159
SnS_2/rGO composite	PIB anode	Sequential wet-chemistry	250 mA h g^{-1} (30 cycles)	120 at 2 A g^{-1}	163
$\text{Sb-P}/\text{C}$ composite	PIB anode	Planetary ball mill	402 mA h g^{-1} (50 cycles)	—	168
P/C nanocomposite	PIB anode	Planetary ball mill	270 mA h g^{-1} (50 cycles)	300 at 2 A g^{-1}	170
Sulfur/carbon nanospheres (yolk-shell)	Li-S battery cathode	Modified Stöber coating	337 mA h g^{-1} (1000 cycles)	400 at 2C	195
CNT/S coated with boron nitride nanosheets/graphene	Li-S battery cathode interlayer	Ball milling and wet-chemistry	700 mA h g^{-1} (1000 cycles)	556 at 6C	200
Li-Mn/graphene	Li-S battery anode	Combination of CVD, hydrothermal and melt infusion	800 cycles at 1 mA cm^{-2} without voltage fluctuation	—	210

bulk of the electrode, providing fast transport channels for the Li ions as well as fast electron transfer to the outer circuit. A mixed metal oxide composite anode of $\text{ZnFe}_2\text{O}_4/\text{C}$ is also prepared by combining sol-gel and ball milling methods where sol-gel synthesised ZnFe_2O_4 nanoparticles are dispersed and attached uniformly along the chains of the carbon matrix. This composite structure features several advantages over the conventional materials, leading to outstanding electrochemical performance in LIBs. Most importantly, a green electrode material of hybrid $\text{Nb}_2\text{O}_5\text{-TiO}_2$ for LIBs is fabricated by adopting the advanced radio frequency sputtering technique, which requires no supplementary support from additives/chemicals. The development of additive-free electrodes based on low-cost and environmentally friendly materials is a significant advance for expansion of sustainable and ecologically friendly energy storage. Another safe LIB anode of Nb_2O_5 with a new morphology of a vein-like nanoporous network was produced using a simple electrochemical anodization method. The demonstrated synthesis method is capable of producing a wide range of functional nanomaterials.

In the case of SIBs, the development of this storage device is hampered due to the lack of suitable anode materials. Our group carried out the first study of sodium electrochemistry with Co_3O_4 in 2014. It is verified that stable cycle life and high rate capability are difficult to achieve with the Co_3O_4 anode in SIBs without incorporation of the carbon matrix. To tackle this problem, a robust composite electrode of $\text{Co}_3\text{O}_4/\text{CNT}$ was designed and produced by a new “liquid plasma” method in a single step process. In this electrode architecture, Co_3O_4 nanoparticle clusters are uniformly dispersed in CNT networks where Co_3O_4 guarantees high electrochemical reactivity towards sodium, while the CNT improves the conductivity and stabilizes the anode structure during cycling.

In terms of cathode materials, layered transition metal oxides and poly-anionic compounds are considered as a suitable cathode host for LIBs and SIBs. However, poor cycling stability and rate capability still exist with these cathode hosts. To advance poly-anionic cathodes, a composite microstructure of $\text{LiFe}_{0.4}\text{Mn}_{0.6}\text{PO}_4/\text{C}$ is proposed and produced using a double carbon coating process by employing a traditional industrial technique (a combination of ball milling, spray drying and annealing). The strategy of double carbon coating is found to be an effective technique to ensure that all particles get electrons from all directions and contribute to the charge-discharge process. A high performance SIB cathode of maricite NaFePO_4 nanoparticle entwined graphene sheets is designed and produced by an innovative approach of combination of a solid-state reaction and a ball milling technique. Entwining particles in a graphene network ensured both electron transfer and ion diffusion simultaneously and most particles contributed to the charge/discharge process. A wet ball-milling method was used to produce the hybrid cathode of $\text{V}_2\text{O}_5/\text{graphene}$ where nanometre-sized V_2O_5 particles/aggregates were well embedded and uniformly dispersed in the crumpled and flexible graphene sheets generated by *in situ* conversion of bulk graphite during ball milling. Improvement in reversible capacity and rate capability is a serious challenge with LiFeO_2 based cathodes in LIBs. A cathode architecture of $\alpha\text{-LiFeO}_2\text{-MWCNTs}$ was

produced by combining a molten salt process and a radio frequency oxygen plasma, which is realised as an advanced cathode with high reversible capacity and high rate capability. To enhance the structural stability of Ni-rich layer structured cathodes ($\text{LiNi}_{1-x-y}\text{Mn}_x\text{Co}_y\text{O}_2$ ($0 \leq x + y \leq 0.5$)), a surface nanocoating with metal oxides such as SiO_2 , ZrO_2 , and Sb doped SnO_2 is proposed. This surface nanocoating suppresses side reactions in the interface between electrolyte and electrode, reduces transition-metal dissolution, and hinders decomposition of the electrolyte, leading to improved electrochemical performance. In-depth *in situ* electrochemical analysis, electrolyte study, and prototype full-cell fabrication by coupling a suitable anode and cathode are expected to be undertaken in the future.

PIBs

Potassium-ion batteries are a new class of high voltage non-aqueous batteries that have received worldwide attention since 2015 and are currently becoming a hot topic in the electrochemical energy storage field. To justify the feasibility of this new type of battery system, the identification of suitable anode electrode materials for this device is very important. Initially, only graphitic carbon anodes were disclosed. The works (material preparation, evaluation of electrochemical properties, and establishment of the charge storage mechanism) carried out by our group are the first to demonstrate non-carbon anodes based on tin (Sn), antimony (Sb) and phosphorus (P) where a number of materials identified are capable of alloying with potassium, delivering capacity higher than graphite. However, it is realised that the stable cycle life of PIBs with alloy anodes is a significant challenge because of large volume variation during potassiation, leading to an abrupt mechanical degradation of the electrodes. To combat volume variation, an effective approach of composite formation with the carbon matrix is proposed. Indeed, composite formation with the carbon matrix does improve the cycling stability of the Sb based anode. In this regard, a combination of three strategies (addition of an electrolyte additive, FEC; choice of the binder, replacement of the CMC with gum arabic; and addition of an extra alloying element to the composite such as black phosphorus, P) is proposed to construct the Sb-P/C composite anode for improving the cycling stability of the Sb based anodes in potassium cells. Surprisingly, no electrochemical reactivity of the silicon based anode with potassium is observed in our experiments. All of these early results in the field have stimulated the research community significantly and have led to the subsequent disclosure of many new non-carbon anode materials for PIBs. In-depth study of reaction mechanisms (reaction mechanisms of electrochemical alloying in potassium cells are quite different from those in previously assessed lithium and sodium cells), creation of certain intermetallic phases (like Sn_4P_3), and fabrication of prototype full-cells with alloy based anodes are to be explored in the future.

Li-S batteries

Significant research achievements have been made through the development of novel strategies for the fabrication of sulfur

cathodes as well as the protection of the Li metal anode in Li-S batteries. A rational novel design of yolk-shell carbon nanospheres composed of a microporous shell and a mesoporous core with a large void between them was found to be an effective sulfur host for the fabrication of conducting and high sulfur loading cathodes. To increase electronic conductivity and prevent shuttling, the formation of an interlayer on the cathode surface is demonstrated as a practical strategy, which significantly improves battery performance. The protection of the Li metal anode is also a significant challenge to relieve volume variation, suppress dendrite formation, and block unfavourable reaction between soluble polysulfides and Li. An advanced molten lithium infusion strategy is proposed for the successful protection of the Li-metal anode to overcome all of these issues. It is anticipated that such a strategy could be extended to other rechargeable batteries. A more comprehensive study including sophisticated electrode design and modification of separators and electrolytes is required to achieve next-generation high performance Li-S batteries.

Conflicts of interest

There are no conflicts to declare.

Acknowledgements

The authors acknowledge financial support from ARC LP (LP170100784) with a major contribution from Bolt Technologies Co. Ltd. Yinchuan, China, as well as support from Deakin Advanced Characterization Facility.

References

- J. Ma, Y. Li, N. S. Grundish, J. B. Goodenough, Y. Chen, L. Guo, Z. Peng, X. Qi, F. Yang, L. Qie, C. A. Wang, B. Huang, Z. Huang, L. Chen, D. Su, G. Wang, X. Peng, Z. Chen, J. Yang, S. He, X. Zhang, H. Yu, C. Fu, M. Jiang, W. Deng, C. F. Sun, Q. Pan, Y. Tang, X. Li, X. Ji, F. Wan, Z. Niu, F. Lian, C. Wang, G. G. Wallace, M. Fan, Q. Meng, S. Xin, Y.-G. Guo and L.-J. Wan, The 2021 battery technology roadmap, *J. Phys. D: Appl. Phys.*, 2021, **54**, 183001.
- M. Zhang, X. Song, X. Ou and Y. Tang, Rechargeable batteries based on anion intercalation graphite cathodes, *Energy Storage Mater.*, 2019, **16**, 65–84.
- V. Etacheri, R. Marom, R. Elazari, G. Salitra and D. Aurbach, Challenges in the development of advanced Li-ion batteries: a review, *Energy Environ. Sci.*, 2011, **4**, 3243–3262.
- D. Deng, Li-ion batteries: basics, progress, and challenges, *Energy Sci. Eng.*, 2015, **3**, 385–418.
- L. Croguennec and M. Rosa, Palacin, Recent achievements on inorganic electrode materials for lithium-ion batteries, *J. Am. Chem. Soc.*, 2015, **137**, 3140–3156.
- N. Yabuuchi, K. Kubota, M. Dahbi and S. Komaba, Research development on sodium-ion batteries, *Chem. Rev.*, 2014, **114**, 11636.
- C. Nithya and S. Gopukumar, Sodium ion batteries: a newer electrochemical storage, *WIREs Energy Environ.*, 2015, **4**, 253–278.
- Y. Marcus, Thermodynamic functions of transfer of single ions from water to nonaqueous and mixed solvents (part 3: standard potentials of selected electrodes), *Pure Appl. Chem.*, 1985, **57**, 1129–1132.
- A. Eftekhari, Z. Jian and X. Ji, Potassium secondary batteries, *ACS Appl. Mater. Interfaces*, 2017, **9**, 4404–4419.
- S. Komaba, T. Hasegawa, M. Dahbi and K. Kubota, Potassium intercalation into graphite to realize high-voltage/high-power potassium-ion batteries and potassium-ion capacitors, *Electrochem. Commun.*, 2015, **60**, 172–175.
- I. Sultana, M. M. Rahman, Y. Chen and A. M. Glushenkov, Potassium-ion battery anode materials operating through the alloying-dealloying reaction mechanism, *Adv. Funct. Mater.*, 2018, **28**, 1703857.
- A. Rosenman, E. Markevich, G. Salitra, D. Aurbach, A. Garsuch and F. F. Chesneau, Review on Li-sulfur battery systems: an integral perspective, *Adv. Energy Mater.*, 2015, **5**, 1500212.
- T. Tao, S. Lu, Y. Fan, W. Lei, S. Huang and Y. Chen, Anode improvement in rechargeable lithium-sulfur batteries, *Adv. Mater.*, 2017, **29**, 1700542.
- F. Cheng, J. Liang, Z. Tao and J. Chen, Functional materials for rechargeable batteries, *Adv. Mater.*, 2011, **23**, 1695–1715.
- L. Pan, J. Dong, D. Yi, Y. Yang and X. Wang, Recent advances in atomic-scale storage mechanism studies of two-dimensional nanomaterials for rechargeable batteries beyond Li-ion, *Chem. Res. Chin. Univ.*, 2020, **36**, 560–583.
- X. Deng, J. Li, L. Ma, J. Sha and N. Zhao, Three-dimensional porous carbon materials and their composites as electrodes for electrochemical energy storage systems, *Mater. Chem. Front.*, 2019, **3**, 2221–2245.
- B. C. Melot and J. M. Tarascon, Design and preparation of materials for advanced electrochemical storage, *Acc. Chem. Res.*, 2013, **46**, 1226–1238.
- H. Chen, S. Cheng, D. Chen, Y. Jiang, E. H. Ang, W. Liu, Y. Feng, X. Rui and Y. Yu, Vanadate-based electrodes for rechargeable batteries, *Mater. Chem. Front.*, 2021, **5**, 1585–1609.
- P. Adelhelm, P. Hartmann, C. L. Bender, M. Busche, C. Eufinger and J. Janek, From lithium to sodium: cell chemistry of room temperature sodium-air and sodium-sulfur batteries, *J. Nanotechnol.*, 2015, **6**, 1016–1055.
- J. Y. Hwang, J. Kim, T. Y. Yu, S. T. Myung and Y. K. Sun, Development of P3-K_{0.69}CrO₂ as an ultra-high performance cathode material for K-ion batteries, *Energy Environ. Sci.*, 2018, **11**, 2821–2827.
- S. Komaba, N. Yabuuchi, T. Nakayama, A. Ogata, T. Ishikawa and I. Nakai, *Inorg. Chem.*, 2012, **51**, 6211–6220.
- M. Sathiyaraj, K. Hemalatha, K. Ramesha, J. M. Tarascon and A. S. Prakash, Synthesis, structure, and electrochemical properties of the layered sodium insertion cathode material: NaNi_{1/3}Mn_{1/3}Co_{1/3}O₂, *Chem. Mater.*, 2012, **24**, 1846–1853.
- A. Leela, M. Reddy, S. R. Gowda, M. M. Shaijumon and P. M. Ajayan, Hybrid nanostructures for energy storage applications, *Adv. Mater.*, 2012, **24**, 5045–5064.

- 24 P. G. Bruce, B. Scrosati and J. M. Tarascon, Nanomaterials for rechargeable lithium batteries, *Angew. Chem., Int. Ed.*, 2008, **47**, 2930–2946.
- 25 F. Liu, S. Song, D. Xue and H. Zhang, Selective crystallization with preferred lithium-ion storage capability of inorganic materials, *Nanoscale Res. Lett.*, 2012, **7**, 149.
- 26 V. Palomares, M. C. Cabanas, E. C. Martínez, M. H. Han and T. Rojo, Update on Na-based battery materials. A growing research path, *Energy Environ. Sci.*, 2013, **6**, 2312–2337.
- 27 P. Poizot, S. Laruelle, S. Grugeon, L. Dupont and J.-M. Tarascon, Nano-sized transition-metal oxides as negative-electrode materials for lithium-ion batteries, *Nature*, 2000, **407**, 496–499.
- 28 J. Cabana, L. Monconduit, D. Larcher and M. R. Palacín, Beyond intercalation-based Li-ion batteries: the state of the art and challenges of electrode materials reacting through conversion reactions, *Adv. Mater.*, 2010, **22**, E170–E192.
- 29 L. Wang, G. Zhang, Q. Liu and H. Duan, Recent progress in Zn-based anodes for advanced lithium ion batteries, *Mater. Chem. Front.*, 2018, **2**, 1414–1435.
- 30 M. V. Reddy, G. V. Subba Rao and B. V. R. Chowdari, Metal oxides and oxysalts as anode materials for Li-ion batteries, *Chem. Rev.*, 2013, **113**, 5364–5457.
- 31 J. A. Jiang, Y. Y. Li, J. P. Liu and X. T. Huang, Building one-dimensional oxide nanostructure arrays on conductive metal substrates for lithium-ion battery anodes, *Nanoscale*, 2011, **3**, 45–58.
- 32 Y. Kim, K. H. Ha, S. M. Oh and K. T. Lee, High-capacity anode materials for sodium-ion batteries, *Chem. – Eur. J.*, 2014, **20**, 11980–11992.
- 33 S. A. Needham, G. X. Wang, K. Konstantinov, Y. Tournayre, Z. Lao and H. K. Liu, Electrochemical performance of Co_3O_4 -C composite anode materials, *Electrochem. Solid-State Lett.*, 2006, **9**, A315–A319.
- 34 N. Y. Nuli, P. Zhang, Z. P. Guo and H. K. Liu, Shape evolution of $\alpha\text{-Fe}_2\text{O}_3$ and its size-dependent electrochemical properties for lithium-ion batteries, *J. Electrochem. Soc.*, 2008, **155**, A196–A200.
- 35 Y. M. Lin, P. R. Abel, A. Heller and C. B. Mullins, $\alpha\text{-Fe}_2\text{O}_3$ nanorods as anode material for lithium-ion batteries, *J. Phys. Chem. Lett.*, 2011, **2**, 2885–2891.
- 36 H. Kang, Y. Liu, K. Cao, Y. Zhao, L. Jiao, Y. Wang and H. Yuan, Update on anode materials for Na-ion batteries, *J. Mater. Chem. A*, 2015, **3**, 17899–17913.
- 37 Z. Jian, P. Liu, F. Li, M. Chen and H. Zhou, Monodispersed hierarchical Co_3O_4 spheres intertwined with carbon nanotubes for use as anode materials in sodium-ion batteries, *J. Mater. Chem. A*, 2014, **2**, 13805–13809.
- 38 D. P. Dubal, O. Ayyad, V. Ruiz and P. Gómez-Romero, Hybrid energy storage: The merging of battery and supercapacitor chemistries, *Chem. Soc. Rev.*, 2015, **44**, 1777–1790.
- 39 C. M. Wang, W. Xu, J. Liu, J. G. Zhang, L. V. Saraf, B. W. Arey, D. Choi, Z. G. Yang, J. Xiao, S. Thevuthasan and D. R. Baer, *In situ* transmission electron microscopy observation of microstructure and phase evolution in a SnO_2 nanowire during lithium intercalation, *Nano Lett.*, 2011, **11**, 1874–1880.
- 40 I. A. Courtney and J. R. Dahn, Electrochemical and *in situ* X-ray diffraction studies of the reaction of lithium with tin oxide composites, *J. Electrochem. Soc.*, 1997, **144**, 2045–2051.
- 41 T. Brousse, R. Retoux, U. Herterich and D. M. Schleich, Thin-film crystalline SnO_2 -lithium electrodes, *J. Electrochem. Soc.*, 1998, **145**, 1–4.
- 42 M. M. Rahman, A. M. Glushenkov, T. Ramireddy, T. Tao and Y. Chen, *Nanoscale*, 2013, **5**, 4910–4916.
- 43 W. Zeng, F. Zheng, R. Li, Y. Zhan, Y. Li and J. Liu, Template synthesis of $\text{SnO}_2/\text{Fe}_2\text{O}_3$ nanotube array for 3D lithium ion battery anode with large areal capacity, *Nanoscale*, 2012, **4**, 2760–2765.
- 44 J. Liu, Y. Li, H. Fan, Z. Zhu, J. Jiang, R. Ding, Y. Hu and X. Huang, Iron oxide-based nanotube arrays derived from sacrificial template-accelerated hydrolysis: large-area design and reversible lithium storage, *Chem. Mater.*, 2010, **22**, 212–2017.
- 45 J. Wang, N. Du, H. Zhang, J. Yu and D. Yang, Large-scale synthesis of SnO_2 nanotube arrays as high-performance anode materials of Li-ion batteries, *J. Phys. Chem. C*, 2011, **115**, 11302–11305.
- 46 W. W. Zhou, C. W. Cheng, J. P. Liu, Y. Y. Tay, J. Jiang, X. Jia, J. Zhang, H. Gong, H. H. Hng, T. Yu and H. J. Fan, Epitaxial growth of branched $\alpha\text{-Fe}_2\text{O}_3/\text{SnO}_2$ nano-heterostructures with improved lithium-ion battery performance, *Adv. Funct. Mater.*, 2011, **21**, 2439–2445.
- 47 W. Zhou, Y. Y. Tay, X. Jia, D. Y. Y. Wai, J. Jiang, H. H. Hoon and T. Yu, Controlled growth of $\text{SnO}_2@/\text{Fe}_2\text{O}_3$ double-sided nanocombs as anodes for lithium-ion batteries, *Nanoscale*, 2012, **4**, 4459–4463.
- 48 Y. Wang, J. Xu, H. Wu, M. Xu, Z. Peng and G. Zheng, Hierarchical $\text{SnO}_2\text{-Fe}_2\text{O}_3$ heterostructures as lithium-ion battery anodes, *J. Mater. Chem.*, 2012, **22**, 21923–21927.
- 49 J. S. Chen, C. M. Li, W. W. Zhou, Q. Y. Yan, L. A. Archer and X. W. Lou, One-pot formation of SnO_2 hollow nanospheres and $\alpha\text{-Fe}_2\text{O}_3@/\text{SnO}_2$ nanorattles with large void space and their lithium storage properties, *Nanoscale*, 2009, **1**, 280–285.
- 50 J. Zhu, Z. Lu, M. O. Oo, H. H. Hng, J. Ma, H. Zhang and Q. Yan, Synergetic approach to achieve enhanced lithium ion storage performance in ternary phased $\text{SnO}_2\text{-Fe}_2\text{O}_3/\text{rGO}$ composite nanostructures, *J. Mater. Chem.*, 2011, **21**, 12770–12776.
- 51 G. Xia, N. Li, D. Li, R. Liu, C. Wang, Q. Li, X. Lü, J. S. Spendelov, J. Zhang and G. Wu, Graphene/ $\text{Fe}_2\text{O}_3/\text{SnO}_2$ ternary nanocomposites as a high-performance anode for lithium-ion batteries, *ACS Appl. Mater. Interfaces*, 2013, **5**, 8607–8614.
- 52 Y. Gu, Z. Jiao, M. Wu, B. Luo, Y. Lei, Y. Wang, L. Wang and H. Zhang, Construction of point-line-plane (0-1-2 dimensional) $\text{Fe}_2\text{O}_3\text{-SnO}_2/\text{graphene}$ hybrids as the anodes with excellent lithium storage capability, *Nano Res.*, 2017, **10**, 121–133.
- 53 S. A. Needham, G. X. Wang, K. Konstantinov, Y. Tournayre, Z. Lao and H. K. Liu, Electrochemical performance of Co_3O_4 -C composite anode materials, *Electrochem. Solid-State Lett.*, 2006, **9**, A315–A319.

- 54 I. Sultana, M. M. Rahman, T. Ramireddy, N. Sharma, D. Poddar, A. Khalid, H. Zhang, Ying Chen and A. M. Glushenkov, Understanding structure-function relationship in hybrid $\text{Co}_3\text{O}_4\text{-Fe}_2\text{O}_3/\text{C}$ lithium-ion battery electrodes, *ACS Appl. Mater. Interfaces*, 2015, 7, 20736–20744.
- 55 H. Wu, M. Xu, Y. Wang and G. Zheng, Branched $\text{Co}_3\text{O}_4/\text{Fe}_2\text{O}_3$ nanowires as high capacity lithium-ion battery anodes, *Nano Res.*, 2013, 6, 167–173.
- 56 Q. Q. Xiong, K. H. Xia, J. P. Tu, J. Chen, Y. Q. Zhang, D. Zhou, C. D. Gu and X. L. Wang, Hierarchical $\text{Fe}_2\text{O}_3@/\text{Co}_3\text{O}_4$ nanowire array anode for high-performance lithium-ion batteries, *J. Power Sources*, 2013, 240, 344–350.
- 57 Y. Luo, D. Kong, J. Luo, Y. Wang, D. Zhang, K. Qiu, C. Cheng, C. M. Lia and T. Yu, Seed-assisted synthesis of $\text{Co}_3\text{O}_4@/\alpha\text{-Fe}_2\text{O}_3$ core-shell nanoneedle arrays for lithium-ion battery anode with high capacity, *RSC Adv.*, 2014, 4, 13241–13249.
- 58 Q. Hou, Q. Man, P. Liu, R. Jin, Y. Cui, G. Li and S. Gao, Encapsulation of $\text{Fe}_2\text{O}_3/\text{NiO}$ and $\text{Fe}_2\text{O}_3/\text{Co}_3\text{O}_4$ nanosheets into conductive polypyrrole for superior lithium ion storage, *Electrochim. Acta*, 2019, 296, 438–449.
- 59 W. Guo, W. Sun and Y. Wang, Multilayer $\text{CuO}@/\text{NiO}$ hollow spheres: microwave-assisted metal organic-framework derivation and highly reversible structure-matched stepwise lithium storage, *ACS Nano*, 2015, 9, 11462–11471.
- 60 G. Xia, N. Li, D. Li, R. Liu, C. Wang, Q. Li, X. Lu, J. S. Spendelov, J. Zhang and G. Wu, Graphene/ $\text{Fe}_2\text{O}_3/\text{SnO}_2$ ternary nanocomposites as a high-performance anode for lithium-ion batteries, *ACS Appl. Mater. Interfaces*, 2013, 5, 8607–8614.
- 61 I. Sultana, M. M. Rahman, S. Mateti, V. G. Ahmadabadi, A. M. Glushenkov and Y. Chen, K-ion and Na-ion storage performances of $\text{Co}_3\text{O}_4\text{-Fe}_2\text{O}_3$ nanoparticle-decorated super P carbon black prepared by a ball milling process, *Nanoscale*, 2017, 9, 3646–3654.
- 62 Y. Zhang, Z. Bakenov, T. Tan and J. Huang, Synthesis of core-shell carbon encapsulated Fe_2O_3 composite through a facile hydrothermal approach and their application as anode materials for sodium-ion batteries, *Metals*, 2018, 8, 461.
- 63 P. C. Rath, J. Patra, D. Saikia, M. Mishra, C. M. Tseng, J. K. Chang and H. M. Kao, Comparative study on the morphology-dependent performance of various CuO nanostructures as anode materials for sodium-ion batteries, *ACS Sustainable Chem. Eng.*, 2018, 6, 10876–10885.
- 64 F. Wu, J. Bai, J. Feng and S. Xiong, Porous mixed metal oxides: design, formation mechanism, and application in lithium-ion batteries, *Nanoscale*, 2015, 7, 17211–17230.
- 65 L. Qiao, X. H. Wang, L. Qiao, X. L. Sun, X. W. Li, Y. X. Zheng and D. Y. He, Single electrospun porous NiO-ZnO hybrid nanofibers as anode materials for advanced lithium-ion batteries, *Nanoscale*, 2013, 5, 3037–3042.
- 66 B. Das, M. V. Reddy, S. Tripathy and B. V. R. Chowdari, A disc-like Mo-metal cluster compound, $\text{Co}_2\text{Mo}_3\text{O}_8$, as a high capacity anode for lithium-ion batteries, *RSC Adv.*, 2014, 4, 33883–33889.
- 67 X. Guo, X. Lu, X. Fang, Y. Mao, Z. Wang, L. Chen, X. Xu, H. Yang and Y. Liu, Lithium storage in hollow spherical ZnFe_2O_4 as anode materials for lithium ion batteries, *Electrochem. Commun.*, 2010, 12, 847–850.
- 68 Y. Wang, D. W. Su, A. Ung, J. H. Ahn and G. X. Wang, Hollow CoFe_2O_4 nanospheres as a high capacity anode material for lithium ion batteries, *Nanotechnology*, 2012, 23, 055402.
- 69 Z. H. Li, T. P. Zhao, X. Y. Zhan, D. S. Gao, Q. Z. Xiao and G. T. Lei, High capacity three-dimensional ordered macroporous CoFe_2O_4 as anode material for lithium ion batteries, *Electrochim. Acta*, 2010, 55, 4594–4598.
- 70 P. Lavela and J. L. Tirado, CoFe_2O_4 and NiFe_2O_4 synthesized by sol-gel procedures for their use as anode materials for Li-ion batteries, *J. Power Sources*, 2007, 172, 379–387.
- 71 Y. Ding, Y. F. Yang and H. X. Shao, High capacity ZnFe_2O_4 anode material for lithium ion batteries, *Electrochim. Acta*, 2011, 56, 9433–9438.
- 72 Y. Sharma, N. Sharma, G. V. S. Rao and B. V. R. Chowdari, Li-storage and cyclability of urea combustion derived ZnFe_2O_4 as anode for Li-ion batteries, *Electrochim. Acta*, 2008, 53, 2380–2385.
- 73 D. Bresser, E. Paillard, R. Kloepsch, S. Krueger, M. Fiedler, R. Schmitz, D. Baither, M. Winter and S. Passerini, Carbon coated ZnFe_2O_4 nanoparticles for advanced lithium-ion anodes, *Adv. Energy Mater.*, 2013, 3, 513–523.
- 74 F. Mueller, D. Bresser, E. Paillard, M. Winter and S. Passerini, Influence of the carbonaceous conductive network on the electrochemical performance of ZnFe_2O_4 nanoparticles, *J. Power Sources*, 2013, 236, 87–94.
- 75 R. M. Thankachan, M. M. Rahman, I. Sultana, A. M. Glushenkov, S. Thomas, N. Kalarikkal and Y. Chen, Enhanced lithium storage in $\text{ZnFe}_2\text{O}_4\text{-C}$ nanocomposite produced by a low-energy ball milling, *J. Power Sources*, 2015, 282, 462–470.
- 76 N. Du, H. Zhang, B. Chen, J. Wu, X. Ma, Z. Liu, Y. Zhang, D. Yang, X. Huang and J. Tu, Porous Co_3O_4 nanotubes derived from $\text{Co}_4(\text{CO})_{12}$ clusters on carbon nanotube templates: A highly efficient material for Li-battery applications, *Adv. Mater.*, 2007, 19, 4505–4509.
- 77 Y. Wang, D. Su, C. Wang and G. Wang, $\text{SnO}_2@/\text{MWCNT}$ nanocomposite as a high capacity anode material for sodium-ion batteries, *Electrochem. Commun.*, 2013, 29, 8–11.
- 78 M. M. Rahman, A. M. Glushenkov, T. Ramireddy and Y. Chen, Electrochemical investigation of sodium reactivity with nanostructured Co_3O_4 for sodium-ion batteries, *Chem. Commun.*, 2014, 50, 5057–5060.
- 79 J. W. Wen, D. W. Zhang, Y. Zang, X. Sun, B. Chen, C. X. Ding, Y. Yu and C. H. Chen, Li and Na storage behavior of bowl-like hollow Co_3O_4 microspheres as an anode material for lithium-ion and sodium-ion batteries, *Electrochim. Acta*, 2014, 132, 193–199.
- 80 Z. Jian, P. Liu, F. Li, M. Chen and H. Zhou, Monodispersed hierarchical Co_3O_4 spheres intertwined with carbon nanotubes for use as anode materials in sodium-ion batteries, *J. Mater. Chem. A*, 2014, 2, 13805–13809.
- 81 Y. Liu, Z. Cheng, H. Sun, H. Arandiyani, J. Li and M. Ahmad, Mesoporous Co_3O_4 sheets/3D graphene networks nanohybrids

- for high-performance sodium-ion battery anode, *J. Power Sources*, 2015, **273**, 878–884.
- 82 Y. Wang, D. Su, C. Wang and G. Wang, SnO₂@MWCNT nanocomposite as a high capacity anode material for sodium-ion batteries, *Electrochem. Commun.*, 2013, **29**, 8–11.
- 83 M. M. Rahman, I. Sultana, Z. Chen, M. Srikanth, L. H. Li, X. J. Dai and Y. Chen, *Ex situ* electrochemical sodiation/desodiation observation of Co₃O₄ anchored carbon nanotubes: a high performance sodium-ion battery anode produced by pulsed plasma in a liquid, *Nanoscale*, 2015, **7**, 13088–13095.
- 84 K. S. Novoselov, A. K. Geim, S. V. Morozov, D. Jiang, Y. Zhang, S. V. Dubonos, I. V. Grigorieva and A. A. Firsov, Electric field effect in atomically thin carbon films, *Science*, 2004, **306**, 666–669.
- 85 G. Wang, X. Shen, J. Yao and J. Park, Graphene nanosheets for enhanced lithium storage in lithium ion batteries, *Carbon*, 2009, **47**, 2049–2053.
- 86 J. Sun, H.-W. Lee, M. Pasta, H. Yuan, G. Zheng, Y. Sun, Y. Li and Y. Cui, A phosphorene-graphene hybrid material as a high-capacity anode for sodium-ion batteries, *Nat. Nanotechnol.*, 2015, **10**, 980–985.
- 87 D. Su, H. J. Ahn and G. Wang, SnO₂-graphene nanocomposites as anode materials for Na-ion batteries with superior electrochemical performance, *Chem. Commun.*, 2013, **49**, 3131–3133.
- 88 Y.-X. Wang, Y.-G. Lim, M.-S. Park, S.-L. Chou, J. H. Kim, H.-K. Liu, S.-X. Dou and Y.-J. Kim, Ultrafine SnO₂ nanoparticle loading onto reduced graphene oxide as anodes for sodium-ion batteries with superior rate and cycling performances, *J. Mater. Chem. A*, 2014, **2**, 529–534.
- 89 Y. Zhang, J. Xie, S. Zhang, P. Zhu, G. Cao and X. Zhao, Ultrafine tin oxide on reduced graphene oxide as high-performance anode for sodium-ion batteries, *Electrochim. Acta*, 2015, **151**, 8–15.
- 90 Z. Li, J. Ding and D. Mitlin, Tin and Tin compounds for sodium-ion battery anodes: phase transformations and performance, *Acc. Chem. Res.*, 2015, **48**, 1657–1665.
- 91 S. Yuan, Y. H. Zhu, W. Li, S. Wang, D. Xu, L. Li, Y. Zhang and X. B. Zhang, Surfactant-free aqueous synthesis of pure single-crystalline SnSe nanosheet clusters as anode for high-energy and power-density sodium-ion batteries, *Adv. Mater.*, 2017, **29**, 1602469.
- 92 Z. Kong, X. Liu, T. Wang, A. Fu, Y. Li, P. Guo, Y. G. Guo, H. Li and X. S. Zhao, Three-dimensional hollow spheres of porous SnO₂/rGO composite as high performance anode for sodium ion batteries, *Appl. Surf. Sci.*, 2019, **479**, 198–208.
- 93 L. Wang, Z. Wei, M. Mao, H. Wang, Y. Li and J. Ma, Metal oxide/graphene composite anode materials for sodium-ion batteries, *Energy Storage Mater.*, 2019, **16**, 434–454.
- 94 X. Xie, S. Wang, K. Kretschmer and G. Wang, Two-dimensional layered compound based anode materials for lithium-ion batteries and sodium-ion batteries, *J. Colloid Interface Sci.*, 2017, **499**, 17–32.
- 95 Y. Chen, X. Chen and Y. Zhang, A Comprehensive review on metal-oxide nanocomposites for high-performance lithium-ion battery anodes, *Energy Fuels*, 2021, **35**, 6420–6442.
- 96 H. Kumar, R. Sharma, A. Yadav and R. Kumari, Recent advancement made in the field of reduced graphene oxide-based nanocomposites used in the energy storage devices: A review, *J. Energy Storage*, 2021, **33**, 102032.
- 97 L. Sun, W. Liu, Y. Cui, Y. Zhang, H. Wang, S. Liu and B. Shan, Non-carbon coating: a new strategy for improving lithium ion storage of carbon matrix, *Green Chem.*, 2018, **20**, 3954–3962.
- 98 M. H. Park, K. Kim, J. Kim and J. Cho, Flexible dimensional control of high-capacity Li-ion-battery anodes: From 0D hollow to 3D porous germanium nanoparticle assemblies, *Adv. Mater.*, 2010, **22**, 415–418.
- 99 J. Gao, M. A. Lowe and H. C. D. Abruna, Spongelike nanosized Mn₃O₄ as a high-capacity anode material for rechargeable lithium batteries, *Chem. Mater.*, 2011, **23**, 3223–3227.
- 100 Z. S. Wu, W. Ren, L. Wen, L. Gao, J. Zhao, Z. Chen, G. Zhou, F. Li and H. M. Cheng, Graphene anchored with Co₃O₄ nanoparticles as anode of lithium-ion batteries with enhanced reversible capacity and cyclic performance, *ACS Nano*, 2010, **4**, 3187–3194.
- 101 H. Wang, L. F. Cui, Y. Yang, C. H. Sanchez, J. T. Robinson, Y. Liang, Y. Cui and H. Dai, Mn₃O₄-Graphene hybrid as a high-capacity anode material for lithium-ion batteries, *J. Am. Chem. Soc.*, 2010, **132**, 13978–13980.
- 102 D. H. Ha, M. A. Islam and R. D. Robinson, Binder-free and carbon-free nanoparticle batteries: A method for nanoparticle electrodes without polymeric binders or carbon black, *Nano Lett.*, 2012, **12**, 5122–5130.
- 103 K. Rana, S. D. Kim and J. H. Ahn, Additive-free thick graphene film as an anode material for flexible lithium-ion batteries, *Nanoscale*, 2015, **7**, 7065–7071.
- 104 C. K. Chan, H. L. Peng, G. Liu, K. McIlwrath, X. F. Zhang, R. A. Huggins and Y. Cui, High-performance lithium battery anodes using silicon nanowires, *Nat. Nanotechnol.*, 2008, **3**, 31–35.
- 105 A. M. Chockla, J. T. Harris, V. A. Akhavan, T. D. Bogart, V. C. Holmberg, C. Steinhagen, C. B. Mullins, K. J. Stevenson and B. A. Korgel, Silicon nanowire fabric as a lithium-ion battery electrode material, *J. Am. Chem. Soc.*, 2011, **133**, 20914–20921.
- 106 Y. Li, X. Lv and J. Li, High performance binder less nanowire arrays electrode for lithium-ion battery, *Appl. Phys. Lett.*, 2009, **95**, 113102.
- 107 C. C. Li, Q. H. Li, L. B. Chen and T. H. Wang, Topochemical synthesis of cobalt oxide nanowire arrays for high performance binderless lithium ion batteries, *J. Mater. Chem.*, 2011, **21**, 11867–11872.
- 108 H. Wu, G. Chan, J. W. Choi, I. Ryu, Y. Yao, M. T. McDowell, S. W. Lee, A. Jackson, Y. Yang, L. Hu and Y. Cui, Stable cycling of double-walled silicon nanotube battery anodes through solid-electrolyte interphase control, *Nat. Nanotechnol.*, 2012, **7**, 310–315.
- 109 X. Yu, L. Xin, Y. Liu, W. Zhao, B. Li, X. Zhou and H. Shen, One-step synthesis of Nb-doped TiO₂ rod@Nb₂O₅ nanosheet core-shell heterostructures for stable high-performance lithium-ion batteries, *RSC Adv.*, 2016, **6**, 27094–27101.

- 110 Y. Liu, L. Lin, W. Zhang and M. Wei, Heterogeneous $\text{TiO}_2@\text{Nb}_2\text{O}_5$ composite as a high-performance anode for lithium-ion batteries, *Sci. Rep.*, 2017, 7, 7204.
- 111 M. M. Rahman, M. Zhou, I. Sultana, S. Mateti, A. Falin, L. H. Li, Z. S. Wu and Y. Chen, Additive-free $\text{Nb}_2\text{O}_5\text{-TiO}_2$ hybrid anode towards low-cost and safe lithium-ion batteries: a green electrode material produced in an environmentally friendly process, *Batteries Supercaps*, 2018, 1, 1–9.
- 112 G. Li, X. Wang and X. Ma, Nb_2O_5 -carbon core-shell nanocomposite as anode material for lithium ion battery, *J. Energy Chem.*, 2013, 22, 357–362.
- 113 M. Liu, C. Yan and Y. Zhang, Fabrication of Nb_2O_5 nanosheets for high-rate lithium-ion storage applications, *Sci. Rep.*, 2015, 5, 8326.
- 114 S. Liu, J. Zhou, Z. Cai, G. Fang, A. Pan and S. Liang, Nb_2O_5 microstructures: a high-performance anode for lithium ion batteries, *Nanotechnology*, 2016, 27, 46LT01.
- 115 M. Sasidharan, N. Gunawardhana, M. Yoshio and K. Nakashima, Nb_2O_5 hollow nanospheres as anode material for enhanced performance in lithium ion batteries, *Mater. Res. Bull.*, 2012, 47, 2161–2164.
- 116 T. Lan, H. Qiu, F. Xie, J. Yang and M. Wei, Rutile TiO_2 mesocrystals/reduced graphene oxide with high-rate and long-term performance for lithium-ion batteries, *Sci. Rep.*, 2015, 5, 8498.
- 117 M. Zhen, X. Guo, G. Gao, Z. Zhou and L. Liu, Rutile TiO_2 nanobundles on reduced graphene oxides as anode materials for Li ion batteries, *Chem. Commun.*, 2014, 50, 11915–11918.
- 118 D. McNulty, E. Carroll and C. O'Dwyer, Rutile TiO_2 inverse opal anodes for Li-ion batteries with long cycle life, high-rate capability, and high structural stability, *Adv. Energy Mater.*, 2017, 7, 1602291.
- 119 M. M. Rahman, R. A. Rani, A. Z. Sadek, A. S. Zoofakar, M. R. Field, T. Ramireddy, K. K. Zadeh and Y. Chen, A vein-like nanoporous network of Nb_2O_5 with a higher lithium intercalation discharge cut-off voltage, *J. Mater. Chem. A*, 2013, 1, 11019–11025.
- 120 R. Pitchai, V. Thavasi, S. G. Mhaisalkar and S. Ramakrishna, Nanostructured cathode materials: a key for better performance in Li-ion batteries, *J. Mater. Chem.*, 2011, 21, 11040–11051.
- 121 M. D. Slater, D. Kim, E. Lee and C. S. Johnson, Sodium-ion batteries, *Adv. Funct. Mater.*, 2013, 23, 947–958.
- 122 Y. Wang and G. Cao, Developments in nanostructured cathode materials for high-performance lithium-ion batteries, *Adv. Mater.*, 2008, 20, 2251–2269.
- 123 S. T. Myung, K. Amine and Y. K. Sun, Nanostructured cathode materials for rechargeable lithium batteries, *J. Power Sources*, 2015, 283, 219–236.
- 124 E. Goikolea, V. Palomares, S. Wang, I. R. de Larramendi, X. Guo, G. Wang and T. Rojo, Na-ion batteries—approaching old and new challenges, *Adv. Energy Mater.*, 2020, 10, 2002055.
- 125 J. Xiao, X. Li, K. Tang, D. Wang, M. Long, H. Gao, W. Chen, C. Liu, H. Liu and G. Wang, Recent progress of emerging cathode materials for sodium ion batteries, *Mater. Chem. Front.*, 2021, 5, 3735–3764.
- 126 J. Ni and Y. Li, Carbon nanomaterials in different dimensions for electrochemical energy storage, *Adv. Energy Mater.*, 2016, 6, 1600278.
- 127 P. Li, K. Zhang and J. H. Park, Dual or multi carbonaceous coating strategies for next-generation batteries, *J. Mater. Chem. A*, 2018, 6, 1900–1914.
- 128 A. K. Padhi, K. S. Nanjundaswamy and J. B. Goodenough, Phospho-olivines as positive-electrode materials for rechargeable lithium batteries, *J. Electrochem. Soc.*, 1997, 144, 1188–1194.
- 129 J. Wang and X. Sun, Olivine LiFePO_4 : the remaining challenges for future energy storage, *Energy Environ. Sci.*, 2015, 8, 1110–1138.
- 130 W. Liu, P. Gao, Y. Mi, J. Chen, H. Zhou and X. Zhang, Fabrication of high tap density $\text{LiFe}_{0.6}\text{Mn}_{0.4}\text{PO}_4/\text{C}$ microspheres by a double carbon coating-spray drying method for high rate lithium ion batteries, *J. Mater. Chem. A*, 2013, 1, 2411–2417.
- 131 Y. P. Huang, T. Tao, Z. Chen, W. Han, Y. Wu, C. Kuang, S. Zhou and Y. Chen, Excellent electrochemical performance of $\text{LiFe}_{0.4}\text{Mn}_{0.6}\text{PO}_4$ microspheres produced using a double carbon coating process, *J. Mater. Chem. A*, 2014, 2, 18831–18837.
- 132 W. Yuan, Y. Zhang, L. Cheng, H. Wu, L. Zheng and D. Zhao, The applications of carbon nanotubes and graphene in advanced rechargeable lithium batteries, *J. Mater. Chem. A*, 2016, 4, 8932–8951.
- 133 M. Casas-Cabanas, V. V. Roddatis, D. Saurel, P. Kubiak, J. Carretero-González, V. Palomares, P. Serras and T. Rojo, Crystal chemistry of Na insertion/de-insertion in $\text{FePO}_4\text{-NaFePO}_4$, *J. Mater. Chem.*, 2012, 22, 17421–17423.
- 134 J. Kim, D. H. Seo, H. Kim, I. Park, J. K. Yoo, S. K. Jung, Y. U. Park, W. A. Goddard and K. Kang, Unexpected discovery of low-cost maricite NaFePO_4 as a high-performance electrode for Na-ion batteries, *Energy Environ. Sci.*, 2015, 8, 540–545.
- 135 B. L. Ellis, W. R. M. Makahnouk, Y. Makimura, K. Toghill and L. F. Nazar, A multifunctional 3.5V iron-based phosphate cathode for rechargeable batteries, *Nat. Mater.*, 2007, 6, 749–753.
- 136 M. M. Rahman, I. Sultana, S. Mateti, J. Liu, N. Sharma and Y. Chen, Maricite $\text{NaFePO}_4/\text{C}/\text{graphene}$: a novel hybrid cathode for sodium-ion batteries, *J. Mater. Chem. A*, 2017, 5, 16616–16621.
- 137 M. M. Rahman, A. M. Glushenkov, Z. Chen, X. J. Dai, T. Ramireddy and Y. Chen, Clusters of $\alpha\text{-LiFeO}_2$ nanoparticles incorporated into multi-walled carbon nanotubes: a lithium-ion battery cathode with enhanced lithium storage properties, *Phys. Chem. Chem. Phys.*, 2013, 15, 20371–20378.
- 138 T. Tao, M. M. Rahman, T. Ramireddy, J. Sunarso, Y. Chen and A. M. Glushenkov, Preparation of composite electrodes with carbon nanotubes for lithium-ion batteries by low-energy ball milling, *RSC Adv.*, 2014, 4, 36649–36655.
- 139 S. Mateti, M. M. Rahman, L. H. Li, Q. Cai and Y. Chen, *In situ* prepared $\text{V}_2\text{O}_5/\text{graphene}$ hybrid as a superior cathode material for lithium-ion batteries, *RSC Adv.*, 2016, 6, 35287–35294.
- 140 Y. Q. Wang, L. Gu, Y. G. Guo, H. Li, X. Q. He, S. Tsukimoto, Y. Ikuhara and L. J. Wan, Rutile- TiO_2 nanocoating for a

- high-rate $\text{Li}_4\text{Ti}_5\text{O}_{12}$ anode of a lithium-ion battery, *J. Am. Chem. Soc.*, 2012, **134**, 7874–7879.
- 141 P. Oh, S. M. Oh, W. Li, S. Myeong, J. Cho and A. Manthiram, High-performance heterostructured cathodes for lithium-ion batteries with a Ni-rich layered oxide core and a Li-rich layered oxide shell, *Adv. Sci.*, 2016, **3**, 1600184.
- 142 B. Song, A facile cathode design combining Ni-rich layered oxides with Li-rich layered oxides for lithium-ion batteries, *J. Power Sources*, 2016, **325**, 620–629.
- 143 K. M. Shaju, G. V. S. Rao and B. V. R. Chowdari, Performance of layered $\text{Li}(\text{Ni}_{1/3}\text{Co}_{1/3}\text{Mn}_{1/3})\text{O}_2$ as cathode for Li-ion batteries, *Electrochim. Acta*, 2002, **48**, 145–151.
- 144 J. Y. Hwang, S. T. Myung, C. S. Yoon, S. S. Kim, D. Aurbach and Y. K. Sun, Novel cathode materials for Na-ion batteries composed of spoke-like nanorods of $\text{Na}[\text{Ni}_{0.61}\text{Co}_{0.12}\text{Mn}_{0.27}]\text{O}_2$ assembled in spherical secondary particles, *Adv. Funct. Mater.*, 2016, **26**, 8083–8093.
- 145 W. Liu, P. Oh, X. Liu, M. J. Lee, W. Cho, S. Chae, Y. Kim and J. Cho, Nickel-rich layered lithium transition-metal oxide for high-energy lithium-ion batteries, *Angew. Chem., Int. Ed.*, 2015, **54**, 4440–4457.
- 146 Y. Cho, P. Oh and J. Cho, A new type of protective surface layer for high-capacity Ni-based cathode materials: nano scaled surface pillaring layer, *Nano Lett.*, 2013, **13**, 1145–1152.
- 147 L. J. Wu, K. W. Nam, X. J. Wang, Y. N. Zhou, J. C. Zheng, X. Q. Yang and Y. M. Zhu, Structural origin of overcharge-induced thermal instability of Ni-containing layered-cathodes for high-energy-density lithium batteries, *Chem. Mater.*, 2011, **23**, 3953–3960.
- 148 S. M. Bak, K. W. Nam, W. Chang, X. Q. Yu, E. Y. Hu, S. Hwang, E. A. Stach, K. B. Kim, K. Y. Chung and X. Q. Yang, Correlating structural changes and gas evolution during the thermal decomposition of charged $\text{Li}_x\text{Ni}_{0.8}\text{Co}_{0.15}\text{Al}_{0.05}\text{O}_2$ cathode materials, *Chem. Mater.*, 2013, **25**, 337–351.
- 149 C. Chen, T. Tao, W. Qi, H. Zeng, Y. Wu, B. Liang, Y. Yao, S. Lu and Y. Chen, High-performance lithium ion batteries using SiO_2 -coated $\text{LiNi}_{0.5}\text{Co}_{0.2}\text{Mn}_{0.3}\text{O}_2$ microspheres as cathodes, *J. Alloys Compd.*, 2017, **709**, 708–716.
- 150 T. Tao, C. Chen, Y. Yao, B. Liang, S. Lu and Y. Chen, Enhanced electrochemical performance of ZrO_2 modified $\text{LiNi}_{0.6}\text{Co}_{0.2}\text{Mn}_{0.2}\text{O}_2$ cathode material for lithium ion batteries, *Ceram. Int.*, 2017, **43**, 15173–15178.
- 151 T. Tao, C. Chen, W. Qi, B. Liang, Y. Yao and S. Lu, Antimony doped tin oxide-coated $\text{LiNi}_{0.5}\text{Co}_{0.2}\text{Mn}_{0.3}\text{O}_2$ cathode materials with enhanced electrochemical performance for lithium-ion batteries, *J. Alloys Compd.*, 2018, **765**, 601–607.
- 152 Z. H. Chen, Y. Qin, K. Amine and Y. K. Sun, Role of surface coating on cathode materials for lithium-ion batteries, *J. Mater. Chem.*, 2010, **20**, 7606–7612.
- 153 H. Gao, X. Guo, S. Wang, F. Zhang, H. Liu and G. Wang, Antimony-based nanomaterials for high-performance potassium-ion batteries, *EcoMat*, 2020, **2**, e12027.
- 154 S. Wang, P. Xiong, X. Guo, J. Zhang, X. Gao, F. Zhang, X. Tang, P. H. L. Notten and G. Wang, A stable conversion and alloying anode for potassium-ion batteries: a combined strategy of encapsulation and confinement, *Adv. Funct. Mater.*, 2020, **30**, 2001588.
- 155 H. Ying and W. Q. Han, Metallic Sn-based anode materials: application in high-performance lithium-ion and sodium-ion batteries, *Adv. Sci.*, 2017, **4**, 1700298.
- 156 B. J. Hassoun, G. Derrien, S. Panero and B. Scrosati, A nanostructured Sn-C composite lithium battery electrode with unique stability and high electrochemical performance, *Adv. Mater.*, 2008, **20**, 3169–3175.
- 157 S.-M. Oh, S.-T. Myung, M.-W. Jang, B. Scrosati, J. Hassoun and Y.-K. Sun, An advanced sodium-ion rechargeable battery based on a tin-carbon anode and a layered oxide framework cathode, *Phys. Chem. Chem. Phys.*, 2013, **15**, 3827–3833.
- 158 J. W. Park, J. Y. Eom and H. S. Kwon, Fabrication of Sn-C composite electrodes by electrodeposition and their cycle performance for Li-ion batteries, *Electrochem. Commun.*, 2009, **11**, 596–598.
- 159 I. Sultana, T. Ramireddy, M. M. Rahman, Y. Chen and A. M. Glushenkov, Tin-based composite anodes for potassium-ion batteries, *Chem. Commun.*, 2016, **52**, 9279–9282.
- 160 Q. Wang, X. Zhao, C. Ni, H. Tian, J. Li, Z. Zhang, S. X. Mao, J. Wang and Y. Xu, Reaction and capacity-fading mechanisms of tin nanoparticles in potassium-ion batteries, *J. Phys. Chem. C*, 2017, **121**, 12652–12657.
- 161 W. Zhang, J. Mao, S. Li, Z. Chen and Z. Guo, Phosphorus-based alloy materials for advanced potassium-ion battery anode, *J. Am. Chem. Soc.*, 2017, **139**, 3316–3319.
- 162 T. Ramireddy, R. Kali, M. K. Jangid, V. Srihari, H. K. Poswal and A. Mukhopadhyay, Insights into electrochemical behavior, phase evolution and stability of Sn upon K-alloying/de-alloying *via in situ* studies, *J. Electrochem. Soc.*, 2017, **164**, A2360–A2367.
- 163 V. Lakshmi, Y. Chen, A. A. Mikhaylov, A. G. Medvedev, I. Sultana, M. M. Rahman, O. Lev, P. V. Prikhodchenko and A. M. Glushenkov, Nanocrystalline SnS_2 coated onto reduced graphene oxide: demonstrating the feasibility of a non-graphitic anode with sulfide chemistry for potassium-ion batteries, *Chem. Commun.*, 2017, **53**, 8272–8275.
- 164 C.-M. Park, J.-H. Kim, H. Kim and H.-J. Sohn, Li-alloy based anode materials for Li secondary batteries, *Chem. Soc. Rev.*, 2010, **39**, 3115–3141.
- 165 L. Baggetto, P. Ganesh, C.-N. Sun, R. A. Meisner, T. A. Awodzinski and G. M. Veith, Intrinsic thermodynamic and kinetic properties of Sb electrodes for Li-ion and Na-ion batteries: experiment and theory, *J. Mater. Chem. A*, 2013, **1**, 7985–7994.
- 166 A. Darwiche, C. Marino, M. T. Sougrati, B. Fraise, L. Stievano and L. Monconduit, Better cycling performances of bulk Sb in Na-ion batteries compared to Li-ion systems: an unexpected electrochemical mechanism, *J. Am. Chem. Soc.*, 2012, **134**, 20805–20811.
- 167 W. D. McCulloch, X. Ren, M. Yu, Z. Huang and Y. Wu, Potassium-ion oxygen battery based on a high capacity antimony anode, *ACS Appl. Mater. Interfaces*, 2015, **7**, 26158–26166.
- 168 I. Sultana, M. M. Rahman, J. Liu, N. Sharma, A. V. Ellis, Y. Chen and A. M. Glushenkov, Antimony-carbon nanocomposites for

- potassium-ion batteries: Insight into the failure mechanism in electrodes and possible avenues to improve cyclic stability, *J. Power Sources*, 2019, **413**, 476–484.
- 169 W. Zhang, J. Mao, S. Li, Z. Chen and Z. Guo, Phosphorus-based alloy materials for advanced potassium-ion battery anode, *J. Am. Chem. Soc.*, 2017, **139**, 3316–3319.
- 170 I. Sultana, M. M. Rahman, T. Ramireddy, Y. Chen and A. M. Glushenkov, High capacity potassium-ion battery anodes based on black phosphorus, *J. Mater. Chem. A*, 2017, **5**, 23506–23512.
- 171 D. Liu, X. Huang, D. Qu, D. Zheng, G. Wang, J. Harris, J. Si, T. Ding, J. Chen and D. Qu, Confined phosphorus in carbon nanotube-backboned mesoporous carbon as superior anode material for sodium/potassium-ion batteries, *Nano Energy*, 2018, **52**, 1–10.
- 172 X. Wu, W. Zhao, H. Wang, X. Qi, Z. Xing, Q. Zhuang and Z. Ju, Enhanced capacity of chemically bonded phosphorus/carbon composite as an anode material for potassium-ion batteries, *J. Power Sources*, 2018, **378**, 460–467.
- 173 J.-K. Yoo, J. Kim, Y. S. Jung and K. Kang, Scalable fabrication of silicon nanotubes and their application to energy storage, *Adv. Mater.*, 2012, **24**, 5452–5456.
- 174 M. Ko, S. Chae, J. Ma, N. Kim, H.-W. Lee, Y. Cui and J. Cho, Scalable synthesis of silicon-nanolayer-embedded graphite for high-energy lithium-ion batteries, *Nat. Energy*, 2016, **16133**, 1–8.
- 175 I. Sultana, M. M. Rahman, Y. Chen and A. M. Glushenkov, Potassium-ion battery anode materials operating through the alloying-dealloying reaction mechanism, *Adv. Funct. Mater.*, 2018, **28**, 1703857.
- 176 T. T. Tran and M. N. Obrovac, Alloy negative electrodes for high energy density metal-ion cells, *J. Electrochem. Soc.*, 2011, **158**, A1411–A1416.
- 177 J. Liang, Z. H. Sun, F. Li and H. M. Cheng, Carbon materials for Li-S batteries: Functional evolution and performance improvement, *Energy Storage Mater.*, 2016, **2**, 76–106.
- 178 R. Xu, I. Belharouak, J. C. M. Li, X. Zhang, I. Bloom and J. Bareño, Role of polysulfides in self-healing lithium-sulfur batteries, *Adv. Energy Mater.*, 2013, **3**, 833–838.
- 179 P. G. Bruce, S. A. Freunberger, L. J. Hardwick and J. M. Tarascon, Li-O₂ and Li-S batteries with high energy storage, *Nat. Mater.*, 2012, **11**, 19–29.
- 180 A. Hu, M. Zhou, T. Lei, Y. Hu, X. Du, C. Gong, C. Shu, J. Long, J. Zhu, W. Chen, X. Wang and J. Xiong, Optimizing redox reactions in aprotic lithium-sulfur batteries, *Adv. Energy Mater.*, 2020, **10**, 2002180.
- 181 X. Yang, X. Gao, Q. Sun, S. P. Jand, Y. Yu, Y. Zhao, X. Li, K. Adair, L.-Y. Kuo, J. Rohrer, J. Liang, X. Lin, M. N. Banis, Y. Hu, H. Zhang, X. Li, R. Li, H. Zhang, P. Kaghazchi, T. K. Sham and X. Sun, Promoting the transformation of Li₂S₂ to Li₂S: Significantly increasing utilization of active materials for high-sulfur-loading Li-S batteries, *Adv. Mater.*, 2019, **31**, 1901220.
- 182 J. Yan, X. Liu and B. Li, Capacity fade analysis of sulfur cathodes in lithium-sulfur batteries, *Adv. Sci.*, 2016, **3**, 1600101.
- 183 S. Waluś, C. Barchasz, R. Bouchet, J.-C. Lepretre, J.-F. Colin, J.-F. Martin, E. Elkaim, C. Baehtz and F. Alloin, Lithium/sulfur batteries upon cycling: structural modifications and species quantification by *in situ* and *operando* X-ray diffraction spectroscopy, *Adv. Energy Mater.*, 2015, **5**, 1500165.
- 184 C. Barchasz, F. Molton, C. Duboc, J. C. Lepretre, S. Patoux and F. Alloin, Lithium/sulfur cell discharge mechanism: an original approach for intermediate species identification, *Anal. Chem.*, 2012, **84**, 3973–3980.
- 185 Y. Yang, G. Zheng, S. Misra, J. Nelson, M. F. Toney and Y. Cui, High-capacity micrometer-sized Li₂S particles as cathode materials for advanced rechargeable lithium-ion batteries, *J. Am. Chem. Soc.*, 2012, **134**, 15387–15394.
- 186 H. Yuan, H.-J. Peng, J.-Q. Huang and Q. Zhang, Sulfur redox reactions at working interfaces in lithium-sulfur batteries: a perspective, *Adv. Mater. Interfaces*, 2019, **6**, 1802046.
- 187 A. Manthiram, Y. Fu, S. H. Chung, C. Zu and Y. S. Su, Rechargeable lithium-sulfur batteries, *Chem. Rev.*, 2014, **114**, 11751–11787.
- 188 F. Li, J. He, J. Liu, M. Wu, Y. Hou, H. Wang, S. Qi, Q. Liu, J. Hu and J. Ma, Gradient solid electrolyte interphase and lithium-ion solvation regulated by bisfluoroacetamide for stable lithium metal batteries, *Angew. Chem., Int. Ed.*, 2021, **60**, 6600–6608.
- 189 Y. Yang, G. Zheng and Y. Cui, Nanostructured sulfur cathodes, *Chem. Soc. Rev.*, 2013, **42**, 3018–3032.
- 190 J. Sun, J. Ma, J. Fan, J. Pyun and J. Geng, Rational design of sulfur-containing composites for high-performance lithium-sulfur batteries, *APL Mater.*, 2019, **7**, 020904.
- 191 R. Kumar, J. Liu, J. Y. Hwang and Y. K. Sun, Recent research trends in Li-S batteries, *J. Mater. Chem. A*, 2018, **6**, 11582–11605.
- 192 S. R. Chen, Y. P. Zhai, G. L. Xu, Y. X. Jiang, D. Y. Zhao, J. T. Li, L. Huang and S. G. Sun, Ordered mesoporous carbon/sulfur nanocomposite of high performances as cathode for lithium-sulfur battery, *Electrochim. Acta*, 2011, **56**, 9549–9555.
- 193 X. Liang, Z. Wen, Y. Liu, H. Zhang, L. Huang and J. Jin, Highly dispersed sulfur in ordered mesoporous carbon sphere as a composite cathode for rechargeable polymer Li/S battery, *J. Power Sources*, 2011, **196**, 3655–3658.
- 194 J. Schuster, G. He, B. Mandlmeier, T. Yim, K. T. Lee, T. Bein and L. F. Nazar, Spherical ordered mesoporous carbon nanoparticles with high porosity for lithium-sulfur batteries, *Angew. Chem.*, 2012, **124**, 3651–3655.
- 195 T. Yang, Y. Zhong, J. Liang, M. M. Rahman, W. Lei, Y. Chen, M. J. Monteiro, Z. Shao and J. Liu, Hierarchical porous yolk-shell carbon nanosphere for high-performance lithium-sulfur batteries, *Part. Part. Syst. Charact.*, 2017, **34**, 1600281.
- 196 Y. S. Su and A. Manthiram, Lithium-sulphur batteries with a microporous carbon paper as a bifunctional interlayer, *Nat. Commun.*, 2012, **3**, 1166.
- 197 S. Chen, B. Sun, X. Xie, A. K. Mondal, X. Huang and G. Wang, Multi-chambered micro/meso porous carbon nanocubes as new polysulfides reservoirs for lithium-sulfur batteries with long cycle life, *Nano Energy*, 2015, **16**, 268–280.
- 198 Y. S. Su and A. Manthiram, A new approach to improve cycle performance of rechargeable Lithium-sulfur batteries

- by inserting a free-standing MWCNT interlayer, *Chem. Commun.*, 2012, **48**, 8817–8819.
- 199 T. G. Jeong, Y. H. Moon, H. H. Chun, H. S. Kim, B. W. Choc and Y. T. Kim, Free standing acetylene black mesh to capture dissolved polysulfide in lithium sulfur batteries, *Chem. Commun.*, 2013, **49**, 11107–11109.
- 200 Y. Fan, Z. Yang, W. Hua, D. Liu, T. Tao, M. M. Rahman, W. W. Lei, S. Huang and Y. Chen, Functionalized boron nitride nanosheets/graphene interlayer for fast and long-life lithium-sulfur batteries, *Adv. Energy Mater.*, 2017, **7**, 1602380.
- 201 H. Kim, G. Jeong, Y. U. Kim, J. H. Kim, C. M. Park and H. J. Sohn, Metallic anodes for next generation secondary batteries, *Chem. Soc. Rev.*, 2013, **42**, 9011–9034.
- 202 W. Xu, J. Wang, F. Ding, X. Chen, E. Nasybulin, Y. Zhang and J. G. Zhang, Lithium metal anodes for rechargeable batteries, *Energy Environ. Sci.*, 2014, **7**, 513–537.
- 203 R. Bouchet, S. Maria, R. Meziane, A. Aboulaich, L. Lienafa, J. P. Bonnet, T. N. T. Phan, D. Bertin, D. Gignes, D. Devaux, R. Denoyel and M. Armand, Single-ion BAB triblock copolymers as highly efficient electrolytes for lithium-metal batteries, *Nat. Mater.*, 2013, **12**, 452–457.
- 204 L. Suo, Y. S. Hu, H. Li, M. Armand and L. Chen, A new class of solvent-in-salt electrolyte for high-energy rechargeable metallic lithium batteries, *Nat. Commun.*, 2013, **4**, 1481.
- 205 S. Qi, H. Wang, J. He, J. Liu, C. Cui, M. Wu, F. Li, Y. Feng and J. Ma, Electrolytes enriched by potassium perfluorinated sulfonates for lithium metal batteries, *Sci. Bull.*, 2021, **66**, 685–693.
- 206 S. Qi, J. He, J. Liu, H. Wang, M. Wu, F. Li, D. Wu, X. Li and J. Ma, Phosphonium bromides regulating solid electrolyte interphase components and optimizing solvation sheath structure for suppressing lithium dendrite growth, *Adv. Funct. Mater.*, 2021, **31**, 2009013.
- 207 H. Wang, J. He, J. Liu, S. Qi, M. Wu, J. Wen, Y. Chen, Y. Feng and J. Ma, Electrolytes enriched by crown ethers for lithium metal batteries, *Adv. Funct. Mater.*, 2021, **31**, 2002578.
- 208 D. Lin, Y. Liu, Z. Liang, H. W. Lee, J. Sun, H. Wang, K. Yan, J. Xie and Y. Cui, Layered reduced graphene oxide with nanoscale interlayer gaps as a stable host for lithium metal anodes, *Nat. Nanotechnol.*, 2016, **11**, 626–632.
- 209 Y. Liu, D. Lin, Z. Liang, J. Zhao, K. Yan and Y. Cui, Lithium-coated polymeric matrix as a minimum volume-change and dendrite-free lithium metal anode, *Nat. Commun.*, 2016, **7**, 10992.
- 210 B. Yu, T. Tao, S. Mateti, S. Lu and Y. Chen, Nanoflake arrays of lithiophilic metal oxides for the ultra-stable anodes of lithium-metal batteries, *Adv. Funct. Mater.*, 2018, **28**, 1803023.
- 211 J. Wang, J. Wan, N. Yang, Q. Li and D. Wang, Hollow multishell structures exercise temporal-spatial ordering and dynamic smart behaviour, *Nat. Rev. Chem.*, 2020, **4**, 159–168.
- 212 J. Wang, Yi Cui and D. Wang, Hollow multishelled structures revive high energy density batteries, *Nanoscale Horiz.*, 2020, **5**, 1287–1292.
- 213 E. H. M. Salhabi, J. Zhao, J. Wang, M. Yang, B. Wang and D. Wang, Hollow multi-shelled structural TiO_{2-x} with multiple spatial confinement for long-life lithium-sulfur batteries, *Angew. Chem., Int. Ed.*, 2019, **58**, 9078–9082.
- 214 J. Zhao, M. Yang, N. Yang, J. Wang and D. Wang, Hollow micro-/nanostructure reviving lithium-sulfur batteries, *Chem. Res. Chin. Univ.*, 2020, **36**, 313–319.
- 215 J. Chen, X. Xu, Q. He and Y. Ma, Advanced current collectors for alkali metal anodes, *Chem. Res. Chin. Univ.*, 2020, **36**, 386–401.